Institut de Chimie, Faculté des Sciences

Metallic Ruthenium Nanoparticles Intercalated in Hectorite for Highly Selective Catalytic Hydrogenations

Thèse présentée à la Faculté des Sciences de l'Université de Neuchâtel
Pour l'obtention du grade de Docteur ès Sciences par

BING SUN

Ingénieur chimiste (*MSc en génie chimque*) de l'Université chinoise
du pétrole à Beijing, République populaire de Chine

Membres du jury:

Prof. Georg Süss-Fink	Directeur de thèse, Université de Neuchâtel
Prof. Bruno Therrien	Rapporteur interne, Université de Neuchâtel
Prof. Thomas Bürgi	Rapporteur externe, Université de Genève

UNIVERSITÉ DE NEUCHÂTEL

Institut de Chimie, Université de Neuchâtel
October 2015 Suisse

swissuniversities

UNIVERSITÉ DE NEUCHÂTEL

Faculté des sciences
Secrétariat-décanat de Faculté
Rue Emile-Argand 11
2000 Neuchâtel - Suisse
Tél: + 41 (0)32 718 2100
E-mail: secretariat.sciences@unine.ch

IMPRIMATUR POUR THESE DE DOCTORAT

La Faculté des sciences de l'Université de Neuchâtel autorise l'impression de la présente thèse soutenue par

Monsieur Bing SUN

Titre:

"Metallic Ruthenium Nanoparticles Intercalated in Hectorite for Highly Selective Catalytic Hydrogenations"

sur le rapport des membres du jury composé comme suit:

- Prof. Georg Süss-Fink, Université de Neuchâtel, directeur de thèse
- Prof. ass. Bruno Therrien, Université de Neuchâtel
- Prof. Thomas Bürgi, Université de Genève

Neuchâtel, le 14 décembre 2015

Le Doyen, Prof. B. Colbois

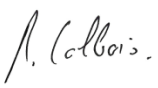

dedicated to my parents

Dingyou Sun & Qin Guo

Acknowledgement

Citing an old Chinese saying, “A teacher for a day is a father for a lifetime”, I am pleased to express my sincere acknowledgement to Prof. Georg Süss-Fink for accommodating and supervising me in the *Laboratoire de chimie organométallique et de catalyse moléculaire* in Neuchâtel. From a hamlet in central China to a metropolis Beijing, further to such a modernized country Switzerland, the discrepancy emerged throughout my life at the beginning. Aside from the maladjustment in this new environment, I often encountered problems in carrying out my research project individually. Here, many thanks to your toleration and instruction on my step into the ruthenium-catalysis world. I benefit very much from your extensive knowledge from inorganic chemistry to catalysis, and even biochemistry. In fact, the whole thesis related to my PhD degree can’t move a small step without your fruitful help. Certainly, what I learned from you not only focuses on the chemistry, but also relates to your personality, gracious, conscientious, strict but generous.... I still remember my first trip in Neuchâtel when you picked me up in the train station. That moment has been engraved in my heart. Danke schön, Prof. Süss-Fink.

Prof. Bruno Therrien, many thanks to you, too. During my PhD study in this group, you often propose smart ideas for my research project. Intercalated ruthenium nanoparticles in hectorite are somewhat a kind of supramolecular host-guest system. Maybe there is a moment where your concept on constructing supramolecular host-guest complexes inspires me to discover more efficient catalysts. Meanwhile, I here stress that I am very grateful to you for inviting me to work together on the book chapter on Elsevier, and thank you for helping me with documents related to my stay in Neuchâtel and return to China. By the way, your distinct North American style makes me a profound impression. Cool!

Prof. Thomas Bürgi, thank you for reviewing my thesis and examining my PhD defense.

I am deeply thankful to Dr. Farooq-Ahmad Khan, who introduced nanocatalysis to me and guided me with his entire passion and experience. From the very basic

custom in French-speaking regions to the critical Schlenk technique handling the air-sensitive ruthenium catalysts, you taught me without any reservation. In my first four months in Neuchâtel, we were madly immersed in the hydrogenations both by day and by night. Your passion and spirit really encouraged me to go forward. I already keep your pet phrase in my mind (…*like machine*…). In a word, thank you.

I am also grateful to Amine Garci and John Peter Justin Paul Raj. Accompanying with Amine for the morning coffee break, I indirectly broadened my knowledge over the chemistry and NE-life, digging out an awesome kebab shop. Justin delivered me his experience over Demonstration experiments for Chimie Générale and trained me a lot. I will preserve this "Demonstration Bible" in case of any show-off chance.

I also thank Dr. Mathiyazhagan Ulaganatha Raja, Dr. Nandhagopal Raja and Dr. Gajendra Gupta for their warm assistance on the chemistry and for their encouragement when I fell into endless depression in losing someone in 2012. Meanwhile, I am grateful to Dr. Mona Anca Furrer, Julien Freudenreich, Jîri Tauchman, Anne-Flore Ibao, Dr. Trieu-Tien Thai, Wassila Aboura, Dr. Tan Yong Leng Kelvin and Dr. Ersin Orhan for all their kind help on my study.

I must express my gratitude to Minghui Yuan and Fan Zhang. During the tough period of my sprint toward the last project, I could not insist without Minghui's concomitance and strong logistics support (*thumbs up for your wonderful cooking*). I often learn chemistry theory and experimental skills from you. I have been used to a morning coffee together with you, sharing some joys and sorrows of life. It will be a nice memory.

I also thank all the other current and previous group members David Stíbal, Thomas Cheminel, Balazs Brem, and Emmanuel Denoyelle Di Muro. Have been working together with David since 2010, no matter in Zürich or Neuchâtel, I always receive his positive suggestions. Thomas takes credit for his excellence in chemical and instrument management, providing us a solid support. Balazs shows his optimistic personality and patience to guide me on the chemical identification. Emmanuel's encouragement and edification kept me from being lost in the past. Thanks so much, guys.

The support from the Neuchâtel Platform of Analytical Chemistry is greatly acknowledged. The chromatography, mass spectroscopy and elemental analysis service is kindly from Dr. Armelle Vallat and nuclear magnetic resonance spectroscopy service from Dr. Diego Carnevale and Dr. Claudio Dalvit. Special thanks to Diego for his contribution to our publication. I also appreciate the assistance of Dr. Mohammad Mehdi Dadras and Dr. Olha Sereda at CSEM for TEM and XRD analysis. Also, the service for optical rotation analysis from Dr. Naomi Sakai at Université de Genève and Julien Pomarole at Universität Bern is thanked. Fruitful discussions with Prof. Robert Deschenaux, Thanh Tung Nguyen and Dr. Christian Invernizzi are acknowledged. I also thank Divambal Appavoo, Thi Luyen Vuong and Thi Minh Nguyet Trinh for warm help on my chemistry.

I am grateful to Mrs. Jocelyne Tissot and Mrs. Emilie Auclair for administration and documents assistance, very graceful and generous. The technician staff Mr. Thierry Delhove, Mr. Dominique Schenker, Mr. Daniel Varidel and others are sincerely thanked. Mr. Habib Abdelkhalek and Mrs. Priscille Bôle are also thanked for chemical and materials ordering.

And my previous colleagues and friends Zhiqiang Ma, Min Wei Tew, Evalyn Mae Alayon, Christiane Kartusch, Martin Makosch, Dr. Matthew Brown and Daniel Fodor in Zürich are thanked for their encouragement and assistance on my study.

Prof. Baojian Shen and Prof. Qiaoxia Guo at China University of Petroleum Beijing are cordially acknowledged for their continuous support and inspiration. You changed me.

Final, I would dedicate this thesis to my parents Mr. Dingyou Sun and Mrs. Qin Guo for their unselfish support throughout my life.

Summary

The design of nanocomposites consisting of functional metals and proper matrices is a very active field of research for the development of recyclable catalysts. Highly active metallic nanoparticles must be stabilized by a suitable support in order to prevent aggregation to bulk metal. Hectorite, a representative smectite clay featured by its unique swelling properties and flexible intercalation capacity, provides an ideal platform for immobilizing metal nanoparticles.

By intercalating organometallic benzene ruthenium complexes or Werner-type ruthenium(III) ions from $RuCl_3 \cdot xH_2O$ as precursor, ruthenium nanoparticles intercalated in hectorite are successfully obtained via a reduction process with molecular hydrogen approach or sodium borohydride. Depending on the properties of solvents and the reduction conditions, a variety of ruthenium nanoparticles with different morphology are formed.

In the catalytic hydrogenation of quinoline, hectorite-intercalated ruthenium nanoparticles show excellent reactivity and selectivity to the specific product. By using water or cyclohexane as reaction medium under a certain pressure of molecular H_2, 1,2,3,4-tetrahydroquinoline and decahydroquinoline were exclusively obtained, repectively. Furthermore, by using sodium borohydride as reducing agent, the catalytic hydrogenation of quinoline proceeds in water under atmospheric pressure with the conversion and selectivity superior to 99%. Isotope labeling experiments combined with semi-empirical calculations reveal that both the sodium borohydride and water participate in the hydrogenation process by means of hydride transfer and proton transfer, respectively.

Furthermore, hectorite-intercalated ruthenium nanoparticles can also be used for the hydrogenation of aromatic amino acids in aqueous media. By screening of the influencing factors, the pH of the solution was found to be critical for the complete conversion of aromatic amino acids. Critically, during the hydrogenation process, the chirality of the substrates remains unchanged.

Keywords

Ruthenium nanoparticles, Hectorite, Hydrogenation, Quinoline, Quinoline derivatives, Quinoline analogues, Aromatic amino acids, Isotope labeling, Semi-empirical calculations.

Mots Clés

Nanoparticules de Ruthénium, Hectorite, Hydrogénation, Quinoléine, Dérivés de quinoléine, Analogues de quinoléine, Acides aminés aromatiques, Marquage isotopique, Calculs semi-empiriques.

Table of Contents

1

Introduction

1.1 Catalysis

Catalysis is an important and fascinating subject. It has been employed in industrial chemical manufacturing for more than 100 years and holds its endless potential for diverse applications in chemistry world. In our modern society, more than 90% of the chemical processes in use throughout the world require catalysts [1]. From the food additives to pharmaceuticals as well as fuel, fabrics, dyes and many other fine chemicals, all these manufacturing processes involve catalysts. Global demand on catalysts was valued at US$33.5 billion in 2014 and would witness a stable and robust growth year by year [2].

A catalyst, a term stemming from Greek καταλύω (meaning 'loosening down'), is generally defined as a substance that accelerates a chemical reaction without itself being consumed [3]. The concept of *catalysis* was initially introduced by the Scottish chemist Elizabeth Fulhame in 1794 [4] and the term *catalysis* was then coined by the Swedish chemist Jöns Jacob Berzelius in 1835 [5]. In 1894, a common definition of *catalysis*, "*Catalysis is the acceleration of a chemical reaction, which proceeds slowly, by the presence of a foreign substance*", was formulated by the German chemist Wilhelm Ostwald (Nobel Prize 1909) [6]. Based on Ostwald's theory, a catalyst accelerates (or inhibits) only the catalytic process, in contrast to the views of Joseph John Thomson (English physicist, Nobel Prize 1906), Henry Edward Armstrong (English chemist) and Christian Friedrich Schönbein (German chemist) according to which a catalyst could initiate a reaction.

To let a chemical reaction occur, a minimum energy is required, which is called *activation energy* (E_a). To let a reaction proceed at a reasonable rate, the energy of reactants must be not lower than the activation energy, a high temperature being essential to overcome the energy barrier. Alternatively, a catalyst provides another path with a requirement of lower activation energy (E_a^*) for carrying out a reaction. As depicted in Figure 1.1, the presence of a catalyst significantly reduces the activation energy for a reaction (E_a^*), turning it energetically much more favorable.

Noticeably, in the cases of the absence and presence of a catalyst, the Gibbs free energy (ΔG) variations remain constant, which means the catalyst only changes the reaction kinetics rather than the thermodynamics (equilibrium constant).

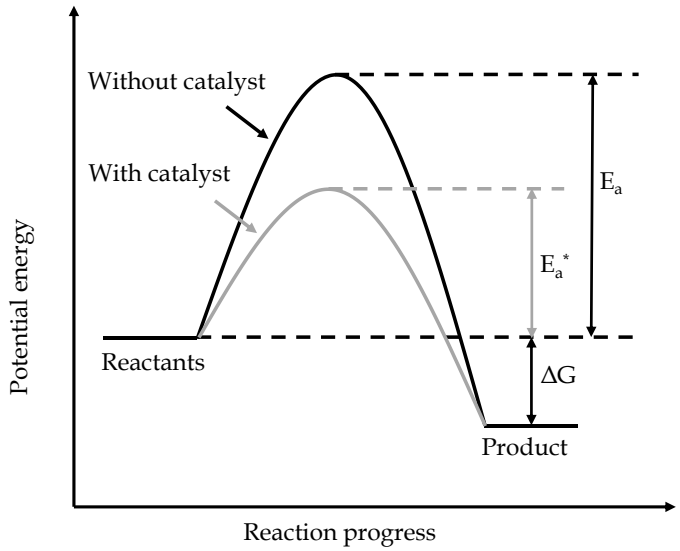

Figure 1.1 Simplified potential energy diagram demonstrating the catalyst effect on a hypothetical exothermic reaction. Activation energy for a non-catalytic reaction (black curve) and catalytic reaction (gray curve) is E_a and E_a^*, respectively. ΔG is the change in Gibbs free energy between the reactants and product.

According to the diversity of the reaction systems, the catalysts can be cataloged as homogeneous catalysts and heterogeneous catalysts. Homogeneous catalysis is featured by a single phase reaction system, in which all the reactants and products are in the same phase as the catalyst. The representative advantages of homogeneous catalysis are commonly attributed to its excellent selectivity to products and milder reaction conditions, however, distressing drawbacks concerning product separation and catalyst recycling seriously limit its large scale application. Heterogeneous catalysis, by contrast, owning to the solid phase of the catalysts, possesses distinct characteristics of easy separation and recycling, being favorable for industrial application.

1.2 Heterogeneous catalytic hydrogenation

Catalytic hydrogenation plays an important role in fine chemical synthesis. Its history can be traced back to the invention of *Döbereiner's lamp* in 1823, when Johann Wolfgang Döbereiner (German chemist) found hydrogen flowing in the air bursts into flame in the presence of metallic platinum. The first hydrogenation process was discovered by the French chemist Paul Sabatier (Nobel Prize 1912) in 1897, named *Sabatier process*, which involves the hydrogenation of CO_2 to produce CH_4 at elevated temperature and pressure catalyzed by a nickel catalyst. In contrast to Sabatier's assertions that only the vaporizable organic compounds can undergo catalytic hydrogenation, the German chemist Wilhelm Normann successfully transformed liquid oleic acid into solid stearic acid with the aid of dispersed nickel as the hydrogenation catalyst. In the early 20^{th} century, the milestone in industrial chemistry was inaugurated by the German chemists Fritz Haber (Nobel Prize 1918) and Carl Bosch (Nobel Prize 1931) for their ingenious contribution to the *Haber–Bosch process*, which converts N_2 to NH_3 by hydrogenation with H_2 using metal catalysts. Meanwhile, the famous *Fischer–Tropsch process* was subsequently developed by the German chemist Franz Fischer and the Czech-German chemist Hans Tropsch in 1925, in which the gaseous CO and H_2 is transformed into liquid hydrocarbons with the aid of transition metals as catalysts [7]. In general, the hydrogenation process refers to the addition of hydrogen to unsaturated hydrocarbons, while hydrogenolysis (another type of hydrogenation) involves the cleavage of C–X bonds. In the catalytic reforming process of petroleum refineries, X usually represents an S, N or O atom. The first commercial reforming process was invented by American chemical engineer Vladimir Haensel in 1949, known as the *Platforming process*, in which the catalytic hydrodesulfurization is included to remove the sulfur compounds.

A large proportion of heterogeneous catalytic hydrogenation involves the use of molecular hydrogen. Commonly, the hydrogen is added onto the unsaturated bonds of the organic compounds via a π-bond in hydrogenation process, however, the hydrogen

is added via a σ-bond in the hydrogenolysis process. In the catalytic hydrogenation of carbon-carbon bonds over metal catalysts, the Horiuti-Polanyi mechanism [8] is widely regarded as the classical mode of action. An illustration of the Horiuti-Polanyi mechanism is depicted in Scheme 1.1. The unsaturated molecule is adsorbed on the surface atoms of the metal catalyst across π-bond, which ruptures to generate two σ-bonds at the *initial state*. Meanwhile, the molecular hydrogen is dissociatively adsorbed on the surface of the metal and splits into surface hydrogen, which is assumed to scoot around the tops of metal surface atoms [9]. Consequently, the first surface hydrogen bonds to one of the unsaturated carbon atoms with a simultaneous breakage of the same carbon atom from metal surface, called *half-hydrogenated state*. All these steps are reversible, which may account for the observed hydrogen exchange between unsaturated reactant and hydrogen. Nevertheless, at the *final hydrogenated state*, the second surface hydrogen irreversibly bonds on the second carbon atom to produce saturated product, followed by a desorption of product from metal surface.

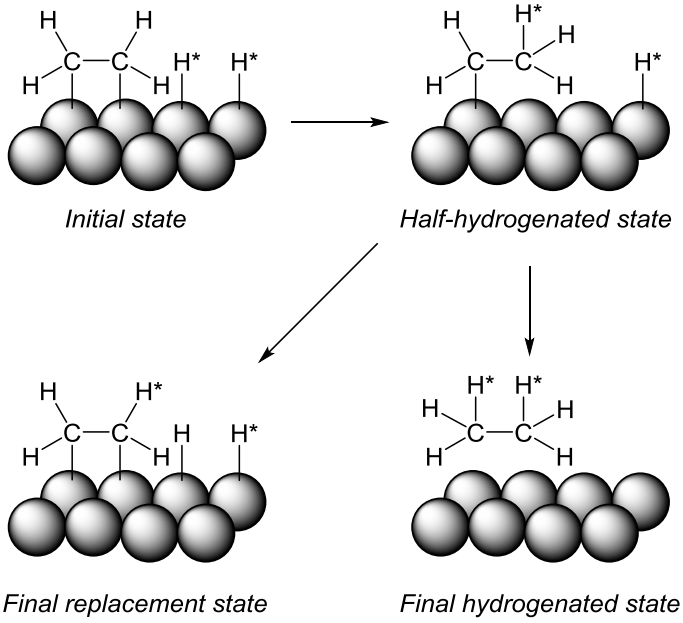

Scheme 1.1 Illustration of the steps in the hydrogenation of C=C double bond on the surface of a metal catalyst (Pt or Ni). The adsorption of reactant on the metal surface is assigned as the initial state, and the addition of hydrogen to the adsorbed carbon atoms involves the half-hydrogenated and final hydrogenated states. The surface hydrogen from the dissociative adsorption of molecular hydrogen (H*) is assumed to be exchangeable with the one from the adsorbed reactant.

Heterogeneous catalysts can be divided into supported catalysts and unsupported catalysts. The active species include metals, alloys, oxides, sulfides, nitrides, carbides, or mixtures of these [3]. To fulfill the multiple requirements for the hydrogenation of each functional group, supported catalysts exhibit distinct advantages such as high dispersion of metal particles over supports, tenacious resistance against sintering under harsh conditions and poisoning, ease separation and recovery [10]. To date, there is evidence for interactions between the active phase and the support [11–17], and the research on this issue is continuously growing. The common materials used as support can be SiO_2, TiO_2, MgO, γ-Al_2O_3, carbon, clays and zeolites et al. [10, 18, 19]. By tuning the morphology of the support, the nanoparticle functionality (catalytic property) can possibly be tailored toward a specific application [20].

1.3 Supported ruthenium nanoparticles

The use of Group VIII metals for catalytic hydrogenations has been unveiled in 1925, when Fischer and Tropsch found that the catalytic reactivity of a series of transition metals for the synthesis of methane from CO and H_2 declines by the order: Ru > Ir > Rh > Os > Pt > Pd [7]. To date, ruthenium catalysts have been proved to be of practical importance in hydrogenation reactions, such as ammonia synthesis [21–23], carbon dioxide methanation [24–27], and hydrogen peroxide synthesis [28]. Besides, a proper support is deeply credited not only for varying the morphology of the metal nanoparticles and further catalytic properties, but also for the addition of support-metal interaction, hydrogen spillover effect, acidity/basicity and sometimes the shape selectivity effects, which are important for practical use.

1.3.1 Ruthenium supported by carbon

Carbon materials have been regarded as a kind of ideal supports (or catalyst) due to its large specific surface area, abundant porosity, excellent stability and rich source

[29–31]. More and more carbon-supported metal catalysts have been and will be discovered for specific reactions. Ruthenium nanoparticles supported by a variety of carbon materials (carbon powder, carbon nanofibers, carbon nanotubes and carbon spheres) for the catalytic hydrogenations are summarized in Figure 1.2. High dispersion and narrow size distribution of ruthenium nanoparticles account for their excellent reactivity and selectivity in the hydrogenation of C=O bond [32, 33], C=C bond [34], N=O bond [35, 36] and C=N bond [37]. Recently, functionalized carbon was shown not only to serve as the catalyst support but to function itself as metal-free catalyst [38, 39].

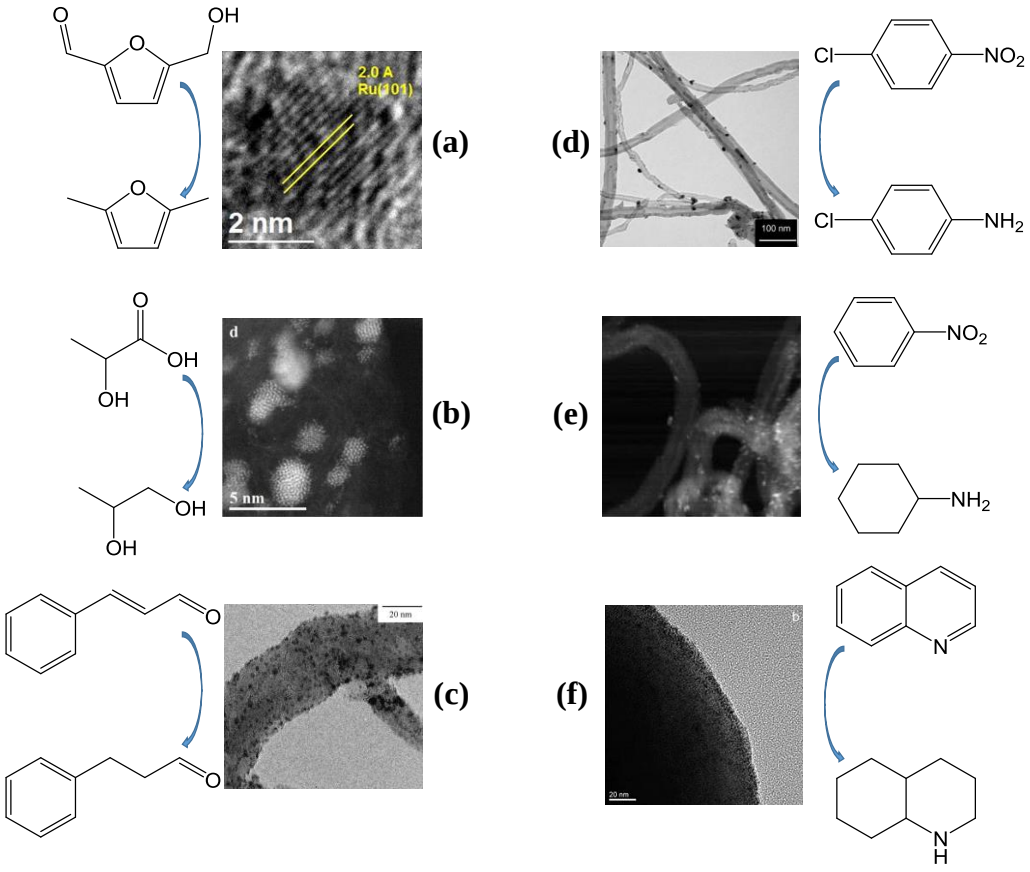

Figure 1.2 Ruthenium nanoparticles supported by various carbon materials for the hydrogenations: (a) Ru supported by carbon for the hydrogenation of hydroxymethylfurfural to dimethylfuran [32]; (b) Ru supported by carbon for the hydrogenation of lactic acid to 1,2-propanediol [33]; (c) Ru supported by carbon nanofiber for the hydrogenation of cinnamaldehyde to hydrocinnamaldehyde [34]; (d) Ru supported by carbon nanotubes for the hydrogenation of *p*-chloronitrobenzene to *p*-chloroaniline [35]; (e) Ru supported by carbon nanotubes for the hydrogenation of nitrobenzene

to cyclohexylamine [36]; (f) Ru supported by glucose-derived carbon spheres for the hydrogenation of quinoline to decahydroquinoline [37]. [34]; (d) Ru supported by carbon nanotubes for the hydrogenation of *p*-chloronitrobenzene to *p*-chloroaniline [35]; (e) Ru supported by carbon nanotubes for the hydrogenation of nitrobenzene to cyclohexylamine [36]; (f) Ru supported by glucose-derived carbon spheres for the hydrogenation of quinoline to decahydroquinoline [37].

1.3.2 Ruthenium supported by oxides

Solid metal oxides and nonmetal oxides are extensively used as supports for a variety of catalysts. Besides the aspects of economics and mechanical strength, the metal-support interaction plays an important role in governing the properties of the catalysts [3, 40]. For the CO hydrogenation process, Ru/γ-Al_2O_3 shows much better reactivity than Ru/SiO_2, which was attributed to the strong metal-support interaction [41]. The migration of O atoms from the alumina lattice to ruthenium clusters causes the partial oxidation of ruthenium [41, 42], which may favor the hydrogen spillover effect [41, 43]. With respect to strong metal-support interaction usually possessing reductive or suppressive effect on the catalytic activities [40, 44], an electronic metal-support interaction is reputed as a beneficial factor for enhancing the catalytic activities [44, 45]. Density functional theory (DFT) calculation on the metal-support interaction between Ru clusters and the TiO_2 surface revealed that electrons transfer from the Ru clusters to the TiO_2 support via the Ru−O bond, which is responsible for the enhanced catalytic activity of Ru clusters [46].

Alkaline earth metal oxides are rich in basic surface oxygen sites, which bear a function as strongly basic sites. For instance, magnesia as a basic catalyst has shown unique properties for several organic reactions [47, 48]. In the selective hydrogenation of quinoline catalyzed by ruthenium nanoparticles supported on magnesia, a combined mechanism of dual-site and dual-pathway was demonstrated by R. A. Sánchez-Delgado et al. [49]. As illustrated in Figure 1.3, during the hydrogenation process, a heterolytic H_2 cleavage into H^+ and H^- occurs over Mg^{2+}−O^{2-} pairs on the MgO surface (site A), while a homolytic H_2 splitting takes place over Mg atoms (site

B) [49, 50]. The *N*-heterocyclic and carbocyclic rings of quinoline were assumed to be hydrogenated, respectively, at sites A via an ionic route to produce 1,2,3,4-tetrahydroquinoline, and sites B via homolytic H_2 splitting to form 5,6,7,8-tetrahydroquinoline [49].

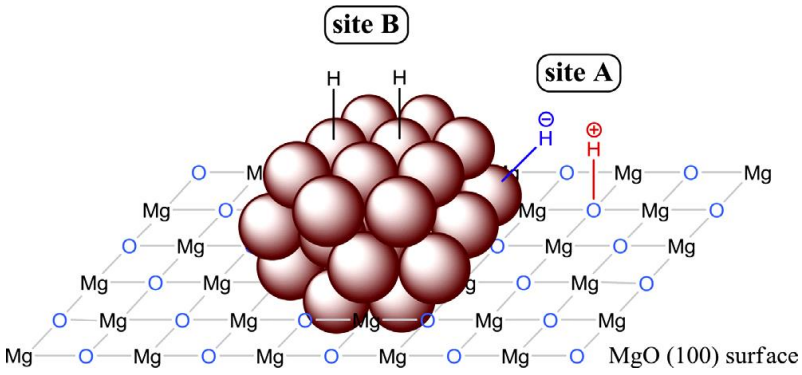

Figure 1.3 Illustration of the proposed dual-site structure on Ru/MgO catalyst. A heterolytic H_2 dissociation into H^+ and H^- occurs over Mg^{2+}–O^{2-} pairs on the MgO surface (site A) while a homolytic H_2 splitting takes place over Mg atoms (site B) [49, 50].

Zeolites are microporous crystalline aluminosilicates with three dimensional channels. Benefiting from their complex porous channels and flexible pore diameters, zeolites are widely used in separation systems including ion exchange and adsorption [51]. In fact, zeolites in their protonated form constitute a series of important industrial catalysts, the key point of which is their acidity [52−55]. Considering the structural features and acidic properties, zeolite-supported metal catalysts have been extensively explored for a variety of reactions [56, 57]. Ruthenium nanoclusters embedded in FAU-type zeolite were highlighted by their superior reactivity and stability in the catalytic hydrogenation of neat benzene and methyl substituted aromatics [58]. The cavities of zeolite greatly enhance the stability of ruthenium nanoclusters from agglomeration, giving rise to the observed resistance against lose in activity and catalytic lifetime [58]. Apart from the constraint effect of the zeolite, the acidity plays an important role in affecting the intrinsic activity of the zeolite supported catalysts in catalytic reactions. Ruthenium nanoparticles supported by zeolite Y were found to

catalyze the hydrogenation of xylose to xylitol, the weak acid sites of high silica HY directing the high selectivity to the targeted product [59]. The same effect was also observed in the hydrogenation of D-glucose to D-sorbitol [60] and of levulinic acid to pentanoic acid [61] over ruthenium nanoparticles supported by HY zeolite. Furthermore, hierarchical micro-mesoporous zeolite, known as a shape-selective catalyst in fluid catalytic cracking process [62], makes full use of these advantages to reach a diverse function. In the Fischer-Tropsch process, mesoporous zeolite-supported ruthenium nanoparticles show superior selectivity to C_5−C_{11} hydrocarbons as compared to microporous zeolite support; the interpretation involves generated mesopores and weak acidity of zeolite with suppressing effects on the consecutive cracking [63, 64].

1.3.3 Ruthenium supported by polymers

Polymers with various functional groups are widely used as supports for organic catalysts and for metallic nanoparticles [65−68]. As it is well known, polar ligands growing in the polymer strongly stabilize metallic nanoparticles and suppress the growth of nanoparticles. Ruthenium nanoparticles supported by poly(styrene-co-divinylbenzene)amine functionalized polymer have an average particle size of 2.5 nm with a homogeneous distribution [69]. This catalyst is highly active for the hydrogenation of xylose to xylitol [69]. By contrast, a dimethylacrylamide potassium 1-methacryloyl ethylene 2-sulphonate-methylene bis(acrylamide) resin (M4KR4) [70] and a hydroxylterminated poly(amidoamine) (PAMAM-OH) dendrimer [71] as hydrophilic supports for ruthenium nanoparticles show a better reactivity than hydrophobic supports for the hydrogenation of benzene and 4-nitrophenol in water. Furthermore, a water-compatible three-dimensional β-cyclodextrin polymer crosslinked with citric acid (poly(CTR-β-CD)) as support for ruthenium nanoparticles additionally constructs individual globular chambers as “microreactors” for the catalytic hydrogenation of biomass-derived furanic compounds [72]. As illustrated in Figure 1.4, β-cyclodextrin

is a torus-shaped cyclic oligosaccharide consisted of seven α-D-glucopyranose units to form a regular cavity. The fabrication of cyclodextrin polymers across the hydroxyl groups develops interconnected nanoporosity, in which the hydrogenation proceeds [72].

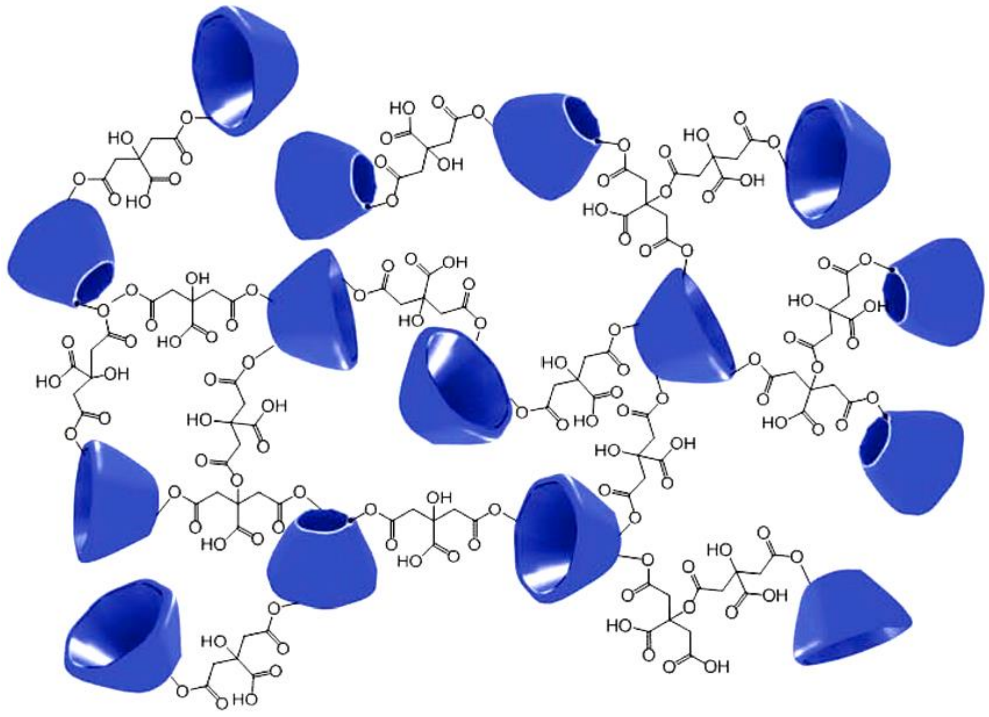

Figure 1.4 Illustration of the two-dimensional structure of the poly(CTR-β-CD) polymer [72].

Despite all the features of the polymers mentioned above, poly(4-vinylpyridine) (PVPy) acts not only as polar ligands for immobilizing the nanoparticles, but as active sites for splitting the molecular hydrogen in the hydrogenation reactions [73]. As depicted in Figure 1.5, the selective hydrogenation of quinoline catalyzed by ruthenium nanoparticles supported on poly(4-vinylpyridine) is thought to proceed with dual-path and dual-sites mechanism, similar to that with Ru/MgO as catalyst [49]. A heterolytic H_2 splitting into H^+ and H^- between support and ruthenium nano-particles, followed by ionic hydrogenation of the polar *N*-heteroaromatic (path a) at Type A sites, while at Type B sites a homolytic hydrogen splitting (path b) is involved

for the hydrogenation of non-polar aromatics [73].

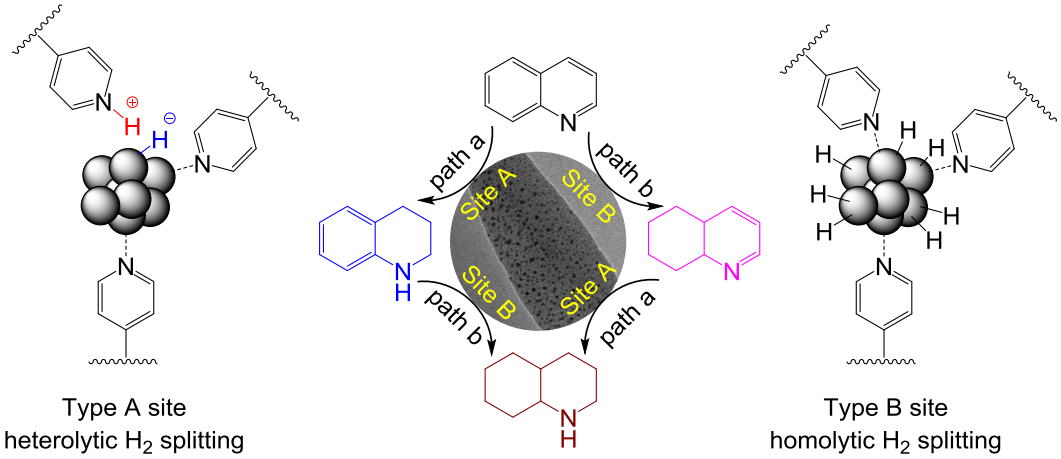

Figure 1.5 Schematic demonstration of the mechanism involved in the hydrogenation of quinoline catalyzed by ruthenium nanoparticles supported on poly(4-vinylpyridine) [73].

1.3.4 Ruthenium supported by clays

Clay minerals are a class of natural abundant materials with diverse porosity. They have been explored for adsorbents, catalysts, and catalyst supports through decades [74, 75]. There are several reviews summarizing the applications of clay-supported catalysts in fine chemical synthesis [76–79]. Smectites, as a representative class of minerals, are well-known for their swelling interlayers, the changeable inter-laminar distance making it a unique platform for the intercalation of metal ions and metal nanoparticles [80]. The most studied smectite clays are montmorillonite and hectorite. In the catalytic hydrogenation process, Pt [81], Rh [82], and Ni [83] nano-particles supported on montmorillonite have been proven to be highly efficient. Mesoporous montmorillonite, post-modified by hydrochloric acid, is suggested to be an improved support for ruthenium nanoparticles, showing a high reactivity in the transfer hydrogenation of substituted nitrobenzenes to the corresponding anilines [84]. Remarkably, ruthenium nanoparticle-intercalated montmorillonite is able to catalyzing the solvent-free alkene hydrogenation reaction with high reactivity and recyclability

[85]. Another supported Ru catalyst by using cetyltrimethylammonium bromide (CTAB)-modified montmorillonite as support exhibits high activity and selectivity in the hydrogenation of quinoline, the modification being responsible for the robust stability of ruthenium nanoparticles [86]. Hectorite has also shown its potential to be a promising support for metal catalysts. Ruthenium nanoparticles intercalated in hectorite bear a superior activity and selectivity in the selective hydrogenation of benzene [87, 88], toluene [88], alkylsubstituted benzenes [89], furfuryl alcohol [90] and α,β-unsaturated ketones to their corresponding saturated products [91].

1.4 Scope and outline

The aim of this thesis is to achieve a controlled synthesis of ruthenium nanoparticles intercalated in hectorite, and to explore their potential as a promising hydrogenation catalyst. Through the optimization over each kind of hydrogenation reactions, the knowledge of the mechanistic understanding is to be enhanced.

This thesis is mainly organized in six chapters. In this chapter, the history and the basic concepts of catalysis are briefly introduced. Specifically, an overview of heterogeneous catalytic hydrogenation is given including the general mechanism of hydrogenation over metal catalysts. Supported ruthenium nanoparticles as catalyst in the hydrogenation are summarized with a kernel on the importance of support. The most common materials used as support, from the organic compounds to inorganic compounds, are concisely discussed, involving the influence of support on the physical and chemical properties of the ruthenium nanoparticles and on the product distribution.

Chapter 2 describes the synthesis and characterization of the ruthenium nanoparticles intercalated in hectorite. The synthetic methods deal with an introduction of organometallic ruthenium complexes and of ruthenium cations into hectorite. The ruthenium catalysts (or precursors) are characterized with various spectroscopic techniques. Chapter 3 describes the catalytic performance of hectorite-supported

ruthenium nanoparticles for the hydrogenation of quinoline. The effect of reaction parameters are discussed and optimized. The role of the solvents, the interpretation of the observed product distribution, and the recyclability of the catalyst are thoroughly discussed. Chapter 4 involves the hydrogenation of quinoline with $NaBH_4$ catalyzed by hectorite-supported ruthenium catalyst in water. With optimized conditions, the scope of a variety of substrates is determined. The role of the water in the transfer hydrogenation is also discussed. Isotope labelling experiments combined with semi-empirical calculations of the electrostatic potentials are employed to go insight into the reaction pathway. The recyclability of the catalyst is also mentioned. Chapter 5 studies the catalytic properties of hectorite-supported ruthenium catalyst for the hydrogenation of aromatic amino acids. Aqueous media with varied pH value are employed to carry out the hydrogenation. The influence of the pH value is discussed as well as the catalyst recyclability. The overall conclusions and perspectives are addressed in Chapter 6, followed by the experimental part and supplementary information.

References

[1] J. M. Thomas, W. J. Thomas, *Principles and Practice of Heterogeneous Catalysis, Second, Revised Edition*, Wiley-VCH, 2015.

[2] *Global Catalyst Market, Third Edition*, Acmite Market Intelligence, 2015.

[3] A. W. Sleight, Science 208 (1980) 895–900.

[4] E. Fulhame, *An Essay On Combustion with a View to a New Art of Dying and Painting, wherein the Phlogistic and Antiphlogistic Hypotheses are Proved Erroneous*, Published by the author, London, 1794.

[5] J. J. Berzelius, *Årsberättelsen om framsteg i fysik och kemi*, Royal Swedish Academy of Sciences, Stockholm, Sweden, 1835.

[6] W. Ostwald, Zeitschrift für physikalische Chemie 15 (1894) 705–706.

[7] I. Horiuti, M. Polanyi, Transactions of the Faraday Society 30 (1934) 1164–1172.

[8] F. Fischer, H. Tropsch, P. Dithey, Brennstoff-Chem. 6 (1925) 265–271.

[9] G. V. Smith, F. Notheisz, *Heterogeneous Catalysis in Organic Chemistry*, Elsevier, 2000.

[10] A. D. O. Cinneide, J. K. A. Clarke, Catal. Rev. 7 (1972) 213–232.

[11] L. M. Falicov, G. A. Somorjai, Proc. Natl. Acad. Sci. 82 (1985) 2207–2211.

[12] S. J. Tauster, Acc. Chem. Res. 20 (1987) 389–394.

[13] D. W. Goodman, Chem. Rev. 95 (1995) 523–536.

[14] B. Coq, F. Figueras, Coord. Chem. Rev. 178–180 (1998) 1753–1783.

[15] S. M. McClure, M. J. Lundwall, D. W. Goodman, Proc. Natl. Acad. Sci. 108 (2011) 931–936.

[16] A. Bruix, J. A. Rodriguez, P. J. Ramírez, S. D. Senanayake, J. Evans, J. B. Park, D. Stacchiola, P. Liu, J. Hrbek, F. Illas, J. Am. Chem. Soc. 134 (2012) 8968–8974.

[17] R. Schlögl, Angew. Chem. Int. Ed. 54 (2015) 3465–3520.

[18] P. Rylander, *Catalytic Hydrogenation over Platinum Metals*, Academic Press, 1967.

[19] P. Rylander, *Catalytic Hydrogenation in Organic Syntheses*, Academic Press, 1979.

[20] C. M. Yim, C. L. Pang, D. R. Hermoso, C. M. Dover, C. A. Muryn, F. Maccherozzi, S. S. Dhesi, R. Pérez, G. Thornton, Proc. Natl. Acad. Sci. 112 (2015) 7903–7908.

[21] T. Lopez, P. Bosch, R. Gomez, React. Kinet. Catal. Lett. 41 (1990) 217–221.

[22] S. Murata, K. Aika, J. Catal. 136 (1992) 118–125.

[23] Y. Kadowaki, K. Aika, J. Catal. 161 (1996) 178–185.

[24] P. J. Lunde, F. L. Kester, Ind. Eng. Chem. Process Des. Dev. 13 (1974) 27–33.

[25] L. T. Luo, S. J. Li, J. Nat. Gas Chem. 13 (2004) 45–48.

[26] Z. Kowalczyk, K. Stołecki, W. Raróg-Pilecka, E. Miśkiewicz, E. Wilczkowska, Z. Karpiński, Appl. Catal. A: General 342 (2008) 35–39.

[27] S. Tada, O. J. Ochieng, R. Kikuchi, T. Haneda, H. Kameyama, Int. J. Hydrogen Energy 39 (2004) 10090–10100.

[28] E. N. Ntainjua, S. J. Freakley, G. J. Hutchings, Top Catal. 55 (2012) 718–722.

[29] H. Jüntgen, Fuel 65 (1986) 1436–1446.

[30] E. Lam, J. H. T. Luong, ACS Catal. 4 (2014) 3393–3410.

[31] F, Yang, D. H. Deng, X. L. Pan, Q. Fu, X. H. Bao. Natl. Sci. Rev. 2 (2015) 183–201.

[32] J. Jae, W. Q. Zheng, R. F. Lobo, D. G. Vlachos, ChemSusChem 6 (2013) 1158–1162.

[33] S. Iqbal, S. A. Kondrat, D. R. Jones, D. C. Schoenmakers, J. K. Edwards, L. Lu, B. R. Yeo, P. P. Wells, E. K. Gibson, D. J. Morgan, C. J. Kiely, G. J. Hutchings, ACS Catal. 5 (2015) 5047−5059.

[34] M. L. Toebes, F. F. Prinsloo, J. H. Bitter, A. J. van Dillen, K. P. de Jong, J. Catal. 214 (2003) 78–87.

[35] M. Oubenali, G. Vanucci, B. Machado, M. Kacimi, M. Ziyad, J. Faria, A. Raspolli-Galetti, P. Serp, ChemSusChem 4 (2011) 950–956.

[36] P. Tomkins, E. Gebauer-Henke, W. Leitner, T. E. Müller, ACS Catal. 5 (2015) 203−209.

[37] D. M. Zhu, H. B. Jiang, L. Zhang, X. L. Zheng, H. Y. Fu, M. L. Yuan, H. Chen, R. X. Li, ChemCatChem 6 (2014) 2954–2960.

[38] D. S. Su, S. Perathoner, G. Centi, Chem. Rev. 113 (2013) 5782–5816.

[39] L. Liu, Y. P. Zhu, M. Su, Z. Y. Yuan, ChemCatChem 7 (2015) 2765–2787.

[40] S. J. Tauster, Acc. Chem. Res. 20 (1987) 389–394.

[41] M. G. Cattania, F. Parmigiani, V. Ragaini, Surf. Sci. 211–212 (1989) 1097–1105.

[42] C. Elmasides, D. I. Kondarides, W. Grünert, X. E. Verykios, J. Phys. Chem. B 103 (1999) 5227–5239.

[43] W. C. Conner, J. L. Falconer, Chem. Rev. 95 (1995) 759–788.

[44] G. Pacchioni, Phys. Chem. Chem. Phys. 15 (2013) 1737–1757.

[45] C. T. Campbell, Nature Chem. 4 (2012) 597–598.

[46] S. T. Zhang, C. M. Li, H. Yan, M. Wei, D. G. Evans, X. Duan, J. Phys. Chem. C 118 (2014) 3514−3522.

[47] S. Ardizzone, C. L. Bianchi, B. Vercelli, Appl. Surf. Sci. 126 (1998) 169–175.

[48] S. Ardizzone, C.L. Bianchi, B. Vercelli, Colloid Surf. A – Physicochem. Eng. Asp. 144 (1998) 9–17.

[49] M. F. Fang, R. A. Sánchez-Delgado, J. Catal. 311 (2014) 357–368.

[50] G. C. Bond, *Catalysis by Metals*, Academic Press, New York, 1962.

[51] C. S. Cundy, P. A. Cox, Chem. Rev. 103 (2003) 663–701.

[52] W. O. Haag, R. M. Lago, P. B. Weisz, Nature, 309 (1984) 589–591.

[53] G. J. Kramer, R. A. van Santen, C. A. Emeis, A. K. Nowak, Nature, 363 (1993) 529–531.

[54] A. Corma, Chem. Rev. 95 (1995) 559–614.

[55] R. A. van Santen, G. J. Kramer, Chem. Rev. 95 (1995) 637–660.

[56] W. M. H. Sachtler, Catal. Today 15 (1992) 419–429.

[57] W. M. H. Sachtler, Z. C. Zhang, Adv. Catal. 39 (1993) 129–220.

[58] M. Zahmakıran, Y. Tonbul, S. Özkar, J. Am. Chem. Soc. 132 (2010) 6541–6549.

[59] D. K. Mishra, A. A. Dabbawala, J. S. Hwang, J. Mol. Catal. A: Chem. 376 (2013) 63–70.

[60] D. K. Mishra, A. A. Dabbawala, J. J. Park, S. H. Jhung, J. S. Hwang, Catal. Today 232 (2014) 99–107.

[61] W. H. Luo, U. Deka, A. M. Beale, E. R. H. van Eck, P. C. A. Bruijnincx, B. M. Weckhuysen, J. Catal. 301 (2013) 175–186.

[62] F. G. Dwyer, T. F. Degnan, Stud. Surf. Sci. Catal. 76 (1993) 499–530.

[63] J. C. Kang, K. Cheng, L. Zhang, Q. H. Zhang, J. S. Ding, W. Q. Hua, Y. C. Lou, Q. G. Zhai, Y. Wang, Angew. Chem. Int. Ed. 50 (2011) 5200–5203.

[64] K. Cheng, J. C. Kang, S. W. Huang, Z. Y. You, Q. H. Zhang, J. S. Ding, W. Q. Hua, Y. C. Lou, W. P. Deng, Y. Wang, ACS Catal. 2 (2012) 441−449.

[65] M. Benaglia, A. Puglisi, F. Cozzi, Chem. Rev. 103 (2003) 3401–3430.

[66] M. Králik, B. Corain, M. Zecca, Chem. Papers 54 (2000) 254–264.

[67] H. Mao, C. Chen, X. P. Liao, B. Shi, J. Mol. Catal. A: Chem. 341 (2011) 51–56.

[68] H. Mao, J. Ma, Y. Liao, S. L. Zhao, X. P. Liao, Catal. Sci. Technol. 3 (2013) 1612–1617.

[69] D. K. Mishra, A. A. Dabbawala, J. S. Hwang, Catal. Commun. 41 (2013) 52–55.

[70] M. Hronec, Z. Cvengrošová, M. Králik, G. Palma, B. Corain, J. Mol. Catal. A: Chem. 105 (1996) 25–30.

[71] N. C. Antonels, R. Meijboom, Langmuir 29 (2013) 13433−13442.

[72] R. Herbois, S. Noël, B. Léger, S. Tilloy, S. Menuel, A. Addad, B. Martel, A. Ponchel, E. Monflier, Green Chem. 17 (2015) 2444–2454.

[73] M. F. Fang, N. Machalaba, R. A. Sánchez-Delgado, Dalton Trans. 40 (2011) 10621–10632.

[74] J. H. Clark, C. N. Rhodes, *Clean Synthesis Using Porous Inorganic Solid Catalysts and Supported Reagents*, RSC, Cambridge, 2000.

[75] A. Gil, S. A. Korili, R. Trujillano, M. A. Vicente, *Pillared Clays and Related Catalysts*, Springer, New York, 2010.

[76] F. Figueras, Catal. Rev. 30 (1988) 457–499.

[77] R. S. Varma, Tetrahedron 58 (2002) 1235–1255.

[78] G. Nagendrappa, Appl. Clay Sci. 53 (2011) 106–138.

[79] D. K. Dutta, B. J. Borah, P. P. Sarmah, Catal. Rev. 57 (2015) 257–305.

[80] T. J. Pinnavaia, Science 220 (1983) 365–371.

[81] J. X. Pan, J. Liu, S. P. Guo, Z. Y. Yang, Catal. Lett. 131 (2009) 179–183.

[82] P. P. Sarmah, D. K. Dutta, Appl. Catal. A Gen. 470 (2014) 355–360.

[83] D. Dutta, D. K. Dutta, Appl. Catal. A Gen. 487 (2014) 158–164.

[84] P. P. Sarmah, D. K. Dutta, Green Chem. 14 (2012) 1086–1093.

[85] P. Upadhyay, V. Srivastava, RSC Adv. 5 (2015) 740–745.

[86] L. M. Zhou, X. L. Qi, X. H. Jiang, Y. F. Zhou, H. Y. Fu, H. Chen, J. Colloid Interface Sci. 392 (2013) 201–205.

[87] G. Süss-Fink, F. A. Khan, J. Boudon, V. Spassov, J. Cluster Sci. 20 (2009) 341–353.

[88] G. Süss-Fink, B. Mollwitz, B. Therrien, M. Dadras, G. Laurenczy, A. Meister, G. Meister, J. Cluster Sci. 18 (2007) 87–95.

[89] A. Meister, G. Meister, G. Süss-Fink, J. Mol. Catal. 92 (1994) L123–L126.

[90] F. A. Khan, A. Vallat, G. Süss-Fink, Catal. Commun. 12 (2011) 1428–1431.

[91] F. A. Khan, A. Vallat, G. Süss-Fink, J. Mol. Catal. A: Chem. 355 (2012) 168–173.

2

Preparation of ruthenium nanoparticles intercalated in hectorite

2.1 State of the art

2.1.1 General description of hectorite materials

Hectorite is a natural mineral featured by smectite structure [1]. Its name "hectorite" originates from a locality at Hector, CA, USA [2]. Pure hectorite often requires a synthetic method, since natural hectorite is often contaminated by bentonite minerals [1]. Synthetic sodium hectorite is a white solid presenting an idealized cell formula of $Mg_{5.5}Li_{0.5}Si_8O_{20}(OH)_4Na \cdot n\ H_2O$. It has a three-layer sheet-like morphology resulted from the two dimensional condensation of silicic acids, two layers of SiO_4 tetrahedra being bridged by a layer of MgO_6 octahedra. Usually, a partial replacement of the Mg^{2+} cations in the octahedral layers by Li^+ cations leads to an excess of anionic charges of the layers, which are compensated by Na^+ cations in the interlaminar space (Figure 2.1).

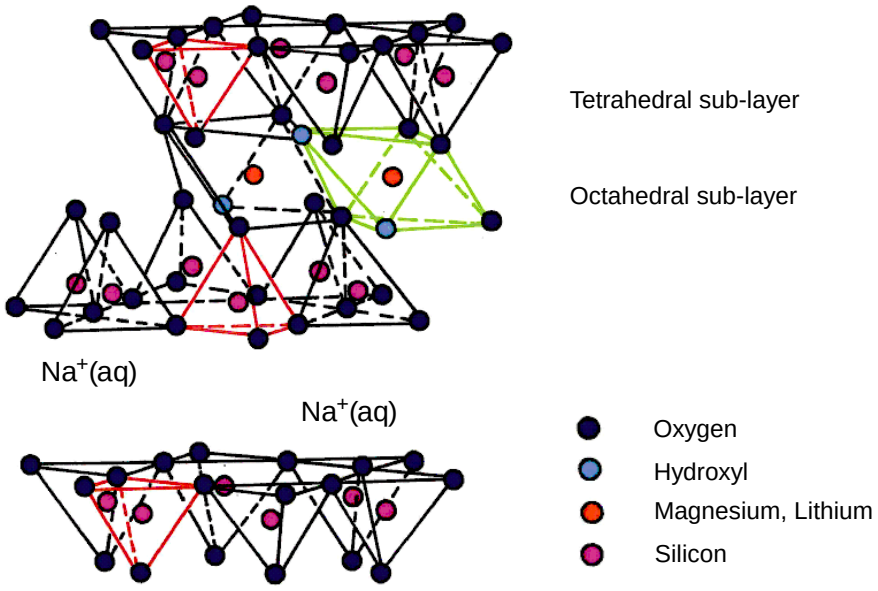

Figure 2.1 Schematic structural model of the synthetic sodium hectorite [4], showing the anionic three-layer sheets and the interlaminar space containing sodium cations.

The sodium-containing hectorite is specifically susceptible to swelling by water [3]. Hydration of the interlaminar Na^+ cations forms $[Na(H_2O)_n]^+$ with a certain osmotic pressure [3], which is responsible for the swelling of interlayers in hectorite when immersed in water, the interlaminar space being to be widened [4].

Noticeably, magnesium and lithium cations locate in the octahedral layer, i.e., the framework of hectorite, however, the sodium cations in the interlaminar space are not bound to the silicate framework. The free sodium cations afford ion-exchange sites for water soluble inorganic, organic or organometallic cations [5].

2.1.2 Intercalation of ruthenium in hectorite

The preparation of highly dispersed metal nanoparticles on a support has attracted much attention [6–8]. The introduction of metal ions as catalyst precursor to a support often relates to a synthetic methodology, which requires a proper transformation of the metal ions to an accessible form [9–11]. The first successful intercalation of ruthenium in hectorite using $[Ru(NH_3)_6]Cl_3$ as a catalyst precursor was reported by T. Uematsu *et al.* [12]. The synthesized precatalyst was reduced under a H_2 atmosphere to obtain a Ru^0/hectorite catalyst, which shows high selectivity for the hydrogenation of olefins [12]. G. Süss-Fink and his co-workers disclosed a synthetic method by using water-soluble organometallic cations such as $[(C_6H_6)Ru(H_2O)_3]^{2+}$ as precursors for the catalyst preparation [13–17]. The ruthenium(II)-containing hectorite precatalyst obtained was then reduced in a variety of solvents under different conditions, generating hectorite-intercalated ruthenium nanoparticles with mean particle size ranging from 3 nm to 20 nm [13–17]. The thus synthesized catalyst shows excellent activity and selectivity in the hydrogenation of benzene [15], toluene [14], alkyl-substituted benzene [13], furfuryl alcohol [16] and α,β-unsaturated ketones [17].

2.2 Results and discussion

2.2.1 Ruthenium nanoparticles derived from benzene ruthenium complexes

The dinuclear complex benzene ruthenium dichloride dimer was synthesized according to the procedure reported by T. Arthur and T. A. Stephenson [18]. The dissolution of the ruthenium dimer in water causes hydrolysis to give, with reversible substitution of chloro ligands by aqua ligands, a mixture of mononuclear benzene ruthenium complexes being in equilibrium [5], as depicted in Scheme 2.1. The ^{1}H NMR signals of benzene in D_2O solution are assigned to $[(C_6H_6)RuCl_2(H_2O)]$ (δ = 5.89 ppm), $[(C_6H_6)RuCl(H_2O)_2]^+$ (δ = 5.97 ppm), and $[(C_6H_6)Ru(H_2O)_3]^{2+}$ (δ = 6.06 ppm) [5, 19]. The dicationic triaqua complex $[(C_6H_6)Ru(H_2O)_3]^{2+}$, isolated as sulfate and fully characterized [20], is the main species in the hydrolytic mixture at pH = 8 based on NMR results.

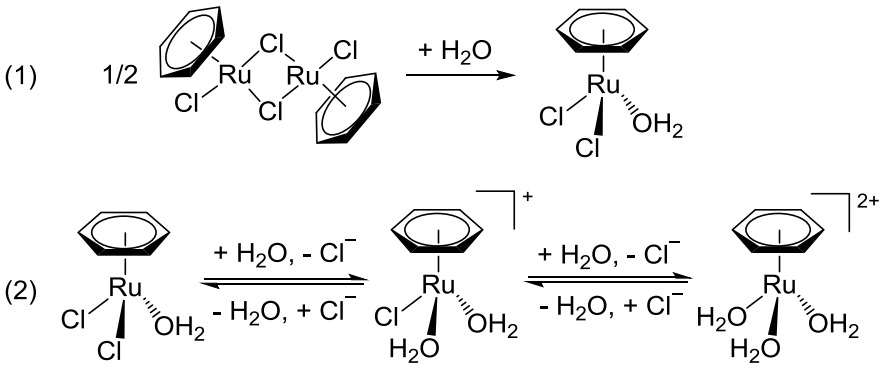

Scheme 2.1 Hydrolysis of the dinuclear ruthenium complex $[(C_6H_6)RuCl_2]_2$ in H_2O to produce a mixture of mononuclear benzene ruthenium complexes.

The intercalation of ruthenium in hectorite is accomplished via ion exchange by mixing the white sodium hectorite with a solution derived from the hydrolysis of the dinuclear ruthenium complex $[(C_6H_6)RuCl_2]_2$ in H_2O. As shown in Figure 2.2, the X-ray diffraction (XRD) patterns of the parent sodium hectorite and the obtained yellow ruthenium(II)-modified hectorite (Ru(II)@hectorite) differ in the d-spacing

(d_{001}) of the interlayers, which are 13.4 Å and 14.6 Å, respectively. The swollen interlayer space refers to the interaction between the adsorbed ruthenium complexes and the intercalant in hectorite [3]. The thus-synthesized Ru(II)@hectorite is very stable in air and can be stored in an open system.

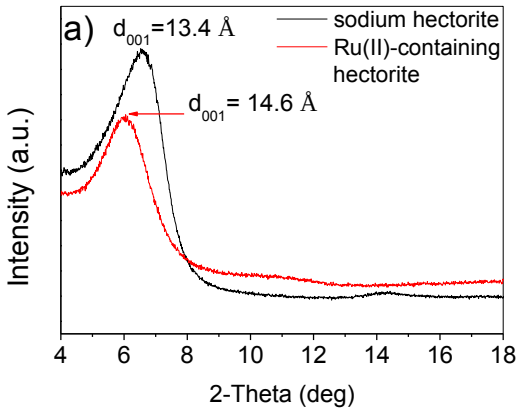

Figure 2.2 XRD patterns of the sodium-containing hectorite and ruthenium(II)-containing hectorite in a scan range of 4–18°. The calculated d-spacing (d_{001}) of Na-hectorite and Ru(II)-containing hectorite are 13.4 Å and 14.6 Å, respectively.

The precatalyst Ru(II)@hectorite suspended in an appropriate solvent can be reduced by molecular hydrogen to give an active *nano*Ru@hectorite catalyst as an air-sensitive black powder. The properties of the solvents are considered to be of great importance in tuning the morphology of the nanoparticles during the reduction process [22–24]. As shown in Figure 2.3 [15], the ruthenium nanoparticles with a hexagonal morphology are obtained in water, the mean particles size being 34.2 nm in a wide distribution (σ = 7.4 nm). A mixture of water and methanol (1:1) as solvent can greatly reduce the mean particles size to 14.9 nm (σ = 1.4 nm) with retaining the hexagonal morphology. However, pure methanol alters the shape of the nanoparticles to spherical with a mean particle size of 7.1 nm (σ = 1.2 nm), which implies that water is essential for the formation of hexagons in hectorite [15]. By contrast, in organic solvents, the ruthenium nanoparticles are always more or less spherical, the mean particle sizes being below 10 nm (Figure 2.3, c, d, e, f). In general, organic solvents

are in favor of the formation of small nanoparticles.

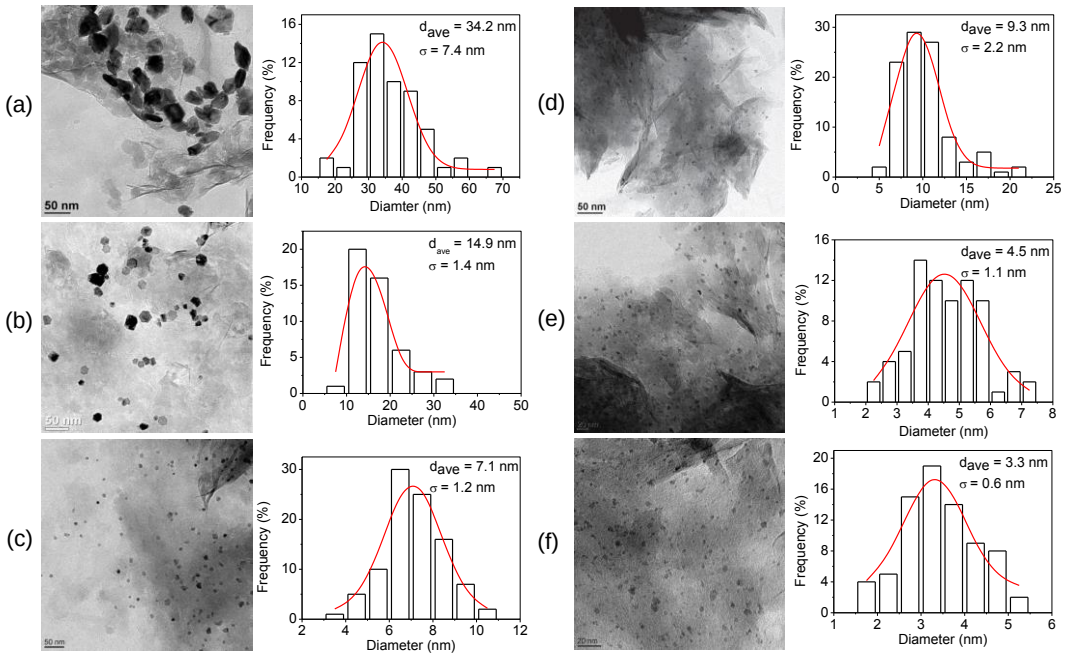

Figure 2.3 TEM images of the hectorite-intercalated ruthenium nanoparticles reduced from ruthenium(II)-containing hectorite precatalyst under a H_2 pressure of 50 bar for 14 h in the solvents (a) water, (b) water/methanol (1:1), (c) methanol, (d) ethanol, (e) isopropanol and (f) 2-butanol [15]. The calculated mean particle size (d_{ave}) are 34.2 ± 7.4 nm, 14.9 ± 1.4 nm, 7.1 ± 1.2 nm, 9.3 ± 2.2 nm, 4.5 ± 1.1 nm and 3.3 ± 0.6 nm, respectively.

2.2.2 Ruthenium nanoparticles reduced from ruthenium(III) ions

Instead of using organometallic ruthenium complexes as precursor, a more general method to prepare supported ruthenium nanoparticles is the immobilization of Werner-type ruthenium(III) ions from $RuCl_3 \cdot xH_2O$ on the support and the subsequent reduction by $NaBH_4$ or molecular H_2. According to the practical requirements for certain reactions, a hectorite-supported ruthenium(III) precatalyst (Ru(III)@hectorite) is prepared by the impregnation method with $RuCl_3 \cdot xH_2O$ in water. As illustrated in Figure 2.4, the interlayer spacing (d_{001}) of the sodium hectorite and Ru(III)@hectorite are calculated from X-ray diffraction patterns to be 13.4 Å and

15.2 Å, respectively. The swollen interlayer distance is attributed to the presence of $[Ru(H_2O)_6]^{3+}$ cations.

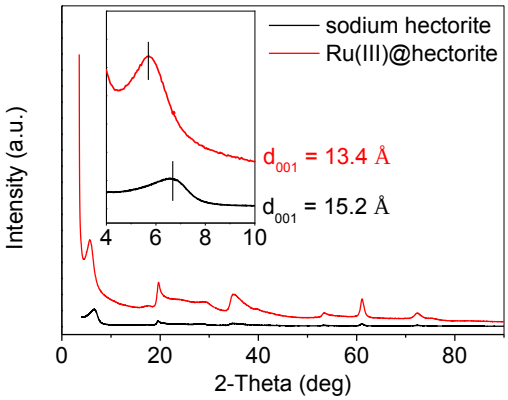

Figure 2.4 XRD patterns of the sodium hectorite and the ruthenium(III)-containing hectorite precatalyst (Ru(III)@hectorite), of which the interlayer spacing (d_{001}) are 13.4 Å and 15.2 Å, respectively. The inset is the zoomed patterns in a scan range of 4–10°.

The reduction of the ruthenium(III)-containing hectorite can be carried out in water under a H_2 atmosphere at elevated temperature or by a reducing agent such as $NaBH_4$. Figure 2.5 shows the characterization results involving the TEM and XRD analysis. The reaction of Ru(III)@hectorite with $NaBH_4$ in water at room temperature yields the ruthenium nanoparticles that are clustered and thoroughly embedded in hectorite with a worm-like morphology, similar to that of the ruthenium nanoparticles intercalated in montmorillonite modified by cetyltrimethylammonium bromide (CTAB) [25]. The mean particle size is calculated to be 4.5 nm (σ = 1.7 nm), which accounts for the observed peak of Ru(011) in X-ray diffraction pattern.

2.3 Conclusions

With respect to the preparation methodology of ruthenium nanoparticles intercalated in hectorite, considerations involving the preparation of the catalyst precursor and the catalyst activation process are essential. Organometallic ruthenium complexes

and classical ionic ruthenium complexes can be successfully intercalated in hectorite via ion-exchange, resulting in stable catalyst precursors. All the samples were examined by X-ray diffraction.

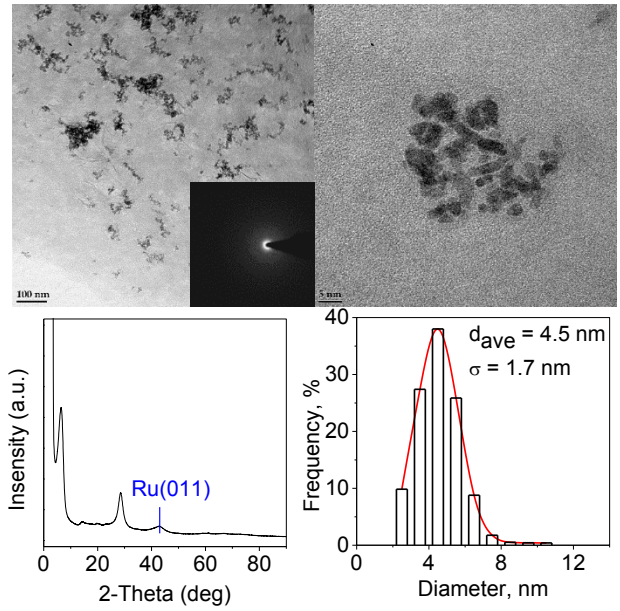

Figure 2.5 TEM and XRD analysis of the hectorite supported ruthenium nanoparticles reduced by $NaBH_4$ in water at room temperature for 4 h. The visible Ru(011) peak in XRD pattern proves the presence of ruthenium nanoparticles. The mean particles size is calculated to be 4.5±1.7 nm.

Depending on the nature of solvent, the reducing agent and reduction conditions, ruthenium nanoparticles with a variety of shapes and sizes are produced. TEM images show that an organic solvent is in favor of generating small nanoparticles, however, the presence of water encourages the formation of hexagonal nanoparticles. Most conveniently, a ruthenium(III)-containing hectorite can be prepared by impregnation of sodium hectorite with an aqueous solution of $RuCl_3 \cdot xH_2O$. Reduced by $NaBH_4$, ruthenium nanoparticles with a worm-like morphology intercalated in hectorite are obtained. The reactivity and selectivity of these ruthenium catalysts will be discussed in the following chapters.

References

[1] A. Gil, S. A. Korili, R. Trujillano, M. A. Vicente, *Pillared Clays and Related Catalysts*, Springer, New York, 2010.

[2] W. F. Foshag, A. O. Woodford, Am. Miner. 21 (1936) 238–244.

[3] T. J. Pinnavaia, Science 220 (1983) 365–371.

[4] R. E. Grim, *Clay Mineralogy 4. Structure of Clay Minerals*, *Smectide Minerals*, McGraw-Hill, USA, 1968.

[5] G. Süss-Fink, F. A. Khan, J. Boudon, V. Spassov, J. Cluster Sci. 20 (2009) 341–353.

[6] L. Jiao, J. R. Regalbuto, J. Catal. 260 (2008) 329–341.

[7] M. S. Hegde, G. Madras, K. C. Patil, Acc. Chem. Res. 42 (2009) 704–712.

[8] M. Flytzani-Stephanopoulos, B. C. Gates, Annu. Rev. Chem. Biomol. Eng. 3 (2012) 545–574.

[9] T. J. Pinnavaia, P. K. Welty, J. Am. Chem. Soc. 97 (1975) 3819–3820.

[10] T. J. Pinnavaia, M. Rameswaran, E. D. Dimotakis, E. P. Giannelis, E. G. Rightor, Faraday Discuss. Chem. Soc. 87 (1989) 227–237.

[11] S. G. Peng, X. J. Fan, J. Zhang, F. Y. Wang, Appl. Catal. B: Environ. 140–141 (2013) 115–124.

[12] S. Shimazu, T. Hirano, T. Uematsu, Appl. Catal. 34 (1987) 255–261.

[13] A. Meister, G. Meister, G. Süss-Fink, J. Mol. Catal. 92 (1994) L123–L126.

[14] G. Süss-Fink, B. Mollwitz, B. Therrien, M. Dadras, G. Laurenczy, A. Meister, G. Meister, J. Cluster Sci. 18 (2007) 87–95.

[15] G. Süss-Fink, F. A. Khan, J. Boudon, V. Spassov, J. Cluster Sci. 20 (2009) 341–353.

[16] F. A. Khan, A. Vallat, G. Süss-Fink, Catal. Comm. 12 (2011), 1428–1431.

[17] F. A. Khan, A. Vallat, G. Süss-Fink, J. Mol. Catal. A: Chem. 355 (2012), 168–173.

[18] T. Arthur, T. A. Stephenson, J. Organomet. Chem. 208 (1981) 369–387.

[19] G. Meister, G. Süss-Fink, Unpublished. See G. Meister (1994) PhD Thesis,

University of Neuchâtel, Switzerland.

[20] M. Stebler-Röthlisberger, W. Hummel, P. A. Pittet, H. B. Bürgi, A. Ludi, A. E. Merbach, Inorg. Chem. 27 (1988) 1358–1363.

[21] A. W. Sleight, Science 208 (1980) 895–900.

[22] C. L. Kitchens, M. C. McLeod, C. B. Roberts, J. Phys. Chem. B 107 (2003) 11331–11338.

[23] M. Anand, M. C. McLeod, P. W. Bell, C. B. Roberts, J. Phys. Chem. B 109 (2005) 22852–22859.

[24] M. Q. Hou, Q. Q. Mei, B. X. Han, J. Colloid Interface Sci. 449 (2015) 488–493.

[25] L. M. Zhou, X. L. Qi, X. H. Jiang, Y. F. Zhou, H.Y. Fu, H. Chen, J. Colloid. Interface Sci. 392 (2013) 201–205.

3

Reactivity and selectivity of ruthenium nanoparticles intercalated in hectorite for the catalytic hydrogenation of quinoline

3.1 Introduction

The hydrogenation of quinolone (Q) and its derivatives is a fascinating area of research, since the hydrogenation products have a variety of industrial applications ranging from the production of petrochemicals and fine chemicals to the development of heterocyclic skeletons for pharmaceuticals and agrochemicals [1–4]. The usual intermediates 1,2,3,4-tetrahydroquinoline (1,2,3,4-THQ) and 5,6,7,8-tetrahydro-quinoline (5,6,7,8-THQ) are initially produced during the catalytic hydrogenation of Q, and can be adsorbed irreversibly at the surface of catalyst, thus hampering the further hydrogenation reaction towards decahydroquinoline (DHQ) [5]. Generally, an acidic media and drastic reaction conditions (> 200 °C, > 100 bar H_2) are essential to obtain DHQ [5–9].

Homogeneous precious metal catalysts have been designed to partially hydrogenate the Q to 1,2,3,4-THQ, but most of these catalysts failed to give satisfactory results due to numerous complications associated with homogeneous catalysis [10–13]. Heterogeneous catalysts such as Au, Pd, Ni, Rh, Ru, Pt and Cu supported on TiO_2, Al_2O_3, SiO_2, coal, hydroxyapatite etc. have been developed in recent years. H. Okazaki *et al*. hydrogenated Q over Raney-nickel at 200 °C and over ruthenium on carbon at 150 °C and studied the rate constants without reporting the selectivities [14]. C. Bianchini *et al*. observed that ruthenium supported on SiO_2 catalyzes the hydrogenation of Q in *n*-octane at 100 °C and 30 bar H_2 to give preferentially 1,2,3,4-THQ with a TOF of 185 h^{-1}, while 5,6,7,8-THQ and DHQ are formed as side products (20 h^{-1} and 4 h^{-1}, respectively) [15]. F. L. Eliel and F. W. Vierhapper reported the hydrogenation of Q catalyzed by PtO_2 in strong acidic media to give preferentially 5,6,7,8-THQ (up to 84%) [16-17]. M. Campanati and co-workers used rhodium-containing catalysts to give selectively 1,2,3,4-THQ with low conversion at 100 °C, but at higher temperatures the selectivity is lost [5]. G. Y. Fan *et al*. reported the hydrogenation of Q over rhodium nanoparticles entrapped in aluminum oxy-hydroxide with DHQ selectivity up to 99.8% [18]. Y. Milkami *et al*.

reported the reversible hydrogenation of Q to produce 1,2,3,4-THQ at 150 °C using a titania supported copper catalyst [19]. Recently, Y. Cao and co-workers demonstrated that TiO_2-supported gold nanoparticles selectively yields 1,2,3,4-THQ in toluene under mild reaction conditions (100%, 60 °C, 20 bar H_2) [20]. K. Kaneda *et al.* developed a catalyst composed of palladium nanoparticles supported by hydroxyapatite, which gives 1,2,3,4-THQ under even milder conditions (98%, 50 °C, 1 bar H_2) [21]. F. Fache was the first to observe that the selectivity of Q hydrogenation can be switched from 1,2,3,4-THQ to DHQ by changing the reaction medium from methanol to hexafluoroisopropanol using an Rh/Al_2O_3 catalyst [22].

Y. P. Sun *et al.* obtained exclusively DHQ from Q at 150 °C and 40 bar H_2 using a hydroxyapatite-supported ruthenium catalyst [23]. However, R. A. Sánchez-Delgado and co-workers reported that poly(4-vinylpyridine) supported ruthenium nanoparticles catalyze the hydrogenation of Q to give almost exclusively 1,2,3,4-THQ at 120 °C and a H_2 pressure of 40 bar in toluene [24, 25]. Very recently, L. Zhou *et al*. reported ruthenium nanoparticles intercalated in CTAB-modified montmorillonite to give exclusively 1,2,3,4-THQ in methanol at 100 °C [26].

Previously it was shown in our group that ruthenium(0) nanoparticles intercalated in hectorite give a black solid material, *nano*Ru@hectorite, which is a highly efficient and reusable catalyst for the hydrogenation of benzene [27–29]. This catalyst showed remarkable selectivities for the hydrogenation of furfuryl alcohol [30] and for the hydrogenation of α,β-unsaturated ketones [31]. In the current chapter, the catalyst *nano*Ru@hectorite is reported to show a switchable selectivity for the hydrogenation of Q. Depending on the reaction medium, the reaction gives either 1,2,3,4-THQ (> 99%) or DHQ (> 99%). Of practical significance is the selective conversion of quinoline to 1,2,3,4-THQ under mild reaction conditions in the benign aqueous medium. This versatile heterogeneous catalyst may have potential applications in the broad field of pharmaceuticals and fine chemicals, where these structural motifs are commonly found in numerous biologically active natural products and pharmacologically relevant therapeutic agents [32].

3.2 Results and discussion

3.2.1 Characterization of the *nano*Ru@hectorite catalyst

The *nano*Ru@hectorite catalyst was prepared from synthetic sodium hectorite and an aqueous solution of benzene ruthenium dichloride dimer containing the aqua complexes $[(C_6H_6)RuCl_2(H_2O)]$, $[(C_6H_6)RuCl(H_2O)_2]^+$ and $[(C_6H_6)Ru(H_2O)_3]^{2+}$ in equilibrium [33] via ion exchange of the sodium cations against benzene ruthenium aqua cations in the interlaminar space. The yellow material obtained is an air-stable catalyst precursor that can be isolated and stored. This catalyst precursor was then reduced, suspended in the appropriate solvent, at elevated temperature by molecular hydrogen to give the active catalyst *nano*Ru@hectorite, an air-sensitive black powder.

The ruthenium loading of *nano*Ru@hectorite was assumed to be 3.3 wt% [27], based upon the molar ratio of $[(C_6H_6)RuCl_2]_2$ consumed (corresponding to 75% of the experimentally determined cation exchange capacity [34]). The presence of metallic ruthenium was proven by its typical reflections in the X-ray diffraction pattern [31]. The specific surface area of *nano*Ru@hectorite was determined by low temperature nitrogen adsorption to be 207 m^2/g, which is much higher than for the unmodified sodium hectorite (87 m^2/g), and the pore size distribution in *nano*Ru@hectorite shows a maximum of 1.98 nm [33]. The size distribution of the ruthenium(0) nanoparticles in *nano*Ru@hectorite was studied by transmission electron microscopy (TEM) using the software ImageJ [35] for analysis, selected area electron diffraction (SAED) and energy-dispersive X-ray spectroscopy (EDS).

The micrographs indicate the ruthenium(0) nanoparticles: At the edges of superimposed silicate layers the nanoparticles are visible, the lighter tone of which is typical for intercalated particles. The mean particle size and standard deviation (σ) were estimated from image analysis of more than 100 particles (Figure 3.1). It was reported earlier that ruthenium(0) nanoparticles intercalated in hectorite possess various shapes (hexagonal or spherical) and sizes (3–38 nm), depending on the reaction conditions

for the reduction process [30–32]. The *nano*Ru@hectorite catalysts prepared here have mean particle sizes of 10 nm (in water) and 3 nm (in cyclohexane) under a H_2 pressure of 50 bar at 100 °C for 14 h.

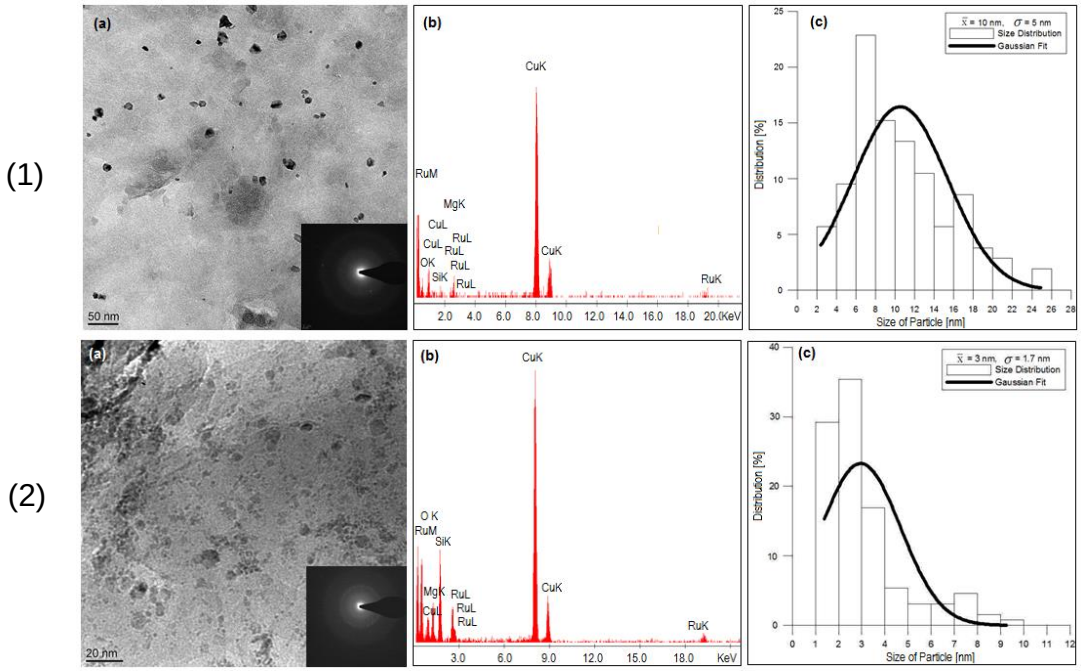

Figure 3.1 Microscopic analysis of the *nano*Ru@hectorite catalysts, (1) reduced in water and (2) reduced in cyclohexane, by TEM, SAED and EDS techniques. The calculated mean particle size for (1) and (2) are 10 ± 5 nm and 3 ± 1.7 nm, respectively.

3.2.2 Optimization of the reaction conditions

The usual intermediates during the hydrogenation of Q to give DHQ are the 1,2,3,4-THQ and 5,6,7,8-THQ, as depicted in Scheme 3.1. The optimized conditions including the proper employment of solvent, temperature, pressure, molar ratio of the reactants and reaction time, often distinctly alter the product distribution. There have been a number of studies probing the nature of solvent in the hydrogenation reactions [36–39]. Both mass transfer and chemical effects are considered to be involved in the heterogeneous system [39]. In the current study, polar and non-polar solvents were selected as probe to discern the optimal system, as summarized in Figure 3.2.

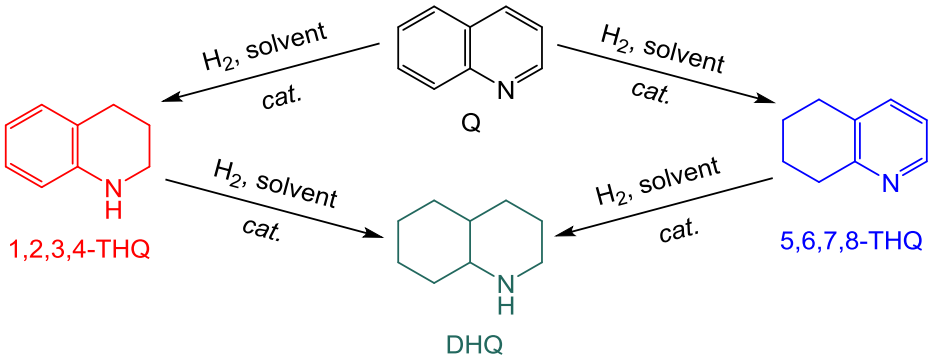

Scheme 3.1 The pathway of the hydrogenation of Q to give DHQ catalyzed by ruthenium nanoparticles intercalated in hectorite. The possible intermediates are 1,2,3,4-THQ and 5,6,7,8-THQ, and the desired products are 1,2,3,4-THQ and DHQ.

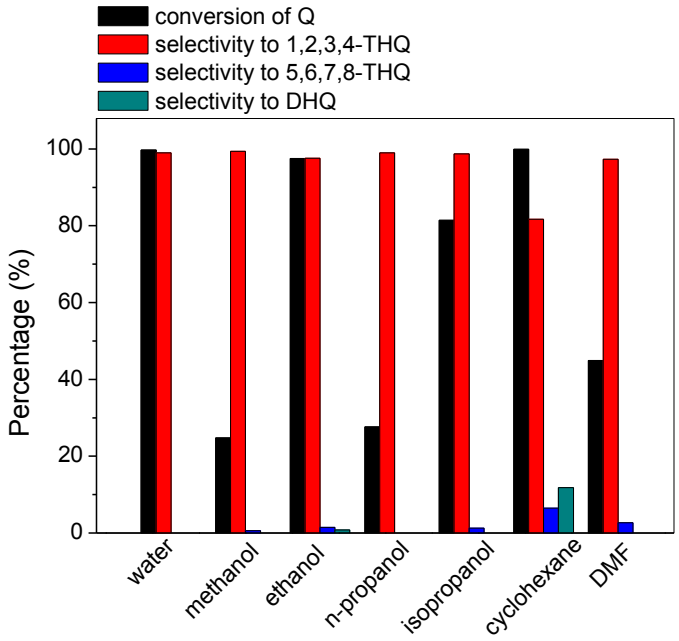

Figure 3.2 Histograms of the relevance of Q conversion and product distribution with various solvents including water, methanol, ethanol, n-propanol, isopropanol, cyclohexane and DMF, under the same reaction conditions.

Water, methanol, ethanol, n-propanol, isopropanol, cyclohexane and dimethyl-formamide (DMF) were studied as reaction media for the hydrogenation of Q under

constant reaction conditions. In the case of water, ethanol or isopropanol as a solvent, the conversion of Q is superior to 95%; however, the selectivity to 1,2,3,4-THQ is superior to 95% for all the tested solvents except for cyclohexane. From the cost-efficient point of view, water is preponderant to all the others in the production of 1,2,3,4-THQ, whereas cyclohexane as solvent can be used for a high selectivity to DHQ. Taking advantage of the various solvents for the hydrogenation of Q, different products can be obtained.

In water as reaction medium, the reaction is very selective for 1,2,3,4-THQ (Table 3.1). At 100 °C and a hydrogen pressure of 30 bar, 1,2,3,4-THQ is obtained almost exclusively (selectivity > 99%) after 3 h. The initial turnover frequency is 330 h^{-1}, the mean turnover frequency 222 h^{-1}. Some 5,6,7,8-THQ (< 1%) was detected by GC-MS analysis, but no traces of DHQ were observed. In a polar non-protic solvent such as DMF, the reaction gives, under the same conditions, 97.3% of 1,2,3,4-THQ and 2.7% of 5,6,7,8-THQ and no traces of DHQ, the conversion being only 44.9%.

Table 3.1

Hydrogenation of Q by *nano*Ru@hectorite in water.

Entry[a]	t, h	T, °C	*p*H2, bar	C_Q, %[b]	Selectivity, %		
					1,2,3,4-THQ	5,6,7,8-THQ	DHQ
1	1	90	30	14.5	> 99.9	-	-
	2	90	30	36.9	98.6	1.4	-
	3	90	30	49.3	99.4	0.6	-
2	1	100	20	27.9	99.5	0.5	-
	2	100	20	54.2	99.1	0.9	-
	3	100	20	76.8	98.6	1.4	-
3	1	100	30	52.1	99.0	1.0	-
	2	100	30	87.5	97.8	2.2	-
	3	100	30	99.6	> 99.0	< 1.0	-

[a] Molar ratio of substrate to metal being 665.

[b] C_Q being Q conversion.

Cyclohexane proved to be the best medium for the complete hydrogenation of quinoline. The selectivity of *nano*Ru@hectorite toward DHQ was found to be highly dependent on the hydrogen pressure (Table 3.2). At 100 °C in cyclohexane under a hydrogen pressure of 60 bar, complete conversion of quinoline to DHQ (selectivity > 99%) was observed within 3 h. The initial turnover frequency is 694 h^{-1}, while the mean turnover frequency is 89 h^{-1}.

Table 3.2

Hydrogenation of Q by *nano*Ru@hectorite in cyclohexane.

Entry[a]	t, h	pH_2, bar	C_Q, %[b]	Selectivity, %		
				1,2,3,4-THQ	5,6,7,8-THQ	DHQ
1	1	20	90.6	79.6	13.3	7.1
	2	20	100	57.9	13.7	28.4
	3	20	100	42.7	11.3	45.9
2	1	30	100	67.9	19.8	12.3
	2	30	100	42.1	14.1	43.8
	3	30	100	28.5	10.8	60.7
3	1	40	100	69.6	18.0	12.4
	2	40	100	37.3	12.2	50.5
	3	40	100	20.9	8.9	70.2
4	1	50	100	51.4	14.2	34.4
	2	50	100	24.2	7.1	68.7
	3	50	100	3.1	3.2	93.7
5	1	60	100	30.9	11.2	57.9
	2	60	100	2.5	2.0	95.5
	3	60	100	0	0	> 99.9

[a] Molar ratio of substrate to metal being 266, reaction temperature 100 °C.

[b] C_Q being Q conversion.

Surprisingly, 5,6,7,8-THQ is observed in relatively high amounts during the hydrogenation of quinoline catalyzed by *nano*Ru@hectorite in cyclohexane (Table 3.2). The 1,2,3,4-THQ selectivity is highly dependent on hydrogen pressure. The highest yields of 5,6,7,8-THQ are observed under a hydrogen pressure of 30 bar at

100 °C (up to 19.8% within 1 h), then a steady decrease in the 5,6,7,8-THQ selectivity is accompanied with increasing H_2 pressure.

3.2.3 Mechanistic considerations

It has been speculated for many years that the high electron density of an aromatic π cloud can act as hydrogen bond acceptor [40–43]. Suzuki *et al.* observed a clear manifestation of hydrogen bond formation with π-electrons in 1:1 clusters of benzene with water [43]. Based on this assumption, the high 1,2,3,4-THQ selectivity is probably due to H-bond formation between water molecules and the π-electrons in the benzene ring of Q, which hampers the adsorption of aromatic ring on the catalyst surface. The nitrogen atom would be likely to coordinate to the ruthenium surface and would thus receive the hydrogen atoms already present at the surface of the nanoparticles, thus yielding 1,2,3,4-THQ almost exclusively (Figure 3.3). In accordance with this hypothesis, the IR spectrum of *nano*Ru@hectorite shows, after a catalytic run, an additional adsorption at 747 cm^{-1}, which may be due to a ruthenium-nitrogen interaction (Figure 3.4). Hydrogen bonding between water and aromatic rings has also been rationalized by theoretical studies [44–47].

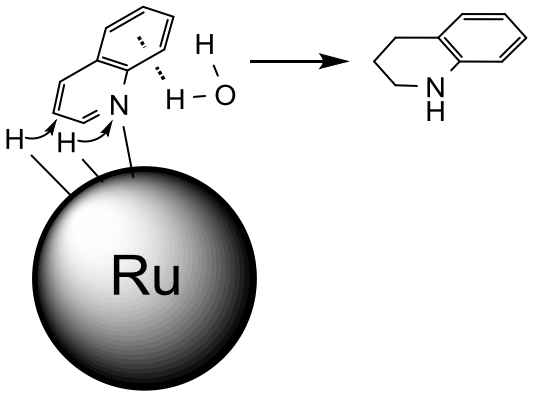

Figure 3.3 Hypothetical explanation for the hydrogenation of Q to 1,2,3,4-THQ in water.

Interestingly, the DHQ selectivity is high in the non-polar medium cyclohexane,

along with the intermediary formation of 5,6,7,8-THQ. It is found that *nano*Ru@hectorite preferentially catalyzes the hydrogenation of the olefinic double bond in the α,β-unsaturated ketones [31]. Recently, B. Chaudret and his co-workers demonstrated an unusual π-coordination of phenyl moiety at the surface of ruthenium nanoparticles [48]. Thus, the surprising selectivity for the intermediary 5,6,7,8-THQ can be tentatively attributed to the vulnerability of the aromatic ring due to the absence of hydrogen bond with cyclohexane (Figure 3.5). The π-electrons now favor the competitive adsorption of the aromatic ring with the heteroaromatic ring on the ruthenium surface, which results in around 20% of the selectivity to 5,6,7,8-THQ (pathway B). In this case, the IR spectra of *nano*Ru@hectorite catalysts show no additional adsorption after a catalytic run (Figure 3.4b).

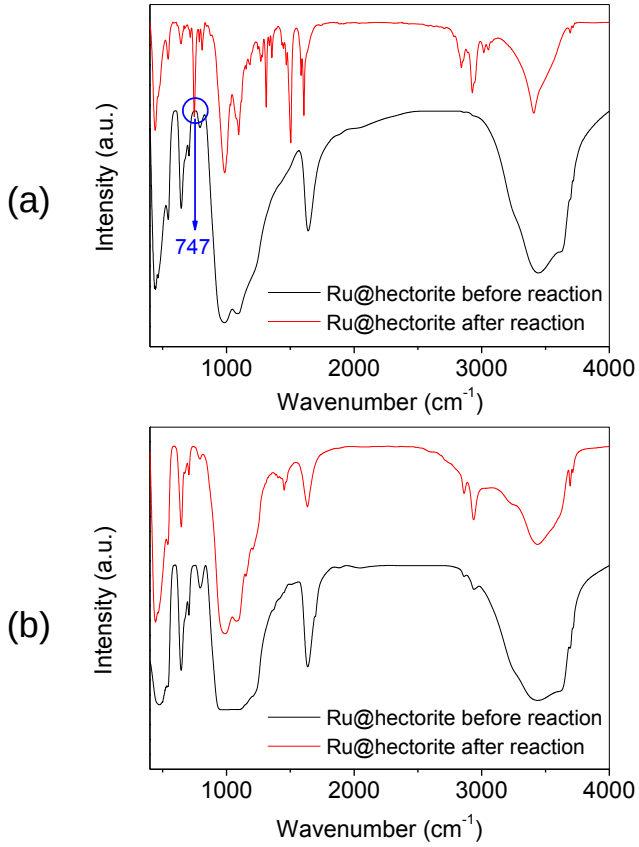

Figure 3.4 Infrared spectra of the *nano*Ru@hectorite collected before and after the reaction in the system of (a) water as solvent and (b) cyclohexane as solvent.

It should be noted that the preferential adsorption of quinoline still occurs via the *N*-heterocycle (pathway A), as evidenced by the high amount of 1,2,3,4-THQ during the catalytic hydrogenation also in non-polar solvents (Table 3.2). Therefore, it can be assumed that even in cyclohexane this reaction predominantly proceeds through pathway A, and not through pathway B.

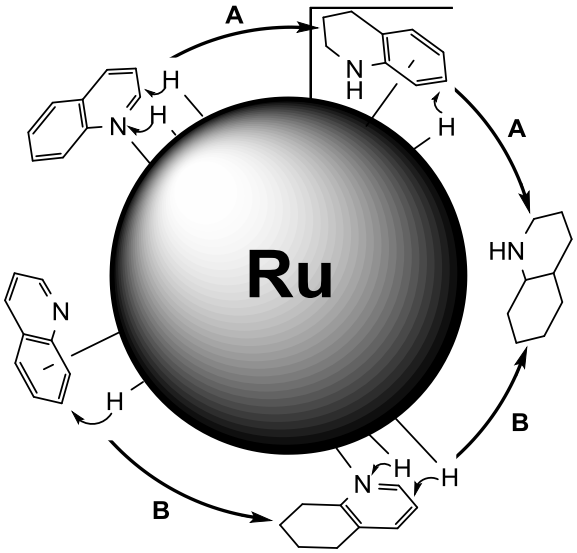

Figure 3.5 Proposed reaction pathways for the hydrogenation of Q to DHQ in cyclohexane.

3.2.4 Recyclability and reusability

The *nano*Ru@hectorite catalyst cannot really be reused for further runs after a catalytic reaction with the same activity and selectivity. We examined the recyclability of the catalyst for four consecutive catalytic runs by separating the catalyst after each run and reactivating it under hydrogen pressure. As shown in Table 3.3, the recycled catalyst remains highly selective in water, giving exclusively 1,2,3,4-THQ, however, it loses rapidly its activity because of separation problems in aqueous media. On the other hand, in cyclohexane the recycled catalyst remains active with conversions over 96%, but loses its selectivity for DHQ.

Table 3.3

Reusability of *nano*Ru@hectorite catalysts in the hydrogenation of Q.

Reuse after the 1st run	C_Q, %[c]	Selectivity, %		
		1,2,3,4-THQ	5,6,7,8-THQ	DHQ
2nd (in H_2O)[a]	23	> 99.9	0	0
3rd (in H_2O)[a]	13	> 99.9	0	0
4th (in H_2O)[a]	4	> 99.9	0	0
2nd (in C_6H_{12})[b]	97	50.4	2.3	47.4
3rd (in C_6H_{12})[b]	97	83.9	2.4	13.7
4th (in C_6H_{12})[b]	96	94.5	1.2	4.3

[a] Reaction conditions: 30 bar H_2, 100 °C, 5 h.

[b] Reaction conditions: 60 bar H_2, 100 °C, 5 h.

[c] C_Q being Q conversion.

3.3 Conclusions

In summary, the *nano*Ru@hectorite catalyst provides a mild and effective method for the catalytic hydrogenation of Q with switchable selectivity between 1,2,3,4-THQ (> 99%) in water and DHQ (> 99%) in cyclohexane. The alternative intermediate 5,6,7,8-THQ, rarely observed in substantial concentrations so far, can be obtained in cyclohexane in yield up to 19.8% by stopping the reaction after 1 h.

References

[1] Y. Gong, P. Zhang, X. Xu, Y. Li, H. Li, Y. Wang, J. Catal. 297 (2013) 272–280.

[2] R. T. Shuman, P. L. Ornstein, J. W. Paschal, P. D. Gesellchen, J. Org. Chem. 55 (1990) 738–741.

[3] F. Glorius, Org. Biomol. Chem. 3 (2005) 4171–4175.

[4] R. Rahi, M. Fang, A. Ahmed, R. A. Sánchez-Delgado, Dalton Trans. 41 (2012) 14490–14497.

[5] M. Campanati, A. Vaccari, O. Piccolo, J. Mol. Catal. A: Chem. 179 (2002) 267–272.

[6] M. Campanati, M. Casagrande, I. Fagiolino, M. Lenarda, L. Storaro, M. Battagliarin, A. Vaccari, J. Mol. Catal. A: Chem. 184 (2002) 287–292.

[7] H. U. Blaser, H. P. Jalett, W. Lottenbach, M. Studer, J. Am. Chem. Soc. 122 (2000) 12675–12682.

[8] O. Piccolo, A. Vaccari, S. Franceschini, M. Campanati, *Catalysis of Organic Reactions*, CRC Press, 2005, 101–110 (chapter 13, and references cited therein).

[9] M. Freifelder, Adv. Catal. 14 (1963) 203–253.

[10] S. M. Lu, X. W. Han, Y. G. Zhou, J. Organomet. Chem. 692 (2007) 3065–3069, (and references cited therein).

[11] H. Mao, C. Chen, X. Liao, B. Shi, J. Mol. Catal. A: Chem. 341 (2011) 51–56.

[12] W. B. Wang, S. M. Lu, P. Y. Yang, X. W. Han, Y. G. Zhou, J. Am. Chem. Soc. 125 (2003) 10536–10537.

[13] H. Zhou, Z. Li, Z. Wang, T. Wang, L. Xu, Y. He, Q. H. Fan, J. Pan, L. Gu, A. S. C. Chan, Angew. Chem. Int. Ed. 47 (2008) 8464–8467.

[14] H. Okazaki, K. Onishi, M. Soeda, Y. Ikefuji, R. Tamura, I. Mochida, Bull. Chem. Soc. Jpn. 63 (1990) 3167–3174.

[15] C. Bianchini, V. D. Santo, A. Meli, S. Moneti, M. Moreno, W. Oberhauser, R. Psaro, L. Sordelli, F. Vizza, J. Catal. 213 (2003) 47–62.

[16] F. W. Vierhapper, E. L. Eliel, J. Org. Chem. 40 (1975) 2729–2734.

[17] M. Hönel, F. W. Vierhapper, J. Chem. Soc. Perkin Trans. 1 (1980) 1933–1939.

[18] G. Y. Fan, J. Wu, Catal. Commun. 31 (2013) 81–85.

[19] Y. Mikami, K. Ebata, T. Mitsudome, T. Mizugaki, K. Jitsukawa, K. Kaneda, Heterocycles, 82 (2011) 1371–1377.

[20] D. Ren, L. He, L. Yu, R. S. Ding, Y. M. Liu, Y. Cao, H. Y. He, K. N. Fan, J. Am. Chem. Soc. 134 (2012) 17592−17598.

[21] N. Hashimoto, Y. Takahashi, T. Hara, S. Shimazu, T. Mitsudome, T. Mizugaki, K. Jitsukawa, K. Kaneda, Chem. Lett. 39 (2010) 832–834.

[22] F. Fache, Synlett 15 (2004) 2827–2829.

[23] Y. P. Sun, H. Y. Fu, D. L. Zhang, R. X. Li, H. Chen, X. J. Li, Catal. Commun. 12 (2010) 188–192.

[24] R. A. Sánchez-Delgado, N. Machalaba, N. Ngaqui, Catal. Commun. 8 (2007) 2115–2118.

[25] M. Fang, N. Machalaba, R. A. Sánchez-Delgado, Dalton Trans. 40 (2011) 10621–10632.

[26] L. Zhou, X. Qi, X. Jiang, Y. Zhou, H. Fu, H. Chen, J. Colloid Interface Sci. 392 (2013) 201–205.

[27] A. Meister, G. Meister, G. Süss-Fink, J. Mol. Catal. 92 (1994) L123–L126.

[28] G. Süss-Fink, B. Mollwitz, B. Therrien, M. Dadras, G. Laurenczy, A. Meister, G. Meister, J. Cluster Sci. 18 (2007) 87–95.

[29] G. Süss-Fink, F. A. Khan, J. Boudon, V. Spassov, J. Cluster Sci. 20 (2009) 341–353.

[30] F. A. Khan, A. Vallat, G. Süss-Fink, Catal. Comm. 12 (2011) 1428–1431.

[31] F. A. Khan, A. Vallat, G. Süss-Fink, J. Mol. Catal. A: Chem. 355 (2012), 168–173.

[32] M. Heitbaum, R. Fröhlich, F. Gloriusa, Adv. Synth. Catal. 352 (2010) 357–362.

[33] G. Meister, G. Süss-Fink, unpublished. See G. Meister (1994) PhD Thesis, University of Neuchâtel, Switzerland.

[34] G. Lagaly, H. Tributh, Ber. Dt. Tonmineralgruppe (1991) 86.

[35] C. A. Schneider, W. S. Rasband, K. W. Eliceiri, Nat. Methods 9 (2012) 671–675.

[36] R. A. Rajadhyaksha, S. L. Karwa, Chem. Eng. Sci. 41 (1986) 1765–1770.

[37] S. Mukherjee, M. A. Vannice, J. Catal. 243 (2006) 108–130.

[38] S. Mukherjee, M. A. Vannice, J. Catal. 243 (2006) 131–148.

[39] B. S. Akpa, C. D'Agostino, L. F. Gladden, K. Hindle, H. Manyar, J. McGregor, R. Li, M. Neurock, N. Sinha, E. H. Stitt, D. Weber, J. A. Zeitler, D. W. Rooney, J. Catal. 289 (2012) 30–41.

[40] M. Levitt, M. F. Perutz, J. Mol. Biol. 201 (1988) 751–754.

[41] M. F. Perutz, in: A. Zewail (Ed.), *The Chemical Bond*, Academic Press, New York, 1992.

[42] S. K. Burley, G.A. Petsko, FEBS Lett. 203 (1986) 139–143.

[43] S. Suzuki, P. G. Green, R. E. Bumgarner, S. Dasgupta, W. A. Goddard, G. A. Blake, Science, New Series 257 (5072) (1992) 942–945.

[44] V. Stefov, Lj. Pejov, B. Šoptrajanov, J. Mol. Struct. 555 (2000) 363–373.

[45] M. A. Muñoz, O. Sama, M. Galán, P. Guardado, C. Carmona, M. Balón, J. Phys. Chem. B 103 (1999) 8794–8798.

[46] W. Pohle, J. Chem. Soc. Faraday Trans. 1. 78 (1982) 2101–2109.

[47] T. Steiner, Angew. Chem. Int. Ed. 41 (2002) 48–76.

[48] I. Favier, S. Massou, E. Teuma, K. Philippot, B. Chaudret, M. Gómez, Chem. Commun. 28 (2008) 3296–3298.

4

Hydrogenation of *N*-heterocycles with $NaBH_4$ and water catalyzed by ruthenium nanoparticles supported on hectorite

4.1 Introduction

As mentioned in Chapter 3, the quinoline (Q) hydrogenation products have important industrial applications ranging from the production of petrochemicals and fine chemicals to the development of heterocyclic skeletons for pharmaceuticals and agrochemicals [1]. Synthetic methods to obtain 1,2,3,4-tetrahydroquinoline (1,2,3,4-THQ) include catalytic cyclization [2–3], Beckman rearrangement [4] and the direct partial hydrogenation of Q. Among these methods, the *N*-cycle-selective hydrogenation of Q is the most interesting process because of its reasonable atom utilization efficiency. A general problem in the selective hydrogenation of *N*-heterocycles is, however, the possible and sometimes irreversible adsorption of the amine formed at the surface of the metal catalyst [5–6], thus blocking the catalytic sites.

Precious metal complexes can be used for the catalytic hydrogenation of Q to 1,2,3,4-THQ, but most of these catalysts failed to give satisfactory results due to numerous complications associated with homogeneous catalysis [7–9]. Heterogeneous metal catalysts such as gold [10], palladium [11–13], rhodium [14–15], and ruthenium [16–18], supported on titania, alumina, silica, coal, hydroxyapatite or polymers have also been developed for this reaction. In most cases, elevated temperature and pressure are essential to convert Q into 1,2,3,4-THQ, the selectivity being tuned by various organic solvents [19].

From the green chemistry point of view, water would be the most interesting solvent, because it is not only a green solvent in organic synthesis, but also plays a promoting role in enhancing the catalyst activity [20]. Only a few heterogeneous catalysts have been found active in the hydrogenation of Q in aqueous medium, such as ruthenium nanoparticles supported on silica spheres with an outer shell of microporous silica [21], palladium nanoparticles stabilized by black wattle tannin [22, 23] and palladium nanoparticles supported by polymers [24].

In our previous work, a heterogeneous catalyst was developed by intercalation of

cationic benzene ruthenium complexes into hectorite, followed by reduction with molecular hydrogen to give a black solid containing metallic ruthenium nanoparticles intercalated in hectorite (*nano*Ru@hectorite) [25–27]. This material was found to catalyze the hydrogenation of Q with switchable selectivity, the reaction in water at 60 °C and 30 bar H_2 giving 1,2,3,4-THQ, conversion and selectivity being superior to 99% [28]. However, high-pressure equipment is required for this reaction.

Inspired by a recent paper by M. M. Dell'Anna on the hydrogenation of Q by sodium borohydride in water catalyzed by polymer-supported palladium nanoparticles [29], we modified our *nano*Ru@hectorite catalyst system, so that it also works with $NaBH_4$ and H_2O as the hydrogen source for the hydrogenation of Q. The simple intercalation of $RuCl_3 \cdot n\ H_2O$ in hectorite gives a black precatalyst, which is stable in air and which catalyzes the selective hydrogenation of Q to 1,2,3,4-THQ with $NaBH_4$ in water under mild conditions in an open reaction vessel; no pressure equipment is required. The actual catalyst, metallic ruthenium nanoparticles intercalated in hectorite (*nano*Ru′@hectorite), can be recovered and reused. Here in the current chapter, the preparation of the precatalyst, the characterization of the catalyst and its performance for *N*-cycle hydrogenation of Q and quinoline derivatives including isoquinoline and quinoxalines are reported.

4.2 Results and discussion

4.2.1 Characterization of the *nano*Ru′@hectorite catalyst

The *nano*Ru'@hectorite precatalyst is accessible from synthetic sodium hectorite and an aqueous solution of $RuCl_3 \cdot n\ H_2O$. The black material is obtained by ion exchange of the sodium cations against ruthenium(III) aqua cations in the interlaminar space. The d-spacing (d_{001}) of the sodium hectorite and Ru(III)-containing hectorite are 13.4 Å and 15.2 Å, respectively (Figure 4.1). The enlarged interlaminar space can be attributed to the actual intercalation of ruthenium(III) aqua cations. The black

Ru(III)-containing catalyst precursor is stable in air and can be isolated and stored. When suspended in water, this precatalyst can be reduced by $NaBH_4$ to give the active *nano*Ru′@hectorite catalyst, an air-sensitive black powder with a d-spacing of 13.6 Å, while the d-spacing of the *in situ* formed *nano*Ru'@hectorite catalyst after a catalytic run is 13.7 Å. The similar d-spacing for the sodium-containing hectorite and *nano*Ru'@hectorite suggests that the ruthenium nanoparticles are thoroughly embedded in the interlayers of the hectorite. Besides, a visible Ru(011) diffraction peak was observed only for the *nano*Ru′@hectorite reduced in pure water, suggesting a larger particle size compared to the *in situ* formed *nano*Ru'@hectorite in a water-quinoline mixture.

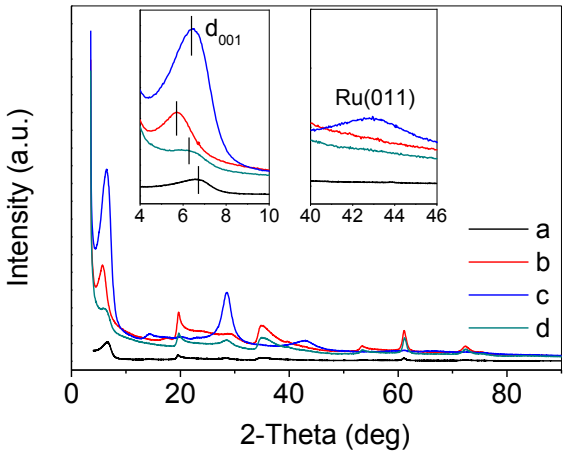

Figure 4.1 Powder X-ray diffraction (XRD) patterns of the samples of (a) the sodium-containing hectorite powder, (b) the Ru(III)-containing hectorite (precatalyst), (c) the *nano*Ru′@hectorite reduced by $NaBH_4$ at 60 °C for 4 h in water under atmospheric pressure without organic agent and (d) the *in situ* generated *nano*Ru′@hectorite after a fresh run for the catalytic hydrogenation of quinoline under atmospheric pressure at 60 °C for 4 h in water. The d_{001} of these samples are calculated to be 13.4 Å, 15.2 Å, 13.6 Å and 13.7 Å, respectively. The insets are the zoomed XRD patterns for clarity.

The morphology of the metallic ruthenium nanoparticles imbedded in the hectorite interlayers of *nano*Ru′@hectorite was studied by transmission electron

microscopy (TEM). The reduction of transition metal salts by sodium borohydride is a common method for the preparation of metallic nanoparticles that allows a certain control of the morphology, important for activity and selectivity for catalytic applications [30]. The reaction medium (organic solvents or water) is also decisive for the morphology of the nanoparticles [27, 31, 32]. Figure 4.2 shows the TEM images of *nano*Ru′@hectorite obtained under different conditions: The ruthenium nanoparticles formed by sodium borohydride reduction of the precatalyst in pure water without a substrate being present is depicted in Figure 4.2a, while Figure 4.2b shows the *in situ* generated ruthenium nanoparticles obtained during a catalytic run in aqueous solution from the precatalyst and sodium borohydride in the presence of Q as the substrate. The recycled *nano*Ru′@hectorite catalyst after a second catalytic run for the hydrogenation of Q is depicted in Figure 4.2c. In all cases, ruthenium is present in the form of nanoparticles the size of which varies between 1 and 10 nm. In pure water, without an organic substrate being present, the ruthenium nanoparticles (mean size 4.5 nm) agglomerate to give worm-like structures, a similar morphology to that observed for ruthenium nanoparticles supported on cetyltrimethylammonium bromide (CTAB) modified montmorillonite [17]. However, the *in situ* formed ruthenium nanoparticles in the presence of Q are smaller (mean size 2.4 nm) and agglomerate to spherical clusters of a diameter of 28.1 nm in average; this is also observed for the recycled *nano*Ru′@hectorite catalyst, where the ruthenium nanoparticles (mean size 2.1 nm) are slightly smaller, while the spherical agglomerates (mean size 41.3 nm) are slightly larger. The observed particle size is consistent with that calculated from XRD analysis.

(a)

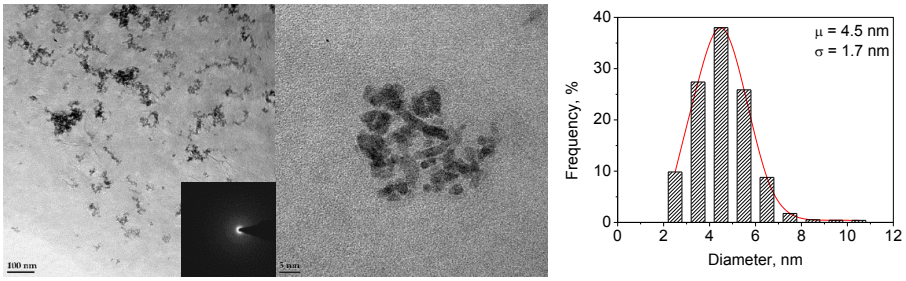

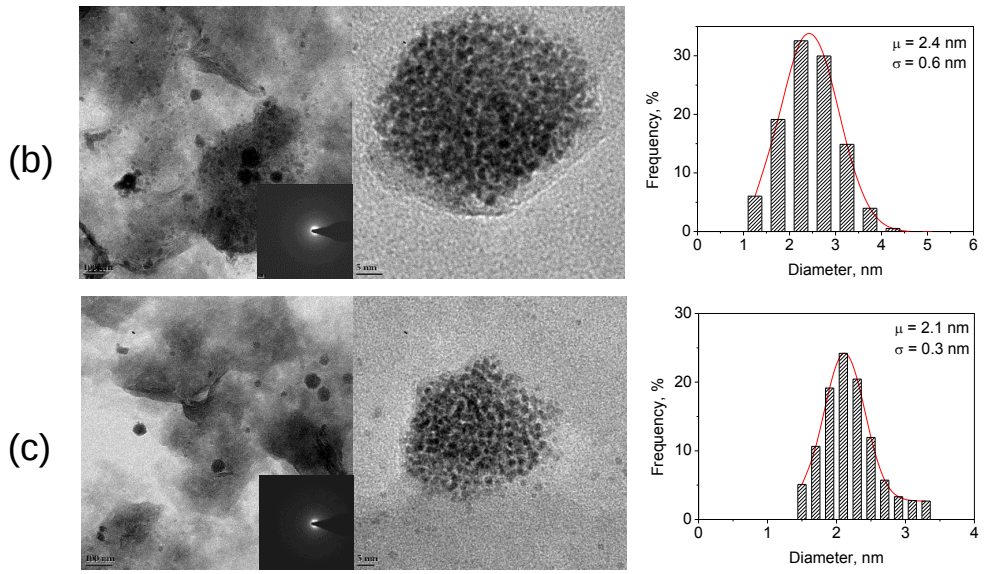

Figure 4.2 TEM images of the samples of (a) *nano*Ru′@hectorite from the reduction of the precatalyst by $NaBH_4$ under atmospheric pressure at 60 °C for 4 h in water without organic agent, (b) the *in situ* generated *nano*Ru′@hectorite catalyst after a fresh run for the catalytic hydrogenation of Q under atmospheric pressure at 60 °C for 4 h in water and (c) the *nano*Ru′@hectorite catalyst after the first recycling run for the hydrogenation of Q under atmospheric pressure at 60 °C for 4 h in water.

4.2.2 Catalytic hydrogenation of quinoline

To optimize the reaction parameters, the hydrogenation of Q was studied by using different solvents and various amounts of $NaBH_4$ in a flask under atmospheric pressure and also in an autoclave under self-generated pressure depending on the amount of $NaBH_4$. In catalytic hydrogenation reactions, the solvent plays an important role in influencing the reaction rate and selectivity [19, 33, 34]. As shown in Table 4.1, several common organic solvents and H_2O have been tested into the hydrogenation under different conditions. The best results were obtained only with H_2O as solvent. Besides the difference in the nature of the solvents, the poor solubility of $NaBH_4$ in aprotic polar solvent (such as THF) and the decomposition of $NaBH_4$ in protic solvents, especially in methanol, can be considered to be the reason of the observed low reactivity. Moreover, H_2O as a solvent has been frequently observed to

be a promoter in stimulating the hydrogenation rate [21, 24, 28]. In the present work, the selective hydrogenation of Q into 1,2,3,4-THQ was successfully conducted in H_2O under atmospheric pressure in a flask (entry 7, Table 4.1), and under self-generated pressure in the autoclave (entry 12, Table 4,1). However, for the reaction in a flask, a higher amount of $NaBH_4$ was necessary to attain complete conversion of Q.

Table 4.1

Hydrogenation of Q to 1,2,3,4-THQ with $NaBH_4$ catalyzed by *nano*Ru′@hectorite.

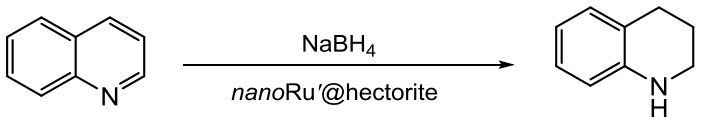

Entry	Solvent[a]	Q/M[b]	H/Q[c]	T, °C	*p*, bar	t, h	C, %[d]	S, %[e]
1	MeOH	50	12	60	a.p.[f]	6	< 5	99
2	EtOH	50	12	60	a.p.[f]	6	12	99
3	THF	50	12	60	a.p.[f]	6	10	99
4	H_2O	50	8	40	a.p.[f]	20	56	99
5	H_2O	50	10	60	a.p.[f]	4	95	99
6	H_2O	50	12	40	a.p.[f]	4	60	99
7	H_2O	50	12	60	a.p.[f]	4	99	99 (95)
8	H_2O	90	8	60	a.p.[f]	20	81	99
9	H_2O	90	14	60	a.p.[f]	20	92	99
10	H_2O	90	20	60	a.p.[f]	20	98	99
11[g]	H_2O	50	8	40	5	5	85	99
12[g]	H_2O	50	8	60	9	3	99	99
13	H_2O	no catalyst	12	60	a.p.[f]	9	51	99
14[g]	H_2O	no catalyst	8	60	9	9	53	99

[a] Solvent volume 5 ml. [b] Molar ratio of Q to ruthenium. The precatalyst was used unless stated otherwise. [c] Molar ratio of $NaBH_4$ to Q. [d] Conversion of Q. [e] Selectivity for 1,2,3,4-THQ, the value in the parentheses being the isolated yield. [f] Atmospheric pressure. [g] Carried out in a pressure vessel, the corresponding pressure being the self-generated pressure.

Throughout all the tests listed in Table 4.1, the hydrogenation of Q into 1,2,3,4-THQ was complete under atmospheric pressure or under self-generated pressure of molecular H_2, both the conversion and selectivity being up to 99%. In comparison with the Pd-*pol* catalyst [29], less $NaBH_4$ (only an 8–12-fold molar excess) was required with *nano*Ru′@hectorite as catalyst. In the blank experiments without catalyst, the conversion was only 51–53%, indicating that the catalyst is essential for the quantitative conversion of Q. However, a higher amount of $NaBH_4$ (20-fold molar excess) generates dihydroquinoline and azo compounds as by-products [29].

4.2.3 Catalytic *N*-cycle hydrogenation of quinoline derivatives and analogues

Since *nano*Ru′@hectorite has been found active for the hydrogenation of Q, the optimized conditions were applied for the hydrogenation of quinoline derivatives and analogues. As depicted in the Table 4.2, several quinoline derivatives and analogues were successfully hydrogenated to the corresponding products shown. It should be noted that sometimes a small amount of an organic co-solvent (ethanol or dimethylformamide) was used to improve the solubility of the organic reagents. In entries 1–3 of Table 4.2, 8-methylquinoline and 6-methylquinoline were efficiently hydrogenated. Under atmospheric pressure, 6-methylquinoline was exclusively transformed into 6-methyl-1,2,3,4-tetrahydroquinoline; however, 8-methylquinoline was only partly hydrogenated to 8-methyl-1,2,3,4-tetraquinoline with a maximum conversion of 53% even after 24 h. This may be explained by the steric effect of the 8-methyl substituent on the nucleophilic attack of the hydride to the C=N bond or by hyperconjugation [29, 35]. Interestingly, a self-generated pressure (3 bar H_2) remarkably improved the hydrogenation of 8-methylquinoline, which was complete in 3 h even at room temperature (25 °C). For comparison, the Q hydrogenation was done under the same conditions as those for 8-methylquinoline, but only a low conversion was observed, suggesting that, under a certain pressure, the electron-donating 8-methyl group is favorable for the hydride transfer to the *N*-cycle. Throughout all the

results for the hydrogenation of Q, 8-methylquinoline and 6-methylquinoline, it can be concluded that the electronic influence exerted by the substituents plays a crucial role in affecting the reactivity. A similar phenomenon was observed in the hydrogenation of 8-methylquinoline and 6-methylquinoline by a platinum oxide catalyst [36].

The catalytic hydrogenation of 2,6-dimethylquinoline did not work under atmospheric pressure, even in the presence of ethanol (1 mL) to dissolve the solid substrate. However, the hydrogenation of 2,6-dimethylquinoline to 2,6-dimethyl-1,2,3,4-tetrahydroquinoline worked under self-generated pressure of 6 bar at 60 °C in the autoclave (entry 5, Table 4.2). The conversion reached 99% after 4 hours; however, the maximum selectivity to 2,6-dimethyl-1,2,3,4-tetrahydroquinoline was only 88%, the by-product being the *C*-cycle-hydrogenated quinoline. This may be attributed to the steric hindrance of the 2-methyl group [19, 24, 37]. Another challenging substrate is 8-hydroxyquinoline, for which there was no conversion under atmospheric pressure; the reaction only occurred in the autoclave at 60 °C (entry 7, Table 4.2). Isoquinoline and quinoxalines also underwent selective *N*-cycle hydrogenation (entry 8–10, Table 4.2). 5-Chloro-8-quinolinol was successfully converted into 5-chloro-1,2,3,4-tetrahydro-8-quinolinol (entry 12, Table 4.2). However, 2-phenyl-quinoline was hydrogenated to give 2-phenyl-5,6,7,8-tetrahydroquinoline, as seen from entry 13 in Table 4.2 (*C*-cycle hydrogenation). This result shows that blocking C(2) by a phenyl substituent encumbers the hydrogenation of the *N*-cycle, suggesting that the attack of the hydride occurs at this carbon atom.

Table 4.2

Hydrogenation of *N*-heterocycles catalyzed by *nano*Ru'@hectorite in aqueous medium.

Entry[a]	Substrate	Product	H/Q[d]	T, °C	*p*, bar[e]	t, h	C, %[f]	S, %[g]
1	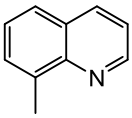	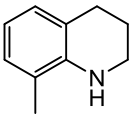	20	60	a.p.	24	53	99
2			3	25	3	3	99	99 (96)
3	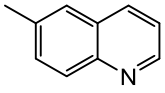	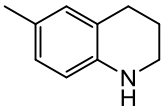	12	60	a.p.	4	99	99 (94)
4	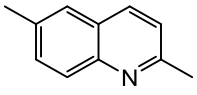	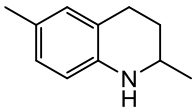	20	60	a.p.	24	0	0
5			6	60	6	4	99	88 (85)
6[b]	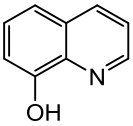	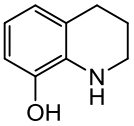	20	60	a.p.	24	0	0
7[b]			8	60	9	3	98	99 (93)
8	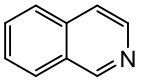	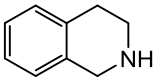	12	60	a.p.	4	99	99 (95)
9	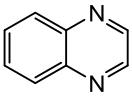	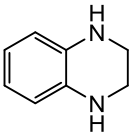	12	60	a.p.	4	99	99 (96)
10	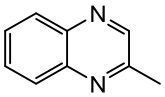	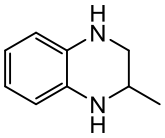	12	60	a.p.	12	98	99 (96)
11[c]	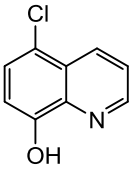	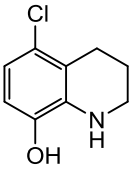	12	60	a.p.	8	77	99
12[c]			8	60	9	3	99	99
13[b]	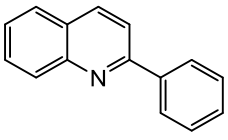	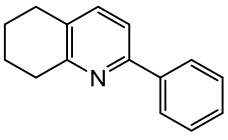	8	60	9	4	97	98

[a] 5 mL H_2O as solvent, the molar ratio of substrate to ruthenium being 50. The precatalyst was used. [b] Ethanol/H_2O (1 mL / 4 mL) as solvent. [c] Dimethylformamide / H_2O (1 mL / 4 mL) as solvent. [d] Molar ratio of $NaBH_4$ to substrate. [e] The atmospheric pressure (a.p.) in the flask, and the self-generated pressure in the autoclave. [f] Conversion of the *N*-heterocycles. [g] Selectivity for the product shown, the value in the parentheses being the isolated yield.

4.2.4 Isotope labeling studies

Sodium borohydride is a convenient reducing agent commonly used in organic synthesis for hydrogenation reactions. Although it undergoes rapid methanolysis with methanol to give molecular hydrogen, sodium hydroxide and trimethylborate, the hydrolysis in water is kinetically blocked, so that $NaBH_4$ is inert in water and can be handled in aqueous solution [38]; however, it is susceptible to a slow H/D exchange in D_2O under acidic conditions [39].

In order to find out if sodium borohydride is the single hydrogen source for the hydrogenation of the *N*-cycle in Q or if water is also involved, we carried out the catalytic reaction with $NaBH_4$ in H_2O, with $NaBD_4$ in H_2O, with $NaBH_4$ in D_2O and with $NaBD_4$ in D_2O and studied the deuteration of the product by NMR spectroscopy. The analysis is not easy, since the situation is complicated by a possible (acid-catalyzed) H/D exchange between the BH_4^- anion and D_2O (or the BD_4^- anion and H_2O) [39] and by the observed H/D exchange of the C-H and N-H functions in the product 1,2,3,4-THQ, even in the *C*-cycle.

Table 4.3

Assignment of ^{13}C and ^{1}H resonances of THQ in a $CDCl_3$ obtained by HSQC and HMBC spectra.

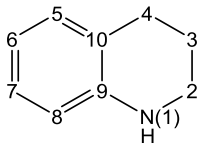

^{13}C (ppm)	^{1}H (ppm)	Assignment
114.86	-	9
129.58	7.00	5
126.79	7.02	7
121.49	-	10
116.98	6.66	6
114.25	6.52	8
42.06	3.35	2
27.06	2.82	4
22.26	2.00	3

Figure 4.3 shows that a pure CH_2 sample may be produced when no deuterium supplied to the reaction. A mixture of CH_2 and CHD groups needs to be taken into account, as soon as ^2H nuclei are involved in the reduction process, either as $NaBD_4$ or D_2O, and when no protic hydrogen is supplied, only CHD groups are obtained. In the cases of $NaBH_4/D_2O$ and $NaBD_4/H_2O$, when both CH_2 and CHD are present, $^{13}C\{^1H\}$ and ^1H line shapes as those shown in Figure 4.4a and 4.4b, are obtained. Only the C(2)H peaks are shown for clarity. With respect to these latter sites, and assuming influences to the chemical environments sensitive to only directly neighboring groups, four possible permutations with repetitions of environments need to be considered, i.e., $C(2)H_2$-$C(3)H_2$, $C(2)H_2$-C(3)HD, C(2)HD-$C(3)H_2$ and C(2)HD-C(3)HD, for both proton and carbon sites. The numerical fits of the experimental spectra of Figure 4a and 4b are performed assuming these four environments. Only $^1J(^{13}C\text{-}^2H)$ and $^3J(^1H\text{-}^1H)$ couplings are considered.

These two CH_2 or CHD environments can be revealed in a ^1H spectrum by monitoring the integral values of the relevant resonances, with pure CH_2 samples resulting in twice the integral values as compared to pure CHD samples. Moreover, the monitoring of these signal intensities for all different sites may cast light on the mechanism of the reaction itself and on the presence of preferred sites of reduction within the Q molecule. For instance, in the case of $NaBD_4/H_2O$ assuming a nucleophilic attack of a D^- anion to C(2), the atom with the lowest electron density, followed by H^+ attack on the electron-rich nitrogen atom, one should expect the presence of an N<u>H</u> signal and a C(2)<u>H</u>D of equal intensities in the ^1H NMR spectrum.

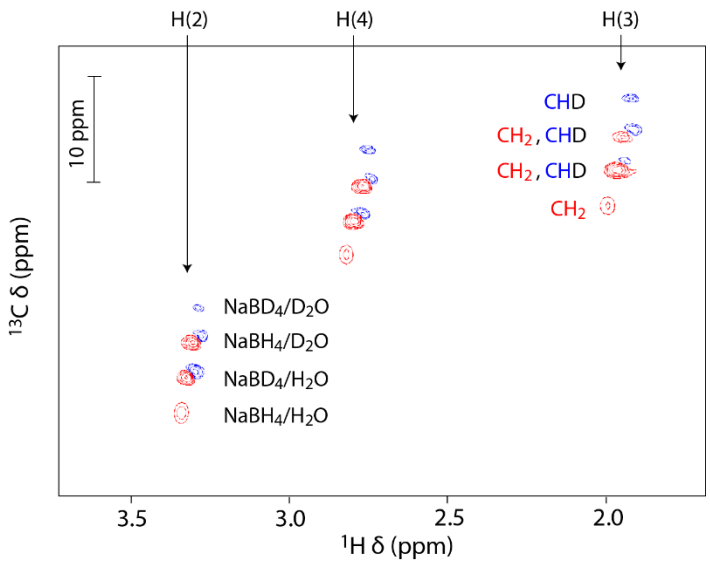

Figure 4.3 Overlay of the aliphatic regions of phase-sensitive multiplicity-edited ^{1}H-^{13}C HSQC spectra of the four samples considered. Red negative correlations indicate CH_2 whereas blue positive correlations indicate CHD groups. The spectra are vertically displaced for clarity.

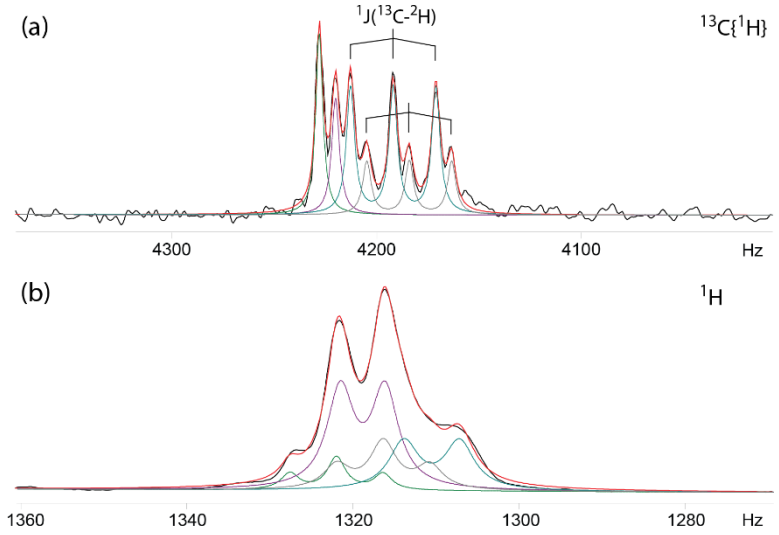

Figure 4.4 (a) Numerical fit (red) of the C(2) region of a proton-decoupled ^{13}C NMR spectrum (black) of THQ prepared with $NaBH_4/D_2O$. The singlets at higher frequencies represent two proton-decoupled CH_2 groups, whereas two 1:1:1 triplets at lower frequencies represent CHD groups. (b) Numerical fit (red) of the H(2) region of a ^{1}H spectrum (black) of the same sample of (a) assuming one C<u>H</u>$_2$-CH_2 as 1:2:1 triplet, one C<u>H</u>$_2$-CHD as 1:1 doublet, one C<u>H</u>D-CH_2 as 1:2:1 triplet and one C<u>H</u>D-CHD as 1:1 doublet, from higher to lower frequencies, respectively, and in agreement with the order of carbon resonances observed in (a). Heteronuclear $^{2,3}J(^{1}H$-$^{2}H)$

couplings are not included in (b), as the resulting splittings (ca. 1–2 Hz) are smaller than the homogeneous/inhomogeneous line width and are implicitly taken into account as line broadening by the numerical fit. For both ^{13}C and ^{1}H spectra, a low-frequency shift is observed as ^{2}H nuclei are progressively added. Numerical fits were performed with the DMfit software [40].

When integrals need to be measured accurately in NMR experiments, one has to make sure that signal averaging is done over experiments performed on fully relaxed systems. This is commonly accomplished by using a recycling delay d_1 between signal acquisitions of $d_1 = 5 \times T_1$. A subsequent measurement of the longitudinal relaxation time constant T_1 was therefore performed on the four samples considered in this study by means of an inversion-recovery experiment. The resulting T_1 values are shown, as histogram, in Figure 4.5.

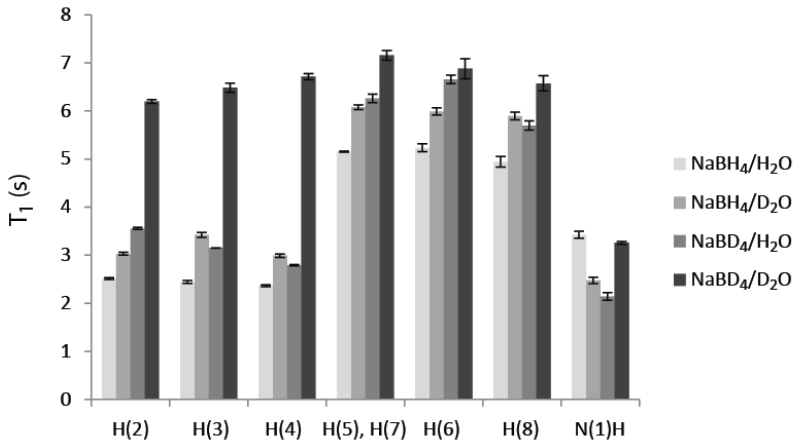

Figure 4.5 Longitudinal relaxation time constants T_1 as measured on the four samples considered in this study with an inversion-recovery experiment. The error bars were calculated as $\pm\sigma$, with σ being the standard deviation of the T_1 values produced by the numerical fits performed on eight data points as produced by the experiment.

It is clear that, as deuterium nuclei are progressively added in the system with the different reduction conditions, an increase of T_1 values is observed as result of the consequent removal of proton-proton intramolecular homonuclear dipolar couplings which act as a source of relaxation. The longest T_1 value for each case was used to estimate the appropriate recycling delay for ^{1}H NMR spectra of the four samples

considered. In such a fashion, the integral values that obtained can be taken as an accurate measurement of the relative levels of deuteration at the various chemical sites within the THQ molecule. The corresponding results are shown in Figure 4.6 as histogram. The integrals were normalized to the value of the signal due to the overlapped H(5) and H(7) at 7.01 ppm.

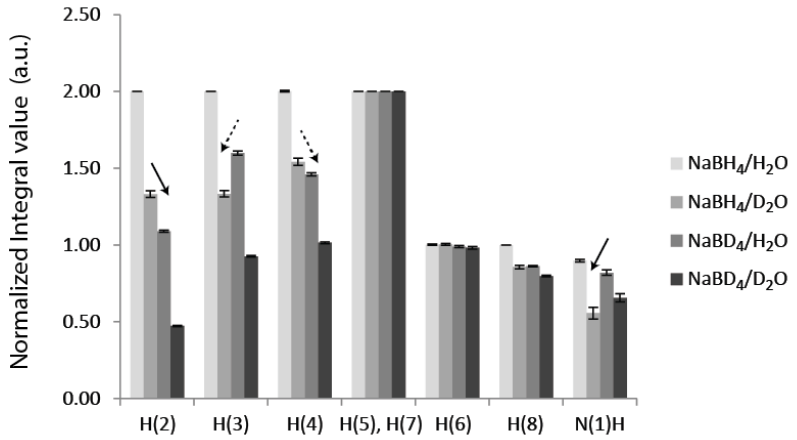

Figure 4.6 Integral values of the various proton resonances of THQ for the various samples considered. The normalization has been performed with respect to the overlapped signals of C(5) and C(7). The error bars were calculated as ±σ, with σ being the standard deviation of the values produced by five independent integrations.

The catalytic quinoline reduction is quantitative, as one can clearly see for the $NaBH_4/H_2O$ case, the measured integral values being 2 and 1 for aliphatic and aromatic protons, respectively, with deviations of only 1%. The N<u>H</u> integral in this case is 0.95. The 5% deviation from the ideal value of this site may be reasonably ascribed to the much larger line width as compared to all other resonances. When ^2H nuclei are involved in the reduction process, one observes a clear decrease of the integrals for the sites 2, 3 and 4, with intensities $1 < I < 2$, representing a mixture of CH_2 and CHD containing species, an ideal and quantitative reduction with only deuterium nuclei would yield $I = 1$ for these sites. Similar results are obtained in the $NaBH_4/D_2O$ and $NaBD_4/H_2O$ cases. Interestingly, also the aromatic site 8 in the *C*-cycle undergoes a significant decrease in signal intensity, which clearly is the result

of a CH → CD exchange/substitution. As only ^{2}H species are involved in the reaction for the $NaBD_4/D_2O$ case, a further decrease in intensity is observed for all aliphatic sites, with $I < 1$, indicating that CD_2 species appear in the sample as a result of a CHD → CD_2 process similar to that observed for site 8. Possible exchanges in sites 5 and 7 cannot be monitored by this approach, since these resonances have been used as reference to calibrate all integral values. One may, however, assume that, if any exchange happens on these sites, it has to be very similar to that of site 6. As the integral of this latter seems to be substantially insensitive to the various experimental conditions explored in this study, we suggest that exchanges in sites 5, 6 and 7 may be ignored in this context. Therefore, the sites that appear to be particularly susceptible to reduction in the quinoline molecule are sites 2, 3, 4 and surprisingly also site 8, from higher to lower reactivity, respectively.

Because of the complications by the known slow H/D exchange between the BH_4^- anion and D_2O (or the BD_4^- anion and H_2O) [38] and also by the observed H/D exchange of the C-H and N-H functions in the THQ molecule (even in the *C*-cycle), the data do not allow unambiguous mechanistic considerations. Nevertheless, it is obvious that, in the most meaningful cases $NaBH_4/D_2O$ and $NaBD_4/H_2O$, all hydrogenated positions are partially deuterated, in the first case the degree of deuteration in C(2) is slightly lower than in the second case, but in the N(1) position this ratio is inversed (black arrows in Figure 4.6), and a similar trend is observed for the positions C(4) and C(3) (dashed arrows in Figure 4.6).

In silico computations of molecular properties can be very useful for the rationalization of experimental data. In particular, semi-empirical methods have been used with success in a variety of structural studies [41–43]. In this context, calculations of the net atomic charges associated to each nuclear site within both Q and 1,2,3,4-THQ molecules were carried out at the PM7 semi-empirical level with the code MOPAC2012 and electrostatic potential surfaces were computed by means of the keyword ESP [44]. Furthermore, 1,2-dihydroquinoline (1,2-DHQ) was considered as a possible intermediate. The results are summarized in Figure 4.7, where the net

charges of Q, 1,2-DHQ and 1,2,3,4-THQ are shown from 4.7a to 4.7c, respectively. In Figure 4.7d–f, the corresponding electrostatic potential surfaces generated by these charges are illustrated. With respect to the Q molecule, the most positively charged carbon atom in the *N*-cycle is, as expected, C(2), suggesting an initial attack of hydride anions to this position. The preferred site for a subsequence proton attack is the nitrogen atom. A second hydride attack on the *N*-cycle finds C(4) as preferred site, given the lower net negative charge as compared to C(3). It is also worth noting that the most positively charged proton on the *C*-cycle is H(8). This is in agreement with the experimental observation that this proton is also exchanged/substituted by deuterium in the $NaBD_4/D_2O$ case.

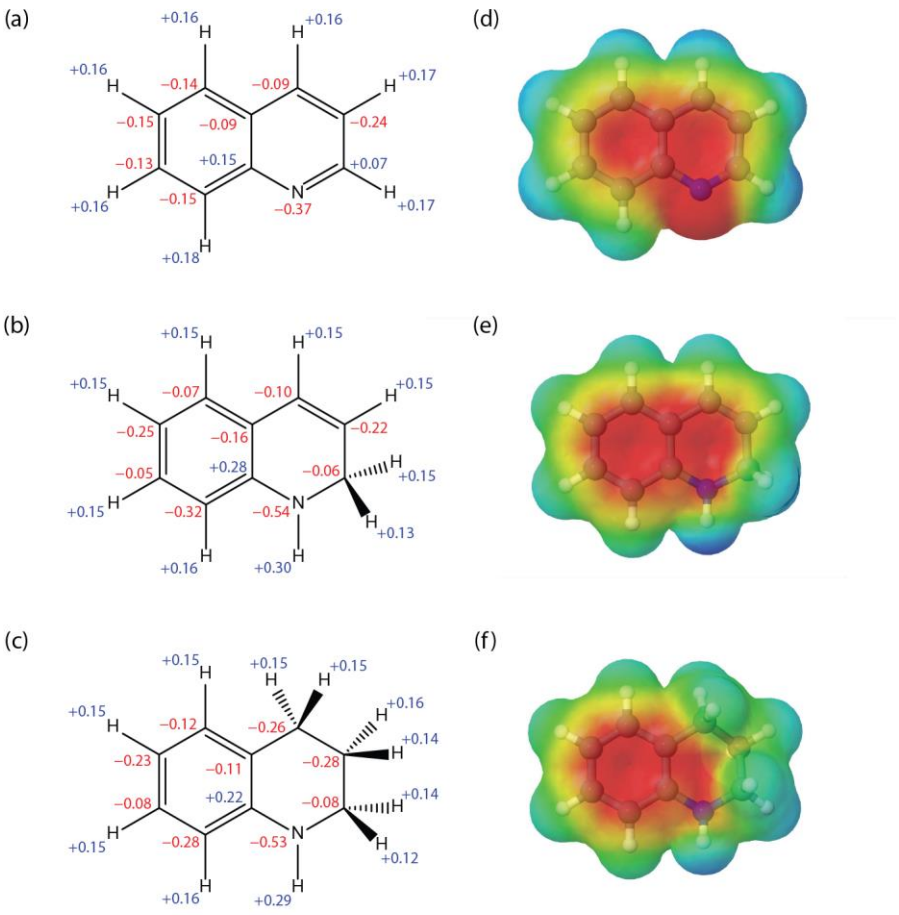

Figure 4.7 Net atomic charges of the nuclear sites in Q, 1,2-DHQ and THQ molecules (a, b and c) along with the surfaces of the electrostatic potentials (d, e and f), plotted from –0.1 V (red) to +0.1 V (blue).

The following conclusions are consistent with the data: i) Sodium borohydride is not the single hydrogen source and water is not an innocent solvent; the hydrogen for the hydrogenation of the *N*-cycle of the quinoline molecule comes from both $NaBH_4$ and H_2O. ii) The hydrogenation seems to be accomplished by a transfer of a hydride (H^-) from the borohydride anion and of a proton (H^+) from the water molecule. iii) The hydride anion is more likely to attack at first the most electron-poor atom of the quinoline molecule C(2), while the proton is likely to attack then the most electron-rich atom of the quinoline molecule N(1). The following step of the reduction involves the attack of a H^- species on C(4), then followed by a H^+ attack on C(3), in accordance with the analysis of the integral values of our isotope labeling study and with the net charges calculated for the different positions (Figure 4.7). This model is also in line with the observed *C*-cycle hydrogenation instead of the *N*-cycle hydrogenation in the case of 2-phenylquinoline, where the C(2) position is blocked by a phenyl substituent (entry 13, Table 4.2).

4.2.5 Catalyst recyclability

The recyclability of *nano*Ru′@hectorite was studied with the hydrogenation of Q to 1,2,3,4-THQ (entry 7, Table 4.1) as model. After a catalytic run, the catalyst was recovered by centrifugation and purified by washing with deionized H_2O and ethyl acetate and dried *in vacuo* at room temperature for 12 h. Then the recycled catalyst was used directly in the next catalytic run without reactivation. As depicted in Figure 4.8, the conversion of Q slightly declined from 99% to 95% after 4 cycles, but the conversion was maintained at 99%. TEM images (Figure 4.2) shows that the clusters of ruthenium nanoparticles retain their spherical shape and the size of the nanoparticles stays within a narrow size distribution of 1.5–3 nm. Ruthenium leaching during the catalytic reactions was found by ICP-OES analysis to be inferior to 2 ppm.

4.3 Conclusions

In summary, we report a simple method for preparing a new hectorite-supported ruthenium precatalyst, which has an exceptional catalytic activity and selectivity for the hydrogenation of the *N*-cycle of quinolines and analogs by sodium borohydride in aqueous media, mostly without pressure equipment. Isotope labelling studies demonstrate the participation of water in the hydrogenation reaction by providing protons. Transition electron microscopy shows the catalyst to contain metallic ruthenium nanoparticles agglomerated to spherical clusters intercalated in the hectorite clay (*nano*Ru′@hectorite). The catalyst can be recycled and reused for further catalytic runs.

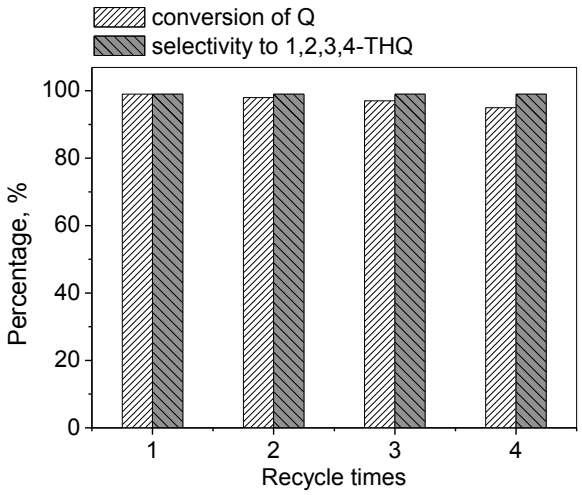

Figure 4.8 Reactivity and selectivity of *nano*Ru'@hectorite catalyst in recycling tests for the hydrogenation of Q to 1,2,3,4-THQ in water under atmospheric pressure at 60 °C for 4 h.

References

[1] V. Sridharan, P. A. Suryavanshi, J. C. Menendez, Chem. Rev. 111 (2011) 7157–7259.

[2] R. Omar-Amrani, A. Thomas, E. Brenner, R. Schneider, Y. Fort, Org. Lett. 5 (2003) 2311–2314.

[3] T. Kubo, C. Katoh, K. Yamada, K. Okano, H. Tokuyama, T. Fukuyama, Tetrahedron 64 (2008) 11230–11236.

[4] K. Maruoka, T. Miyazaki, M. Ando, Y. Matsumura, S. Sakane, K. Hattori, H. Yamamoto, J. Am. Chem. Soc. 105 (1983) 2831–2843.

[5] C. H. Bartholomew, Appl. Catal. A: Gen. 212 (2001) 17–60.

[6] S. Nishimura, *Handbook of Heterogeneous Catalytic Hydrogenation for Organic Synthesis*, WILEY, New York, 2001.

[7] S. M. Lu, X. W. Han, Y. G. Zhou, J. Organomet. Chem. 692 (2007) 3065–3069 (and references cited therein).

[8] W. B. Wang, S. M. Lu, P. Y. Yang, X. W. Han, Y. G. Zhou, J. Am. Chem. Soc. 125 (2003) 10536–10537.

[9] H. Zhou, Z. Li, Z. Wang, T. Wang, L. Xu, Y. He, Q. H. Fan, J. Pan, L. Gu, A. S. C. Chan, Angew. Chem. Int. Ed. 47 (2008) 8464–8467.

[10] D. Ren, L. He, L. Yu, R. S. Ding, Y. M. Liu, Y. Cao, H. Y. He, K. N. Fan, J. Am. Chem. Soc. 134 (2012) 17592–17598.

[11] N. Hashimoto, Y. Takahashi, T. Hara, S. Shimazu, T. Mitsudome, T. Mizugaki, K. Jitsukawa, K. Kaneda, Chem. Lett. 39 (2010) 832–834.

[12] R. Rahi, M. Fang, A. Ahmed, R. A. Sánchez-Delgado, Dalton Trans. 41 (2012) 14490–14497.

[13] Y. Gong, P. Zhang, X. Xu, Y. Li, H. Li, Y. Wang, J. Catal. 297 (2013) 272–280.

[14] M. Campanati, A. Vaccari, O. Piccolo, J. Mol. Catal. A: Chem. 179 (2002) 267–272.

[15] M. Campanati, M. Casagrande, I. Fagiolino, M. Lenarda, L. Storaro, M. Battagliarin, A. Vaccari, J. Mol. Catal. A: Chem. 184 (2002) 287–292.

[16] M. Fang, N. Machalaba, R. A. Sánchez-Delgado, Dalton Trans. 40 (2011)10621–10632.

[17] L. M. Zhou, X. L. Qi, X. H. Jiang, Y. F. Zhou, H. Y. Fu, H. Chen, J. Colloid. Interface Sci. 392 (2013) 201–205.

[18] M. Fang, R. A. Sánchez-Delgado, J. Catal. 311 (2014) 357–368.

[19] F. Fache, Synlett 15 (2004) 2827–2829.

[20] C. Michel, J. Zaffran, A. M. Ruppert, J. Matras-Michalska, M. Jędrzejczyk, J. Grams, P. Sautet, Chem. Commun. 50 (2014) 12450–12453.

[21] L. Zhang, X.Y. Wang, Y. Xue, X.J. Zeng, H. Chen, R. X. Li, S. L. Wang, Catal. Sci. Technol. 4 (2014) 1939–1948.

[22] H. Mao, C. Chen, X. Liao, B. Shi, J. Mol. Catal. A: Chem. 341 (2011) 51–56.

[23] H. Mao, J. Ma, Y. Liao, S. L. Zhao, X. P. Liao, Catal. Sci. Technol. 3 (2013) 1612–1617.

[24] M. M. Dell'Anna, V. F. Capodiferro, M. Mali, D. Manno, P. Cotugno, A. Monopoli, P. Mastrorilli, Appl. Catal. A: Gen. 481 (2014) 89–95.

[25] A. Meister, G. Meister, G. Süss-Fink, J. Mol. Catal. 92 (1994) L123–L126.

[26] G. Süss-Fink, B. Mollwitz, B. Therrien, M. Dadras, G. Laurenczy, A. Meister, G. Meister, J. Clust. Sci. 18 (2007) 87–95.

[27] G. Süss-Fink, F. A. Khan, J. Boudon, V. Spassov, J. Clust. Sci. 20 (2009) 341–353.

[28] B. Sun, F. A. Khan, A. Vallat, G. Süss-Fink, Applied Catal. A: Gen. 467 (2013) 310–314.

[29] M. M. Dell'Anna, G. Romanazzi, S. Intini, A. Rizzuti, C. Leonelli, A. F. Piccinni, P. Mastrorilli, J. Mol. Catal. A: Chem. 402 (2015) 83–91.

[30] D. Astruc, *Nanoparticles and Catalysis*, WILEY-VCH, Weinheim, 2008.

[31] C. L. Kitchens, M. C. McLeod, C. B. Roberts, J. Phys. Chem. B 107 (2003) 11331–11338.

[32] J. Song, D. Kim, D. Lee, Langmuir 27 (2011) 13854–13860.

[33] B. S. Akpa, C. D'Agostino, L. F. Gladden, K. Hindle, H. Manyar, J. McGregor, R. Li, M. Neurock, N. Sinha, E. H. Stitt, D. Weber, J. A. Zeitler, D. W. Rooney, J. Catal. 289 (2012) 30–41.

[34] H. J. Wan, A. Vitter, R. V. Chaudhari, B. Subramaniam, J. Catal. 309 (2014) 174–184.

[35] R. Yang, S. G. Schulman, Luminescence 16 (2001) 129–133.

[36] M. Hönel, F. W. Vierhapper, J. Chem. Soc., Perkin Trans. 1 (1980) 1933–1939.

[37] Y. P. Sun, H. Y. Fu, D. L. Zhang, R. X. Li, H. Chen, X. J. Li, Catal.Commun. 12 (2010) 188–192.

[38] R. E. Mesmer, W. L. Jolly, Inorg. Chem. 1 (1962) 608–612.

[39] R. E. Davis, E. Bromels, C. L. Kibby, J. Am. Chem. Soc. 84 (1962) 885–892.

[40] D. Massiot, F. Fayon, M. Capron, I. King, S. Le Calvé, B. Alonso, J. O. Durand, B. Bujoli, Z. H. Gan, G. Hoatson, Magn. Reson. Chem. 40 (2002) 70–76.

[41] D. Carnevale, V. Del Amo, D. Philp, S. E. Ashbrook, Tetrahedron 66 (2010) 6238–6250.

[42] D. Carnevale, A. J. Perez Linde, G. Bauer, G. Bodenhausen, Chem. Phys. Lett. 580 (2013) 172–178.

[43] N. Salvi, J. Frey, D. Carnevale, M. Grätzel, G. Bodenhausen, Dalton Trans. 43 (2014) 6389–6395.

[44] B. H. Besler, K. M. Merz Jr., P. A. Kollman, J. Comp. Chem, 11 (1990) 431–439.

5

Chemoselective hydrogenation of aromatic amino acids catalyzed by ruthenium nanoparticles intercalated in hectorite

5.1 Introduction

The design of nanocomposites consisting of functional metals and proper matrices is a very active field of research for the development of recyclable catalysts. Highly active metallic nanoparticles must be stabilized by a suitable support in order to prevent aggregation to bulk metal [1]. As mentioned in the previous chapters, hectorite is naturally occurring clay with smectite structure that possesses the features of cation exchange, intercalation and swelling properties [2]. The sodium cations in the interlaminar space are susceptible to ion exchange [2–4]. There have been a number of reports on the immobilization of transition metal particles or metal complexes by hectorite involving rhodium [5, 6] and platinum [7] for the catalytic hydrogenation of olefins and α,β-unsaturated aldehydes. Ruthenium-supported hectorite catalysts have been reported by Shimazu et al. using $[Ru(NH_3)_6]^{3+}$ as precursor [8] and by our group using $[(C_6H_6)Ru(H_2O)_3]^{2+}$ cations [9–14] or $[(C_6H_6)_4Ru_4H_4]^{2+}$ cations [15] as precursors for the intercalation. In particular, ruthenium nanoparticles (3–27 nm) intercalated in hectorite (*nano*Ru@hectorite) proved to be a highly active and selective catalyst for the hydrogenation of benzene [9–11], furfuryl alcohol [12], α,β-unsaturated ketones [13] and quinoline [14].

Unnatural amino acids are important structural motifs for peptides, peptide-mimetics, synthetases and pharmaceuticals [16–18]. The synthesis of unnatural amino acids has received a tremendous impact from homogeneous [19–21], heterogeneous [22–28] and enzymatic catalysis [29–32]. Featured by high efficiency and enantioselectivity as well as by comparatively mild operating conditions, homogeneous catalysis and enzymatic catalysis show advantages as compared with their heterogeneous counterpart. However, considering the increasing demand of unnatural amino acids and the possibility of the contamination by the catalyst to the product in the separation section, a heterogeneous process for the manufacturing of these compounds would be more attractive. From this point of view, supported metal catalysts for the synthesis of optically pure unnatural amino acids have been

developed.

A number of heterogeneous catalytic systems have been exploited to selectively convert phenyl rings into saturated cyclohexyl rings. Noble metals, such as Pd [22, 33], Pt [23], Ru [24, 26] and Rh [25, 27, 28] supported on carbon or Al_2O_3, are the most widely studied catalysts. The solubility of the aromatic amino acids in water is low, but it can be improved in acidic or basic medium. Depending on the catalyst employed, the pH plays an important role in the hydrogenation of aromatic amino acids. For example, for the hydrogenation of (R)-phenylglycine, palladium on charcoal under basic conditions gave only phenylacetic acid [33], however, the expected (R)-cyclohexylglycine can be formed over $Pd(OH)_2$ on charcoal in the pH range of 4.5 to 8.0 with 66% conversion and 84% *e.e*. [22]. To the best of our knowledge, a very limited number of supported catalysts have been reported to selectively hydrogenate phenyl-substituted amino acids into cyclohexyl-substituted amino acids with high *e.e.*, such as Ru on carbon [24, 26], Rh on carbon [25] and Rh on Al_2O_3 [27]. Among these catalytic systems, only Rh on carbon seems to be recyclable.

In this chapter, metallic ruthenium nanoparticles intercalated in hectorite (*nano*Ru@hectorite) are reported as a highly active and selective catalyst for the hydrogenation of aromatic amino acids in aqueous solution. The effect of the pH on the hydrogenation processes is thoroughly discussed. The recovery and reusability of the *nano*Ru@hectorite catalyst for further runs are investigated.

5.2 Results and discussion

5.2.1 Characterization of the *nano*Ru@hectorite catalyst

The *nano*Ru@hectorite catalyst is prepared from the ruthenium(II)-containing hectorite precatalyst described in Chapter 2 and 3. The d-spacing (d_{001}) of the sodium hectorite and Ru(II)-containing hectorite are 13.4 Å and 14.6 Å, respectively (Figure

2.2). The swelling layers distance refers to the interaction between the adsorbed ruthenium complexes and the intercalant in hectorite [2]. When suspended in the appropriate solvent, this precursor can be then reduced by molecular hydrogen to give the active *nano*Ru@hectorite catalyst, an air-sensitive black powder [10].

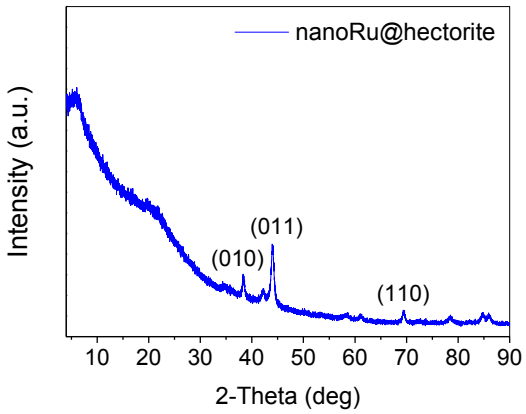

Figure 5.1 XRD pattern of Ru(0) nanoparticles intercalated in hectorite (*nano*Ru@hectorite) obtained under a H_2 pressure of 50 bar at 100 °C for 14 h in water (10 ml).

The ruthenium loading of *nano*Ru@hectorite is assumed to be 3.2 wt% [9], based upon the molar ratio of $[(C_6H_6)RuCl_2]_2$ used (corresponding to 75% of the experimentally determined cation exchange capacity [34]) and the presence of the metallic ruthenium is evidenced by its typical reflections in the XRD pattern (Figure 5.1). Calculated from the line broadening of Ru(011) X-ray reflection using the Scherrer equation, the crystal system being assumed hexagonal (Figure 5.2b), the crystallite size is approximately 15 nm. However, a typical TEM micrograph with a statistical diameter calculation (Figure 5.2a, 5.2d) results in a mean particle size (d_{ave}) of 24 nm and the standard deviation (σ) of 3.5 nm. The different diameters from XRD and TEM suggest that the ruthenium nanoparticles are partially polycrystalline, which is shown by selected area electron diffraction (SAED) pattern (Figure 5.2c).

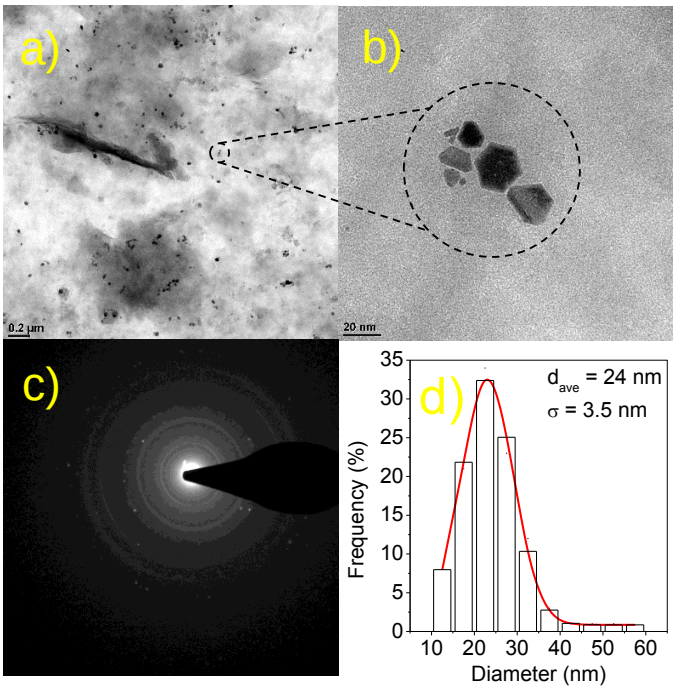

Figure 5.2 (a) TEM micrograph (the scale bar 0.2 µm) of the dispersed ruthenium nanoparticles in hectorite. (b) The enlarged TEM micrograph (the scale bar 20 nm) for ruthenium nanoparticles clearly shows a hexagonal morphology. (c) A SAED pattern displays a series of bright rings relevant to the polycrystalline. (d) The size distribution of the ruthenium nanoparticles is presented in the histogram, the diameter ranging from 10 to 60 nm with a mean particle size of 24 ± 3.5 nm.

5.2.2 Catalytic hydrogenation of amino acids

The hydrogenation of chiral aromatic amino acids often requires mild conditions in order to avoid racemization. The protection of the benzylic C–N bond and carboxylic group is a common method to avoid the hydrogenolytic cleavage of C–N bond [27]. Water as a solvent allows the variation of the pH, which can be used to dissolve the tested amino acids, because in acidic or basic solution amino acids are present in cationic or anionic form. With *nano*Ru@hectorite as a heterogeneous catalyst, the hydrogenation of a series of aromatic amino acids can be catalyzed to produce the corresponding cyclohexyl-substituted amino acids.

The solvents effect on the product selectivity in the catalytic reactions has been proven in a number of studies [35–38]. A series of solvents examined for the

hydrogenation of L-phenylalanine (LPA), as shown in Figure 5.3. The preliminary results indicate that water is so far the best reaction medium, in which the conversion of LPA reaches to 99%. A continuous optimization is required for the hydrogenation of amino acids in the aqueous reaction system.

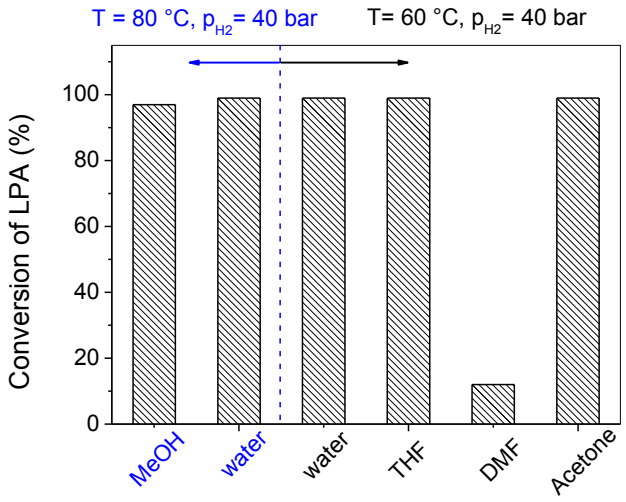

Figure 5.3 The histograms of the correlation of solvents and LPA conversion under a constant H_2 pressure of 40 bar at 60 °C and 80 °C for methanol, water, THF, DMF and acetone.

Since *nano*Ru@hectorite catalyst is prepared from the ruthenium(II)-containing hectorite precursor by hydrogen reduction in aqueous solution, the suspension of *nano*Ru@hectorite in water is slightly basic (pH = 9). Table 5.1 shows activity and selectivity of the catalyst for LPA hydrogenation under different reaction conditions. Under a H_2 pressure of 40 bar with a low substrate to metal ratio (entry 1, Table 5.1), the catalytic hydrogenation of LPA to give L-cyclohexylalanine is complete in 120 h at room temperature without racemization, the selectivity being over 99%. With a higher substrate to metal mole ratio of 76, the conversion is only 52% under the same conditions, although the selectivity is still high (entry 2, Table 5.1), the main reason being that the aqueous solution at pH = 9 does not fully dissolve the substrate at room temperature. The solubility can be improved by higher temperature and the best conditions are 60 °C and 40 bar H_2 with a substrate to metal mole ratio of 106, which

gives full conversion and high selectivity (entry 4, Table 5.1). A higher loading of substrate does not lead to full conversion even at higher temperature for 24 h (entry 6, 7, Table 5.1). A blank experiment was carried out without a catalyst (entry 5, Table 5.1), however, no conversion was observed, proving that *nano*Ru@hectorite is essential for the studied catalytic hydrogenation.

Table 5.1

Hydrogenation of LPA over *nano*Ru@hectorite in aqueous solution.

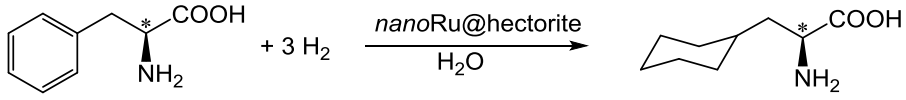

Entry[a]	S/M[b]	T, °C	p_{H2}, bar	t, h	C, %[c]	S, %[d]
1	38	20	40	120	> 99	> 99
2	76	20	40	120	52	> 99
3	106	60	30	24	96	> 99
4	106	60	40	18	> 99	> 99 (92)
5[e]	106	60	40	18	0	0
6	114	90	40	24	64	> 99
7	114	100	40	24	87	> 99

[a] The catalysts being prepared under a H_2 pressure of 50 bar at 100 °C for 14 h in 10 mL water (the same catalyst *nano*Ru@hectorite hereinafter, otherwise noted). [b] Substrate to metal mole ratio (hereinafter referred to as S/M, otherwise noted). [c] Conversion of LPA. [d] Selectivity for L-cyclohexylalanine, the value in parentheses being the isolated yield. [e] No catalyst in the system.

We varied the pH of the aqueous solution from 1 to 14 by adding appropriate amount of acid (2N HCl or 1N H_2SO_4) or base (1N NaOH or KOH). As shown in Table 5.2, LPA can be hydrogenated exclusively to L-cyclohexylalanine in all cases (entry 3–7, Table 5.2). Unlike Ru supported on carbon [24, 26] and Rh on Al_2O_3 [27], *nano*Ru@hectorite catalyzes the hydrogenation of LPA even under neutral aqueous solution, which offers a good opportunity for a scale-up production.

Table 5.2

Hydrogenation of LPA over *nano*Ru@hectorite in water at different pH.

Entry[a]	pH	S/M	T, °C	p_{H2}, bar	t, h	C[b], %	S[c], %
1	1[d]	114	100	40	24	60	> 99
2	9	114	100	40	24	87	> 99
3	1[d]	106	60	40	12	> 99	> 99
4	4[d]	106	60	40	18	> 99	> 99
5	7[d]	106	60	40	18	> 99	> 99
6	9	106	60	40	18	> 99	> 99 (92)
7	14[e]	106	60	40	12	> 99	> 99

[a] The catalysts *nano*Ru@hectorite. [b] Conversion of LPA. [c] Selectivity for L-cyclohexylalanine, the value in parentheses being the isolated yield. [d] pH adjusted by adding 2N HCl or 1N H_2SO_4. [e] pH adjusted by adding 2N NaOH or 2N KOH.

Table 5.3

Hydrogenation of LPG over *nano*Ru@hectorite in water at different pH.

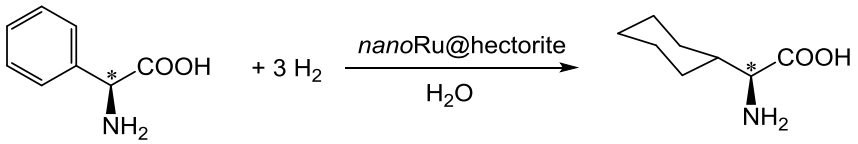

Entry[a]	pH[b]	S/M	T, °C	p_{H2}, bar	t, h	C[c], %	S[d], %
1	1	118	60	40	12	> 99	> 99
2	9	118	60	40	48	89	> 99
3	11	118	60	40	24	89	> 99
4	13	118	60	40	24	90	> 99
5	14	118	60	40	12	> 99	> 99 (94)

[a] The catalysts *nano*Ru@hectorite. [b] pH adjusted by adding 2N NaOH (KOH), or 2N HCl (1N H_2SO_4). [c] Conversion of LPG. [d] Selectivity for L-cyclohexylglycine, the value in parentheses being the isolated yield.

We also examined other aromatic amino acids containing aromatic substituents for the hydrogenation over *nano*Ru@hectorite in aqueous solution. It turned out that the reaction works well when the substrate contains an unsubstituted phenyl group as

in LPA. As shown in Table 5.3, L-phenylglycine (LPG) is successfully converted into L-cyclohexylglycine with more than 99% conversion and selectivity, either in very acidic (pH=1) or basic condition (pH=14). However, incomplete conversion of LPG was observed over a pH range from 2 to 13, the reason being the low solubility of LPG in a less acidic or basic solution.

We also extended our study to L-tyrosine (LTR), which contains a hydroxyl group at the aromatic ring. Initially examined by Waser et al. [39], the hydrogenation of tyrosine under acidic conditions (1N HCl) produced a mixture of hexahydrotyrosine (10%) and β-cyclohexylalanine (90%) catalyzed by PtO_2. The electrostatic stability of the hydroxyl-substituted phenyl group is higher than that of phenyl ring, since the hydroxyl function increases the electron density of the phenyl ring. Therefore, harsher conditions are required to activate the hydrogenation process. As shown in Table 5.4, with *nano*Ru@hectorite as catalyst, the conversion of LTR only proceeds under acidic and harsh conditions (100 °C, 50 bar H_2, 24 h) to give a maximum conversion of 93% with a selectivity of 50%, the by-product being cyclohexylalanine. The selectivity for L-hexahydrotyrosine can be increased to 65% but at the expense of the conversion (76%) by lowing pressure and temperature.

Table 5.4

Hydrogenation of LTR over *nano*Ru@hectorite in water at different pH.

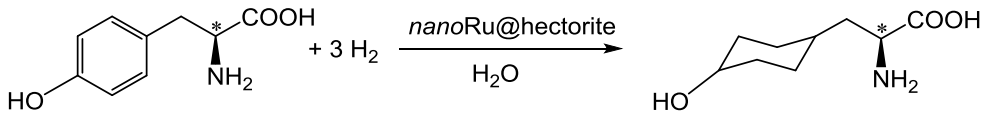

Entry[a]	pH[b]	S/M	T, °C	p_{H2}, bar	t, h	C[c], %	S[d], %
1	1	106	60	40	18	76	65
2	1	78	100	50	24	93	50
3	14	106	60	40	24	0	0
4	14	106	100	50	24	0	0

[a] The catalysts *nano*Ru@hectorite. [b] pH adjusted by adding 2N NaOH (KOH) or 2N HCl (1N H_2SO_4). [c] Conversion of LTR. [d] Selectivity for L-hexahydrotyrosine.

L-3-(octahydroindolyl)alanine is an important unusual amino acid in the synthesis of peptides. Therefore the catalytic hydrogenation of L-tryptophan (LTP) to produce this amino acid is an attractive process. Until today, there is no heterogeneous catalyst reported for this reaction. We examined the *nano*Ru@hectorite catalyst for the hydrogenation of LTP in aqueous solution with different pH, as summarized in Table 5.5. Both acidic and basic conditions are possible for the hydrogenation of LTP, but complete conversion was obtained at pH = 14 with 63% selectivity. However, under all these conditions, L-4,5,6,7-tetrahydrotryptophan as by-product was always formed, which may be explained by the poisoning effect of the amine group in the indole moiety to the catalyst [40, 41], which hampers the further hydrogenation of the pyrrole ring.

Table 5.5

Hydrogenation of L-tryptophan (LTP) over *nano*Ru@hectorite in water at different pH.

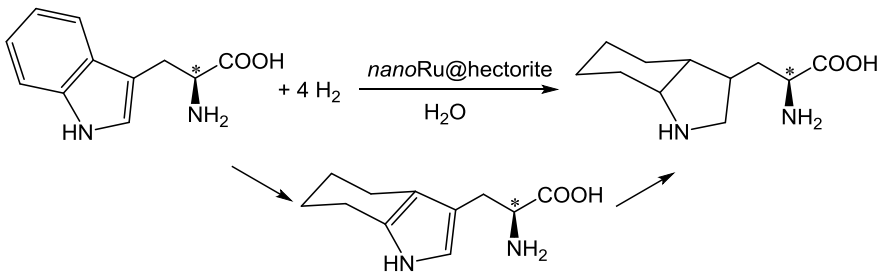

Entry[a]	pH[b]	S/M	T, °C	p_{H2}, bar	t, h	C[c], %	S[d], %
1	1	53	60	40	24	33	50
2	1	53	80	40	24	53	50
3	1	78	100	50	24	65	77
4	14	78	100	50	24	> 99	63
5	14	106	100	50	24	91	58

[a] The catalysts *nano*Ru@hectorite. [b] pH adjusted by adding 2N NaOH (KOH), or 2N HCl (1N H_2SO_4). [c] Conversion of LTP. [d] Selectivity for L-3-(octahydroindolyl)alanine.

5.2.3 Catalyst recyclability

The recyclability of the catalyst for four consecutive catalytic runs by separating the catalyst after each run and reactivating it under hydrogen pressure has been examined in the case of LPA (entry 3, Table 5.2). As shown in Figure 5.4, the recycled catalyst remains highly active and selective in the first three runs, giving exclusively L-cyclohexylalanine without racemization. However, in the fourth recycling process, the diameter of the ruthenium nanoparticles increased from 24 nm to 45 nm in average, resulting in hexagonal nanoparticles with a broader size distribution (Figure 5.5). Furthermore, partial aggregation of the ruthenium nanoparticles is observed, which leads to a drop in the catalytic activity, the conversion being decreased to 28%, the selectivity being still over 99% (Figure 5.4). Ruthenium leaching (2 ppm) is negligible, according to the ICP-OES analysis of the filtrate. The catalyst deactivation, caused by aggregation of the ruthenium nanoparticles, may be avoided by modifying the reactivation conditions of *nano*Ru@hectorite [10].

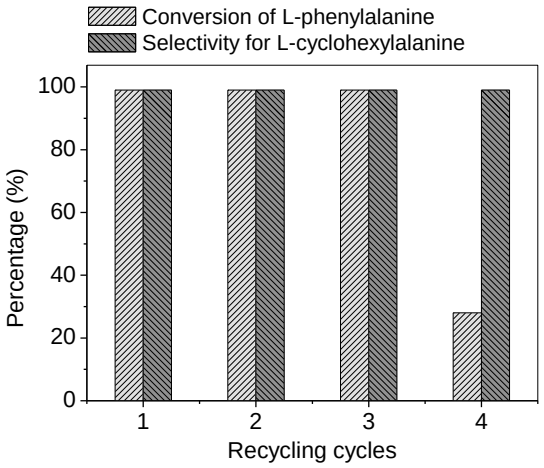

Figure 5.4 The recyclability of the *nano*Ru@hectorite catalyst for four catalytic runs of LPA. The first recycling was conducted following the regular catalytic run with fresh catalyst under the conditions of 40 bar H_2 at 60 °C for 18 h (as entry 4 in Table 5.1). All the recycling runs were performed under the same conditions as those with fresh catalyst.

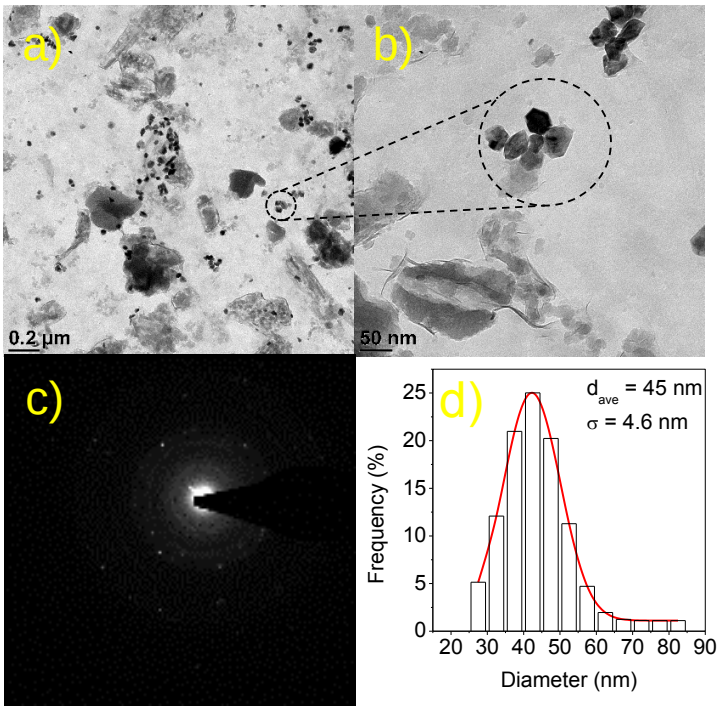

Figure 5.5 TEM micrographs of the *nano*Ru@hectorite catalyst after three catalytic runs of LPA (a, b). (c) A SAED pattern displays a series of bright rings relevant to the ruthenium poly-crystalline. (d) The mean particle size is 45 ± 4.6 nm.

5.3 Conclusions

In conclusion, the activity and selectivity of *nano*Ru@hectorite catalyst in the hydrogenation of chiral aromatic amino acids under different reaction conditions has been studied. *Nano*Ru@hectorite is a highly active catalyst that can catalyze the hydrogenation of L-phenylalanine in aqueous solution even at room temperature. The pH value plays an important role in varying the activity of the catalyst. Aromatic amino acids are hydrogenated to give the corresponding cyclohexyl-substituted amino acids without racemization. Recycling experiments show *nano*Ru@hectorite to be a stable catalyst that can be recovered and reused at least three times without loss of activity and selectivity.

References

[1] D. Astruc, F. Lu, J. R. Aranzaes, Angew. Chem. Int. Ed. 44 (2005) 7852–7872.

[2] T. J. Pinnavaia, Science 220 (1983) 365–371.

[3] J. L. Valverde, A. de Lucas, P. Sánchez, F. Dorado, A. Romero, Appl. Catal. B 43 (2003) 43–56.

[4] B. M. Choudary, M. L. Kantam, K. V. S. Ranganath, K. K. Rao, Angew. Chem. Int. Ed. 44 (2005) 322–325.

[5] T. J. Pinnavaia, P. K. Welty, J. Am. Chem. Soc. 97 (1975) 3819–3820.

[6] T. J. Pinnavaia, R. Raythatha, J. G. S. Lee, L. J. Halloran, J. F. Hoffman, J. Am. Chem. Soc. 101 (1979) 6891–6897.

[7] M. Dhanagopal, D. Duraiswami, R. A. Valentine, M. R. Viswanathan, S. Thiripuranthagan, Chin J Catal. 31 (2010) 1200–1208.

[8] S. Shimazu, T. Hirano, T. Uematsu, Appl. Catal. 34 (1987) 255–261.

[9] A. Meister, G. Meister, G. Süss-Fink, J. Mol. Catal. 92 (1994) L123–L126.

[10] G. Süss-Fink, B. Mollwitz, B. Therrien, M. Dadras, G. Laurenczy, A. Meister, G. Meister, J. Cluster Sci. 18 (2007) 87–95.

[11] G. Süss-Fink, F. A. Khan, J. Boudon, V. Spassov, J. Cluster Sci. 20 (2009) 341–353.

[12] F. A. Khan, A. Vallat, G. Süss-Fink, Catal. Comm. 12 (2011) 1428–1431.

[13] F. A. Khan, A. Vallat, G. Süss-Fink, J. Mol. Catal. A: Chem. 355 (2012) 168–173.

[14] B. Sun, F. A. Khan, A. Vallat, G. Süss-Fink, Appl. Catal. A 467 (2013) 310–314.

[15] G. Meister, G. Süss-Fink, unpublished. See G. Meister PhD Thesis, University of Neuchâtel, Switzerland, (1994).

[16] R. H. Thomson, *The Chemistry of Natural Products*. Springer Science + Business Media, B.V. (1993) 183–200.

[17] K. Aarstad, T. L. Zimmer, S. G. Laland, Eur. J. Biochem. 112 (1980) 335–338.

[18] G. Tóth, E. Ioja, C. Tömböly, S. Ballet, D. Tourwé, A. Péter, T. Martinek, N. N. Chung, P. W. Schiller, S. Benyhe, A. Borsodi, J. Med. Chem. 50 (2007) 328–333.

[19] R.M. Williams, J. A. Hendrix, Chem. Rev. 92 (1992) 889–917.

[20] C. Nájera, J. M. Sansano, Chem. Rev. 107 (2007) 4584–4671.

[21] Y. K. Chen, A. E. Lurain, P. J. Walsh, J. Am. Chem. Soc. 124 (2002) 12225–12231.

[22] M. Tamura, K. Harada, Synth. Commun. 8 (1978) 345–351.

[23] P. F. Schuda, W. J. Greenlee, P. K. Chakravarty, P. Eskola, J. Org. Chem. 53 (1988) 873–875.

[24] T. Sato, Y. Honda, K. Izawa, Eur. Pat. Appl. 97305973.6, (1997).

[25] A. J. Minnaard, W. H. J. Boesten, H. J. M. Zeegers, Synth. Commun. 29 (1999) 4327–4332.

[26] T. Sato, Y. Honda, K. Izawa, U.S. Pat. 6316660 B1, (2001).

[27] D. J. Ager, I. Prakash, Org. Process Res. Dev. 7 (2003) 164–167.

[28] T. Maegawa, A. Akashi, K. Yaguchi, Y. Iwasaki, M. Shigetsura, Y. Monguchi, H. Sajiki, Chem. Eur. J. 15 (2009) 6953–6963.

[29] C. G. Baker, A. Meister, J. Am. Chem. Soc. 73 (1951) 1336–1338.

[30] D. Rudman, A. Meister, J. P. Greenstein, J. Am. Chem. Soc. 74 (1952) 551–551.

[31] M. Beller, M. Eckert, H. Geissler, B. Napierski, H. P. Rebenstock, E. W. Holla, Chem. Eur. J. 4 (1998) 935–941.

[32] M. X. Wang, S. J. Lin, J. Org. Chem. 67 (2002) 6542–6545.

[33] K. Harada, J. Org. Chem. 32 (1967) 1790–1793.

[34] G. Lagaly, H. Tributh, Ber. Dt. Tonmineralgruppe 86 (1996).

[35] R. A. Rajadhyaksha, S. L. Karwa, Chem. Eng. Sci. 41 (1986) 1765–1770.

[36] S. Mukherjee, M. A. Vannice, J. Catal. 243 (2006) 108–130.

[37] S. Mukherjee, M. A. Vannice, J. Catal. 243 (2006) 131–148.

[38] B. S. Akpa, C. D'Agostino, L. F. Gladden, K. Hindle, H. Manyar, J. McGregor, R. Li, M. Neurock, N. Sinha, E. H. Stitt, D. Weber, J. A. Zeitler, D. W. Rooney, J. Catal. 289 (2012) 30–41.

[39] E. Waser, E. Brauchli, Helv. Chim. Acta 7 (1924) 740–758.

[40] C. H. Bartholomew, Applied Catalysis A: General 212 (2001) 17–60.

[41] L. Hegedűs, T. Máthé, Applied Catalysis A: General 226 (2002) 319–322.

6

Conclusions and perspectives

The aim of this thesis was to achieve a controlled synthesis of hectorite-supported ruthenium nanoparticles for catalytic hydrogenations and to explore their potential as a promising hydrogenation catalyst. Thanks to the screening of various ruthenium catalysts used for a variety of hydrogenation reactions, the mechanistic understanding of ruthenium-catalyzed hydrogenation has been also improved.

The synthetic approach for preparing the hectorite-intercalated ruthenium nano-particles includes the hydrolysis of benzene ruthenium dichloride dimer and the subsequent intercalation of benzene ruthenium(II) species into hectorite, followed by a reduction process. The *nano*Ru@hectorite thus prepared was found to be highly active and selective in catalyzing the hydrogenation of quinoline under mild conditions. As illustrated in Figure 6.1, a switchable selectivity was observed for exclusively yielding 1,2,3,4-tetrahydroquinoline or decahydroquinoline by using water or cyclohexane as reaction medium. The pathway of quinoline hydrogenation is presumably depending on the polarity of solvents.

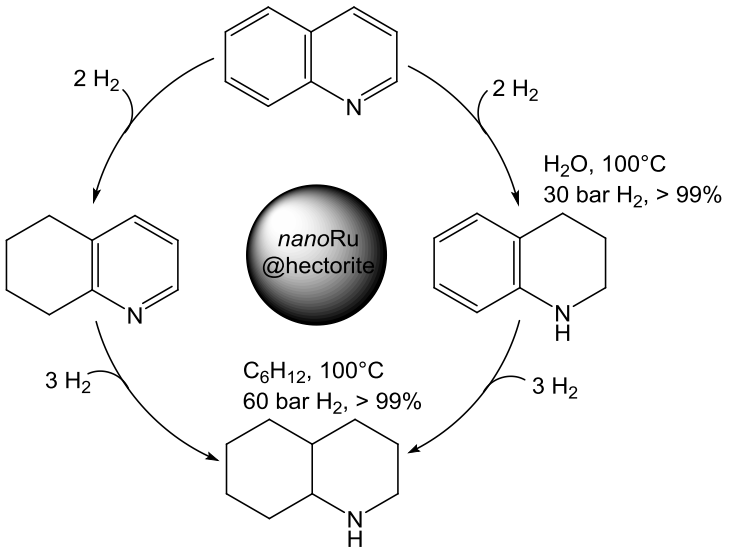

Figure 6.1 Graphical abstract of the hydrogenation of quinoline over *nano*Ru@hectorite.

Another hectorite-supported ruthenium(III) precatalyst was prepared via impregnation of sodium-hectorite with an aqueous solution of $RuCl_3 \cdot xH_2O$. The

hectorite-supported ruthenium nanoparticles, *in situ* formed from this material during the hydrogenation of quinoline with sodium borohydride in water, were found to catalyze the reaction efficiently. A variety of quinoline derivatives and analogues were, under atmospheric pressure, exclusively converted into the corresponding *N*-cycle-hydrogenated products. Isotope labeling experiments combined with semi-empirical calculations reveal that both the sodium borohydride and water participate in the hydrogenation process by means of hydride transfer and proton transfer, respectively, as illustrated in Figure 6.2.

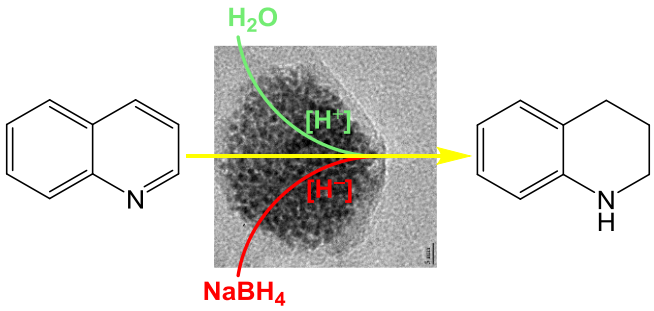

Figure 6.2 Graphical abstract of the hydrogenation of quinoline with sodium borohydride and water over *nano*Ru′@hectorite.

The catalytic properties of the hectorite-intercalated ruthenium nanoparticles can also be used for the hydrogenation of aromatic amino acids in aqueous media, as depicted in Figure 6.3. By screening of the influencing factors, the pH of the solution was found to be critical for the complete conversion of aromatic amino acids. The scope of the substrates susceptible to the *nano*Ru@hectorite catalyst includes L-phenylglycine, L-tyrosine, and L-tryptophan as well as L-phenylalanine. Under the catalytic reaction conditions, all these substrates are completely converted with high selectivity. Noticeably, during these reactions the chirality of the substrates remains unchanged.

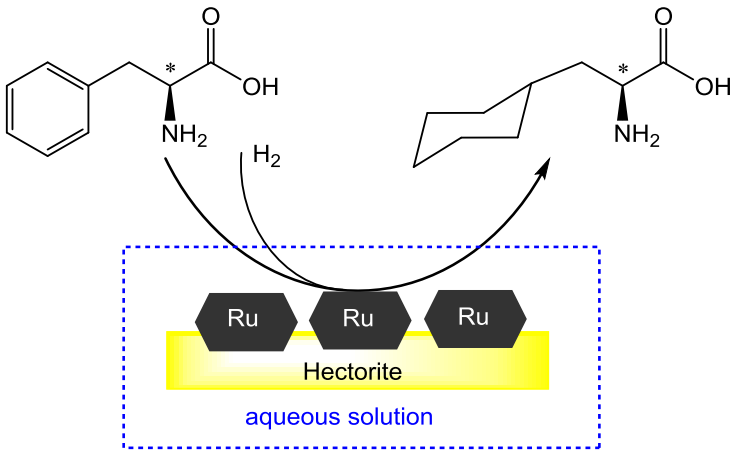

Figure 6.3 Graphical abstract of the hydrogenation of L-phenylalane over *nano*Ru@hectorite.

Among all the precious metals employed as catalysts, ruthenium owes its unique advantages to a relatively low price and to satisfactory catalytic properties. To date, a great number of studies on ruthenium catalysts stress on homogeneous conditions, although the number of heterogeneous catalysts is growing gradually. Accompanied by a sense of cost-effective and green chemistry, the replacement of expensive metals with cheaper ones has been attempted and will be sustaining. Noticeably, supported ruthenium catalysts have found their wide use in oxidation, olefin metathesis, nitrile hydration, azide-alkyne cycloaddition as well as in hydrogenation. From a perspective point of view, the design of highly efficient metal catalysts remains significantly attractive, the mechanistic understanding of the structure-performance relationship being critical. The ruthenium catalysts studied in this thesis, *nano*Ru@hectorite and *nano*Ru′@hectorite, are easily accessible in the form of Ru(II) or Ru(III)-containing precatalysts, which are air-stable and can be easily stored and used. It is expected that they may also catalyze other important hydrogenation reactions such as the hydrogenation of aliphatic nitro compounds and dinitro compounds, oximes, reductive alkylations, dehydrohalogenations, miscellaneous hydrogenolysis and more.

7

Experimental section

7.1 Experimental part for chapter 2

General synthesis

White sodium-containing hectorite powder was synthesized according to the method of Bergk and Woldt [1]. The sodium cation exchange capacity, determined under the method of Lagaly and Tributh [2], was found to be 104 mEq per 100 g. The dimeric complex $[(C_6H_6)_2RuCl_2]_2$ was synthesized following the procedure reported by Arthur and Stephenson [3].

Preparation of the ruthenium(II)-containing catalyst precursor

The neutral complex $[(C_6H_6)RuCl_2]_2$ (83.8 mg, 0.17 mmol) was thoroughly dissolved in distilled and N_2-saturated water (50 ml), giving a bright yellow solution after vigorous stirring for 1 h. The pH of this solution was adjusted to 8 (using a glass electrode) by adding the appropriate amount of 0.1 M NaOH. After filtration this solution was added to 1 g of finely powdered and degassed (1 h high vacuum, then N_2-saturated) sodium hectorite. The resulting suspension was stirred for 4 h at 20 °C. Then the yellow ruthenium(II)-containing hectorite was filtered off and dried *in vacuo* for 12 h.

Preparation of the ruthenium(III)-containing catalyst precursor

White sodium hectorite powder (1 g) was degassed *in vacuo* for 1 h and followed by the N_2 saturation, then the calculated amount of $RuCl_3 \cdot n\ H_2O$ (0.40 mmol) dissolved in 85 ml H_2O (black solution) was transferred dropwise to the hectorite powder. The suspension was stirred for 3 h at room temperature, then treated by filtration and washing with deionized H_2O (black solid) until no chloride ion was detected. The obtained solid product was dried *in vacuo* at 50 °C for 12 h and then

ground to give a fine powder, containing 0.39 μmol/mg Ru (2 mol%) based on ICP-OES analysis.

Preparation of the nanoRu@hectorite catalyst

The *nano*Ru@hectorite catalyst was obtained by reacting a suspension of the black ruthenium(II)-containing hectorite (50 mg, 0.01592 mmol Ru) in a magnetically stirred stainless-steel autoclave (volume 100 ml) under a pressure of H_2 (50 bar) at 100 °C for 14 h using different solvents. After pressure release and cooling, the *nano*Ru@hectorite catalyst was isolated as a black material.

Preparation of the nanoRu'@hectorite catalyst

The *nano*Ru′@hectorite was obtained by reacting a suspension of the yellow ruthenium(III)-containing hectorite (50 mg) with fresh sodium borohydride (12 mmol) in 10 ml degassed water at 60 °C for 4 h under atmospheric pressure. After the reaction, the mixture was quenched and centrifuged. The obtained black solid material was thoroughly washed with distilled water and finally dried *in vacuo* at room temperature for 12 h. The *nano*Ru′@hectorite catalyst was therefore obtained.

Characterization of the as-synthesized hectorite-supported ruthenium nanoparticles

The powder X-ray diffraction (XRD) patterns of the catalysts were collected by XRD Application LAB in CSEM (Switzerland). The samples were measured in air at 20 °C on a STOE STADIP high-resolution X-ray diffractometer using CuKα radiation. D-spacing (d) determination of the interlamellar spacing in hectorite, based on hectorite (001) reflection, was calculated from Bragg's law [4]:

$$n \lambda = 2 d \sin\theta$$

where n is an integer (herein n = 1), λ is the X-ray wavelength (for the CuKα, λ = 1.5418 Å). θ is the angle between incident beam and scattering planes. Based on the Ru(011) reflection with the Si standard as a reference for the instrument peak broadening, the crystallite size L was calculated using the Scherrer equation [5]:

$$L = K \lambda / (\beta \cos\theta)$$

where λ is the X-ray wavelength (λ = 1.5418 Å), K is a constant related to crystallite shape, here taken as 0.94. β is the full width at half maximum (FWHM) of the peak profile, and θ is the Bragg angle.

Transmission electron microscopy (TEM) was conducted in CSEM on a Philips CM 200 Transmission Electron Microscope (operating at 200 kV) coupled with Energy Dispersive X-ray spectrometry (EDS) for chemical analysis. The solid catalyst samples are thoroughly dispersed in ethanol and deposited on carbon film coated square mesh copper grids. The calculation of the nanoparticle size was obtained from TEM images with a number of over 100 nanoparticles by using the software ImageJ [6]. Inductively coupled plasma optical emission spectrometry (ICP-OES, Perkin-Elmer Optima 3300 DV) was employed to analyze the amount of *in situ* formed ruthenium in hectorite and ruthenium leaching in the centrifuged supernatant after the catalytic run.

7.2 Experimental part for chapter 3

The catalyst used in this chapter is *nano*Ru@hectorite, which were prepared through an organometallic approach. A variety of the solvents were tested for the preparation of the catalyst and for the catalytic hydrogenation.

Catalytic hydrogenation of quinoline

The selective hydrogenation of quinoline was carried out in a magnetically

stirred stainless-steel autoclave (100 ml). The air in the autoclave was displaced by purging three times with hydrogen prior to use. The quantitative chemical analysis of hydrogenation products was completed by GC–MS analysis. The GC separation was carried out on a ZB-5MS column (30 m × 0.25 mm, 0.25 μm) using a temperature program of 35–200 °C at 5 °C/min. The instrument used was ThermoFinnigan®Trace GC-Polaris Q. The data was collected by using extracted ion chromatograms of marker m/z values for each molecule from the total ion chromatograms (TIC).

A freshly prepared suspension of *nano*Ru@hectorite and the desired amount of quinoline was used. Then the autoclave was pressurized with hydrogen (20–60 bar) and then heated to 100 °C. After the reaction, the pressure was released, the solution was filtered (0.22 μm, PTFE) and analyzed in order to determine the substrate conversion and selectivity (in %). The catalytic reaction was followed by gas chromatography coupled to a mass detector. The products were separated on an apolar column and identified by their retention time and their mass spectrum using the electron impact (EI) ionization method.

Catalyst recycling and recovery

After the catalytic run, the *nano*Ru@hectorite catalyst was separated by decantation of the centrifuged reaction mixture. Then the catalyst was washed with diethyl ether and cyclohexane, and then reactivated in the autoclave under H_2 pressure (50 bar) at 100 °C for14 h in the reaction medium used for the next catalytic run. After pressure release and cooling, a new batch of quinoline was added for the next catalytic run.

7.3 Experimental part for chapter 4

The catalyst involved in this chapter is *nano*Ru′@hectorite. However, the ruthenium(III)-containing hectorite precatalyst was used into the hydrogenation

without any reduction. The *nano*Ru′@hectorite was in situ formed in the presence of sodium borohydride during the hydrogenation process, which is considered to be the real catalyst.

Catalytic hydrogenation N-cycle of quinolines

Deionized water was made from tap water by ionic exchange resins and degassed before use. All the *N*-cyclic chemicals were purchased from commercially available sources and used as received. $NaBH_4$ and $NaBD_4$ (D, 98 atom %) were purchased from Aldrich, and D_2O (D, 99.9%) from Cambridge Isotope Laboratories.

The precatalyst (50 mg), $NaBH_4$ (or $NaBD_4$) (3–12 mmol), 1 mmol of the *N*-cyclic substrate and 5 ml deionized and degassed water (or D_2O) were placed in a 25 ml three-necked flask equipped with a reflux condenser and a pressure release valve to discharge the hydrogen gas self-generated during the reactions. The operation was carried out under inert atmosphere. The reaction mixture was vigorously stirred at different temperatures (25–60 °C) for the time selected. The complete conversion of substrate was determined by submitting small samples to spot thin layer chromatography (TLC). After completion, the slurry was centrifuged to separate the catalyst. The solid phase obtained was washed with deionized H_2O and then several times with ethyl acetate to remove all organic residues. The filtrate was collected, extracted with ethyl acetate and the extract dried over anhydrous $MgSO_4$. After removal of the solvent *in vacuo*, the corresponding product was obtained. In some cases, a silica-gel column chromatography was used to purify the product (isolated yield). The product analysis and identification was conducted by comparing the NMR spectral data with those of the published pure substances (all analyzed by ^{1}H NMR and ^{13}C NMR on Bruker Avance II 400 MHz spectrometer).

Alternatively, the reaction was performed in a magnetically stirred stainless-steel autoclave (100 ml) in cases where the reaction failed to be complete under atmospheric pressure. The loading procedure was the same as that in a flask. After

purging three times with nitrogen, the autoclave was quickly fixed in the preheated oil bath. Once the reaction was complete, the autoclave was quenched in cold water, the pressure was released, and the product was isolated as described above.

Isotope labeling experiments were done for the hydrogenation of quinoline with $NaBH_4/D_2O$ and with $NaBD_4/H_2O$ (and for comparison with $NaBH_4/H_2O$ and with $NaBD_4/D_2O$), under the same conditions as those of entry 7 in Table 1 (see below). All NMR spectra were recorded with a narrow-bore Bruker 400 spectrometer (9.4 T) operating at $\omega_0/2\pi$ = 400.0 and 100.6 MHz for ^1H and ^{13}C, respectively, and equipped with an AVANCE-II console and a 5 mm double resonance probe. The *rf*-field strengths of all hard $\pi/2$ and π pulses were $\omega_1/2\pi$ = 26 kHz and 27 kHz, for ^1H and ^{13}C channels, respectively. Quantitative proton spectra were acquired with a recycling delay $d_1 = 5 \times T_1$, with longitudinal relaxation time constraints T_1 of the as measured with inversion-recovery experiments. Semi-empirical calculations were performed with the PM7 method as implemented in MOPAC2012 [7]. The optimized geometries were used for calculations of the electrostatic potentials by means of the keyword ESP.

Catalyst recycling and recovery

The recyclability of the nanoRu′@hectorite catalyst was examined for the hydrogenation of quinoline under atmospheric pressure in a flask. After a catalytic run, the catalyst was recovered by centrifugation and purified by washing with deionized H_2O and ethyl acetate and dried *in vacuo* at room temperature for 12 h. Then the recycled catalyst was used for the next catalytic run without any reactivation.

7.4 Experimental part for chapter 5

The catalyst used in this chapter is *nano*Ru@hectorite, which was prepared through an organometallic approach.

Catalytic hydrogenation of chiral aromatic amino acids

The selective hydrogenation of the optically active phenyl amino acid was carried out in a magnetically stirred stainless-steel autoclave (100 ml). Prior to the loading of the catalyst, the autoclave was purged three times with hydrogen to expel the air. Typically, a freshly prepared suspension of *nano*Ru@hectorite (0.01592 mmol Ru, 10 ml H_2O) and the appropriate amount of the substrate were carefully transferred into the autoclave under inert atmosphere, and then the autoclave was charged with H_2 to the desired pressure. The autoclave was placed into the pre-heated heating mantle and the magnetic stirring was started for the indicated reaction time. After the reaction, the autoclave was cooled down and the pressure was released. The reactor was thoroughly rinsed with 2N NaOH solution to wash out the entire product (in the case of acidic system, 2N HCl was used). All the collected solutions were filtered (0.22 μm, PTFE) to remove the catalyst and then treated with diluted HCl (or NaOH) solution to adjust the pH to 5.5, which caused the partial precipitation of the product. The suspension was then reduced *in vacuo* to 10 ml in order to complete the precipitation. The precipitate was filtered off, washed with distilled water and dried *in vacuo* at room temperature for 12 h.

The white product was analyzed through ^{1}H and ^{13}C NMR in methanol-d_4 or D_2O using a Bruker Avance II 400 MHz spectrometer using tetramethylsilane (TMS) as internal standard. IR spectra were recorded with a PerkinElmer FT-IR 1720 X spectrometer. Optical rotation was measured by a SCHMIDT HAENSCH Polartronic H532 polarimeter. The optical purity of the product was further examined by HPLC-UV technique (Ultimate 3000RS Dionex system with Acquity UPLC® BEH HILIC column). Electrospray ionization mass spectra (ESI-MS) were obtained in negative ion mode on a Bruker FTMS 4.7T BioAPEX II mass spectrometer. Inductively coupled plasma optical emission spectrometry (ICP-OES, Perkin-Elmer Optima 3300 DV) was used to analysis the ruthenium leaching after the catalytic run.

Catalyst recycling and recovery

After a catalytic run, the *nano*Ru@hectorite catalyst was separated by decantation from the centrifuged reaction mixture. The supernatant was analyzed by ICP-OES to detect the Ru leaching. The catalyst was washed with 2N NaOH (in the case of acidic system, 2N HCl was used) solution and then with degassed water to extract traces of the catalytic product. After drying *in vacuo* for 12 h, the recycled catalyst was dispersed in the reaction medium under ultrasonic conditions and reactivated in the autoclave under a H_2 pressure of 50 bar at 100°C for 14 h. After pressure release and cooling, the amino acid substrate, the amount of which was calculated from the weight of the corresponding recycled catalyst, was added for the next catalytic run.

7.5 Spectroscopic analysis

1,2,3,4-Tetrahydroquinoline: oil, ^{1}H NMR (400 MHz, $CDCl_3$): δ = 6.45–7.01 (m, 4H, CH), 3.83 (s, 1H, NH), 3.31 (t, 2H, CH_2), 2.79 (t, 2H, CH_2), 1.96 (q, 2H, CH_2); ^{13}C NMR (400 MHz, $CDCl_3$): δ = 142.60, 128.26, 125.32 120.01, 115.23, 112.89, 40.54, 25.75, 20.48.

6-Methyl-1,2,3,4-tetrahydroquinoline: oil, ^{1}H NMR (400 MHz, $CDCl_3$): δ = 7.01 (b, 1H, CH), 6.78 (s, 1H, CH), 6.43 (s, 1H, CH), 3.28 (t, 2H, CH_2), 2.74 (t, 2H, CH_2), 2.21 (s, 3H, CH_3), 1.93 (q, 2H, CH_2); ^{13}C NMR (400 MHz, $CDCl_3$): δ = 141.53, 130.01, 128.5, 127.93, 121.5, 42.15, 26.69, 22.15, 20.36.

8-Methyl-1,2,3,4-tetrahydroquinoline: solid, ^{1}H NMR (400 MHz, $CDCl_3$): δ = 6.63–6.95 (m, 3H, CH), 3.66 (s, 1H, NH), 3.43 (t, 2H, CH_2), 2.85 (t, 2H, CH_2), 2.14 (s, 3H, CH_3), 2.01 (q, 2H, CH_2); ^{13}C NMR (400 MHz, $CDCl_3$): δ = 142.73, 127.86,

127.39, 121.17, 120.85, 116.39, 42.36, 27.33, 22.19, 17.18.

2,6-Dimethyl-1,2,3,4-tetrahydroquinoline: solid, ^{1}H NMR (400 MHz, $CDCl_3$): δ = 6.43–6.83 (m, 3H, CH), 3.60 (s, 1H, NH), 3.39 (m, 1H, CH), 2.75–2.86 (t, 2H, CH_2), 2.25 (s, 3H, CH_3), 1.59–1.93 (q, 2H, CH_2), 1.23 (s, 3H, CH_3); ^{13}C NMR (400 MHz, $CDCl_3$): δ = 142.45, 129.80, 127.21, 126.16, 121.16, 114.24, 47.3, 31.37, 26.58, 22.71, 22.58.

8-Hydroxy-1,2,3,4-tetrahydroquinoline: solid, ^{1}H NMR (400 MHz, $CDCl_3$): δ = 6.49–6.60 (m, 3H, CH), 3.69 (s, 1H, NH), 3.24 (t, 2H, CH_2), 2.76 (t, 2H, CH_2), 1.91 (q, 2H, CH_2); ^{13}C NMR (400 MHz, $CDCl_3$): δ = 142.12, 135.20, 121.95, 120.01, 117.21, 113.05, 42.11, 27.21, 22.21.

1,2,3,4-Tetrahydroisoquinoline: oil, ^{1}H NMR (400 MHz, $CDCl_3$): δ = 7.01–7.14 (m, 4H, CH), 4.02 (s, 2H, CH_2), 3.15 (t, 2H, CH_2), 2.81 (t, 2H, CH_2); ^{13}C NMR (400 MHz, $CDCl_3$): δ = 136.21, 134.75, 129.32, 126.01, 125.75, 125.47, 48.11, 43.75, 29.05.

1,2,3,4-Tetrahydroquinoxaline: oil, ^{1}H NMR (400 MHz, $CDCl_3$): δ = 6.51–6.57 (m, 4H, CH), 3.43 (s, 4H, CH_2); ^{13}C NMR (400 MHz, $CDCl_3$): δ = 137.79, 122.41, 118.93, 40.95.

2-Methyl-1,2,3,4-tetrahydroquinoxaline: solid, ^{1}H NMR (400 MHz, $CDCl_3$): δ = 6.50–6.61 (m, 4H, CH), 3.52 (s, 2H, NH), 3.31–3.51 (t, 2H, CH_2), 3.02–3.07 (m, 1H, CH); ^{13}C NMR (400 MHz, $CDCl_3$): δ = 133.52, 133.14, 118.66, 118.65, 114.45, 114.40, 48.22, 45.69, 19.84.

5-Chloro-8-hydroxy-1,2,3,4-tetrahydroquinoline: solid, ^{1}H NMR (400 MHz, $CDCl_3$): δ = 6.52 (s, 2H, CH), 3.27 (t, 2H, CH_2), 2.75 (t, 2H, CH_2), 1.95 (q, 2H, CH_2); ^{13}C NMR (400 MHz, $CDCl_3$): δ = 142.88, 142.08, 127.2, 124.6, 122.5, 112.68, 41.04,

24.53, 21.43.

2-Phenyl-5,6,7,8-tetrahydroquinoline: solid, ^{1}H NMR (400 MHz, $CDCl_3$): δ = 7.99–8.00 (s, 2H, CH), 7.40–7.50 (m, 5H, CH), 3.05 (t, 2H, CH_2), 2.81 (t, 2H, CH_2), 1.86–1.96 (q, 4H, CH_2); ^{13}C NMR (400 MHz, $CDCl_3$): δ = 156.43, 150.65, 136.34, 134.78, 128.01, 128.00, 127.4, 127.3, 127.0, 118.98, 32.01, 27.21, 22.69, 22.68.

L-cyclohexylalanine: white solid, ^{1}H NMR (400 MHz, CD_3OD): δ = 3.55–3.58 (m, 1H, CH), 0.92–1.84 (m, 13H, C_6H_{11}, CH_2); ^{13}C NMR (400 MHz, CD_3OD): δ = 173.65, 52.50, 38.89, 33.58, 33.29, 32.02, 26.02, 25.79, 25.59; ESI-MS (methanol): *m/z* = 170.1 ($[M–H]^-$); $[\alpha]^{25}_D$ = +14.60°, c = 2, TFA (the reported results: [α] = +14.06°, c = 2, TFA, see the reference [8]).

L-cyclohexylglycine: white solid, ^{1}H NMR (400 MHz, D_2O): δ = 4.59–4.60 (m, 1H, CH), 1.07–1.96 (m, 11H, C_6H_{11}); ^{13}C NMR (400 MHz, D_2O): δ = 174.17, 59.91, 38.74, 28.76, 27.34, 25.58, 25.53; ESI-MS (H_2O + methanol): *m/z* = 140.6 ($[M–OH]^-$); $[\alpha]^{20}_D$ = +31°, c=1, 1 N HCl (the reported results: $[\alpha]^{20}_D$ = +31°, c=1, 1 N HCl, see the reference [9]).

Energy Dispersive X-ray Spectrometry (EDS) analysis of nanoRu'@hectorite

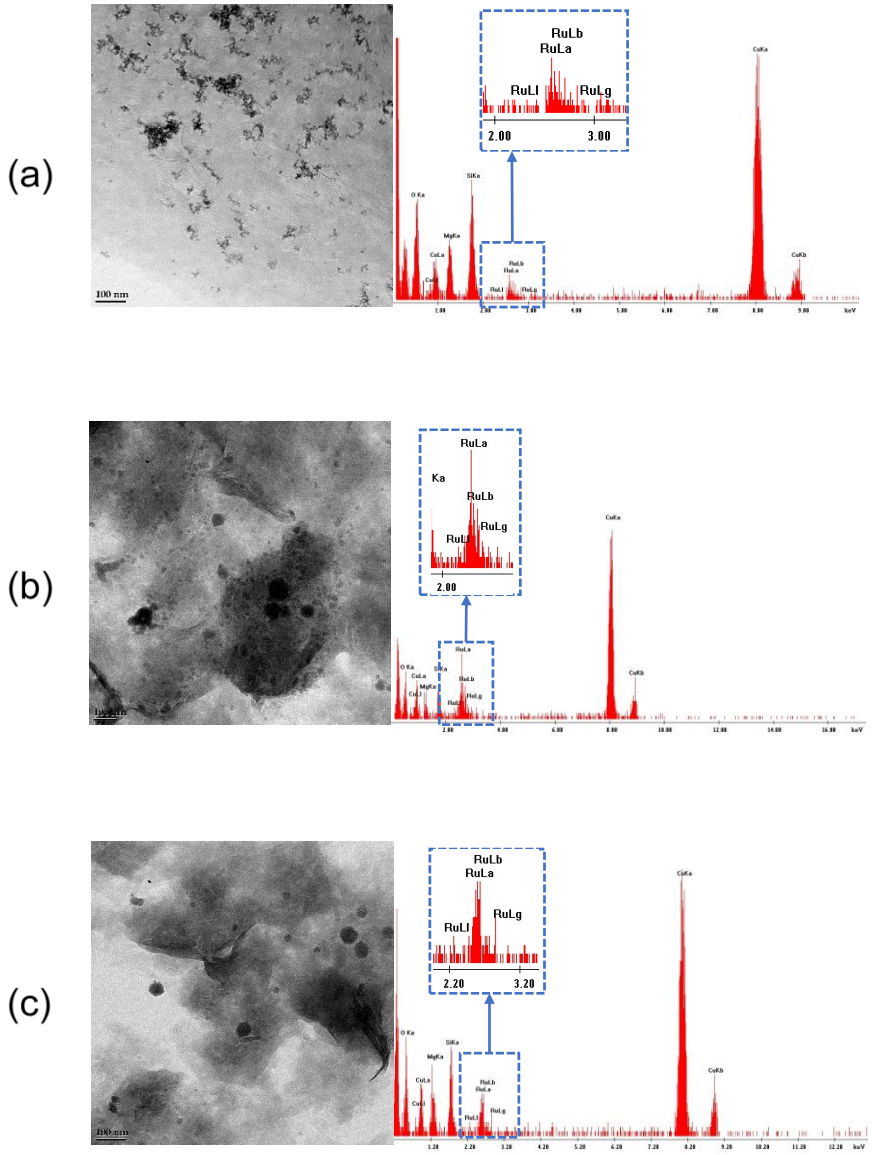

Figure 7.1 EDS analysis of the samples of (a) the *nano*Ru'@hectorite from the direct reduction of the precatalyst under atmospheric pressure at 60 °C for 4 h in water without organic agent, (b) the *in situ* generated *nano*Ru'@hectorite catalyst after a fresh run for the catalytic hydrogenation of quinoline under atmospheric pressure at 60 °C for 4 h in water and (c) the *nano*Ru'@hectorite catalyst after the first recycling run for the hydrogenation of quinoline under atmospheric pressure at 60 °C for 4 h in water.

Energy Dispersive X-ray Spectrometry (EDS) analysis of nanoRu@hectorite

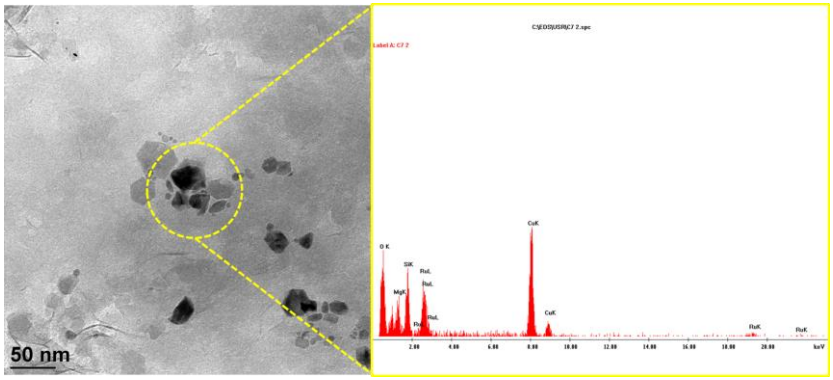

Figure 7.2 EDS analysis of the freshly prepared *nano*Ru@hectorite catalyst

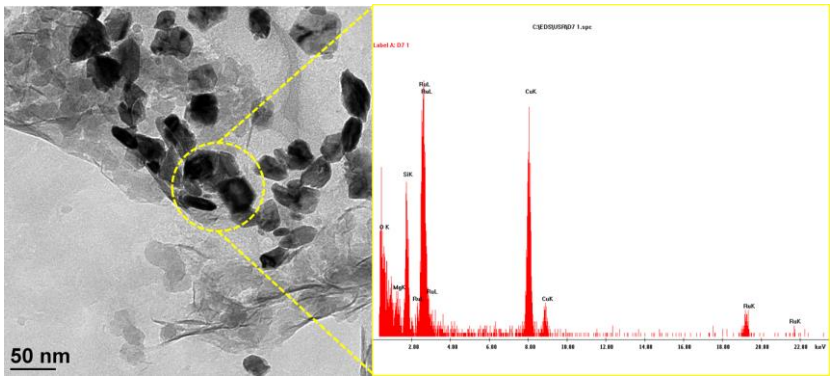

Figure 7.3 EDS analysis of the recycled *nano*Ru@hectorite catalyst after three times catalytic hydrogenation run of L-phenylalanine in water.

References

[1] K. H. Bergk, D. Woldt, unpublished. See D. Woldt, PhD Thesis, University of Halle-Wittenberg, Germany, 1988.

[2] G. Lagaly, H. Tributh, Ber. Dt. Tonmineralgruppe 86 (1996).

[3] T. Arthur, T. A. Stephenson, J. Organomet. Chem. 208 (1981) 369–387.

[4] W. L. Bragg, Proc. Camb. Philos. Soc. (1913) 43–57.

[5] P. Scherrer, Nachrichten von der Gesellschaft der Wissenschaften zu Göttingen, Mathematisch-Physikalische Klasse 1918 (1918) 98–100.

[6] C. A. Schneider, W. S. Rasband, K. W Eliceiri, Nat. Methods 9 (2012) 671–675.

[7] J. J. P. Stewart, Stewart Computational Chemistry, Version 13.073W web: HTTP://OpenMOPAC.net.

[8] D. J. Ager, I. Prakash, Org. Process Res. Dev. 7 (2003) 164–167.

[9] M. Beller, M. Eckert, H. Geissler, B. Napierski, H.-P. Rebenstock, E. Wolfgang Holla, Chem. Eur. J. 4 (1998) 935–941.

List of publications

1. B. Sun, D. Carnevale, G. Süss-Fink, Selective *N*-cycle hydrogenation of quinolines with sodium borohydride in aqueous media catalyzed by hectorite-supported ruthenium nanoparticles. J. Organomet. Chem. 2015, *submitted*.
2. B. Sun, G. Süss-Fink, Chemselective hydrogenation of aromatic amino acids in aqueous media catalyzed by *nano*Ru@hectorite. J. Organomet. Chem. 2015, doi:10.1016/j.jorganchem.2015.09.011.
3. B. Sun, F. A. Khan, B. Therrien, G. Süss-Fink, Metal Catalysts Intercalated in Smectite Clays (invited book chapter for *Encapsulated Catalysts*). Elsevier, 2015, *in preparation*.
4. B. Sun, F. A. Khan, A. Vallat, G. Süss-Fink, *Nano*Ru@hectorite: A heterogeneous catalyst with switchable selectivity for the hydrogenation of quinoline. Appl. Catal. Gen: A. 467 (2013) 310–314.

Conference contributions

1. Fall Meeting of the Swiss Chemical Society 2014, 11.09.2014, Zürich, Poster.
2. Subject Days "Modern Synthetic Methods and their Application in the context of Natural Products", 11.06.2013, Neuchâtel, Switzerland, Oral presentation.
3. Fall Meeting of the Swiss Chemical Society 2013, 06.09.2013, Lausanne, Poster.
4. Swiss Summer School "Synthesis and Catalysis", Villars, Switzerland, 12.07.2013 – 16.07.2013, Poster.
5. Fall Meeting of the Swiss Chemical Society 2012, 13.09.2012, Zürich, Poster.
6. 1st Year Graduate Student Symposium 2012, 10.09.2012 – 11.09.2012, Bern, Switzerland, Oral presentation.
7. Swiss Summer School "Hydrogen Bonding", Villars, Switzerland, 20.08.2012 – 24.08.2012, Poster.

The design of nanocomposites consisting of functional metals and proper matrices is a very active field of research for the development of recyclable catalysts. Highly active metallic nanoparticles must be stabilized by a suitable support in order to prevent aggregation to bulk metal. Hectorite, a representative smectite clay featured by its unique swelling properties and flexible intercalation capacity, provides an ideal platform for immobilizing metal nanoparticles.

In the catalytic hydrogenation of quinoline, hectorite-intercalated ruthenium nanoparticles show excellent reactivity and selectivity to the specific product. By using water or cyclohexane as reaction medium under a certain pressure of H_2, 1,2,3,4-tetrahydroquinoline and decahydroquinoline were exclusively obtained, respectively. Furthermore, by using sodium borohydride as reducing agent, the catalytic hydrogenation of quinoline proceeds in water under atmospheric pressure with the conversion and selectivity superior to 99%. Isotope labeling experiments combined with semi-empirical calculations reveal that both the sodium borohydride and water participate in the hydrogenation process by means of hydride transfer and proton transfer, respectively.

Furthermore, hectorite-intercalated ruthenium nanoparticles can also be used for the hydrogenation of aromatic amino acids in aqueous media. By screening of the influencing factors, the pH of the solution was found to be critical for the complete conversion of aromatic amino acids. Critically, during the hydrogenation process, the chirality of the substrates remains unchanged.